U.S. Department of Transportation
Federal Railroad Administration

Weld Repair of Manganese Frogs for Enhanced Performance

Office of Research, Development, and Technology
Washington, DC 20590

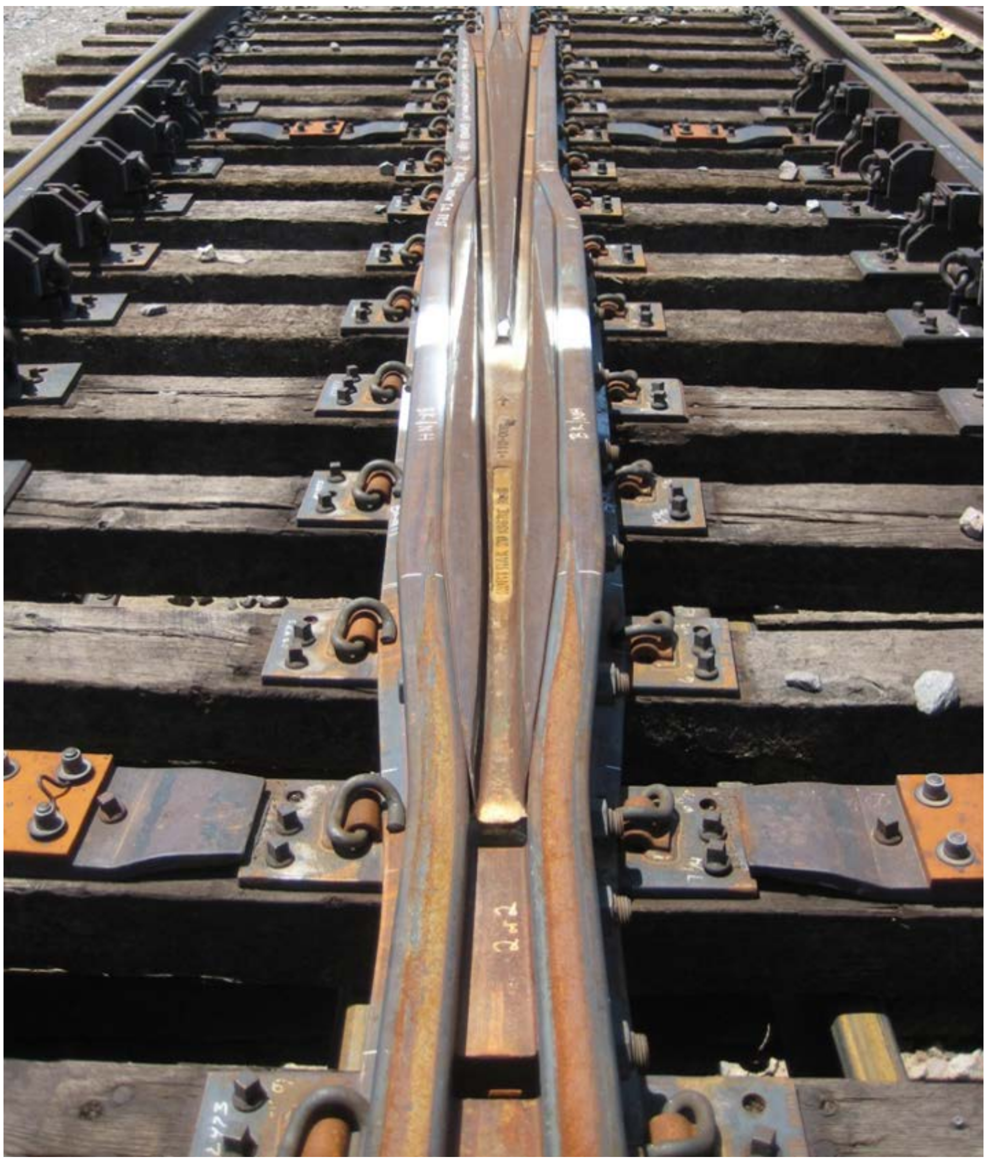

DOT/FRA/ORD-17/01

Final Report
January 2017

REPORT DOCUMENTATION PAGE

Form Approved
OMB No. 0704-0188

1. AGENCY USE ONLY (Leave blank)	2. REPORT DATE	3. REPORT TYPE AND DATES COVERED
	January 2017	Final

4. TITLE AND SUBTITLE
Weld Repair of Manganese Frogs for Enhanced Performance

5. FUNDING NUMBERS
Contract No.
DTFR53-13-C-00037

6. AUTHOR(S)
Marc Alan Purslow

7. PERFORMING ORGANIZATION NAME(S) AND ADDRESS(ES)
EWI
1250 Arthur E. Adams Drive
Columbus, OH 43221

8. PERFORMING ORGANIZATION REPORT NUMBER
53744GTH

9. SPONSORING/MONITORING AGENCY NAME(S) AND ADDRESS(ES)
U.S. Department of Transportation
Federal Railroad Administration
Office of Railroad Policy and Development
Office of Research and Development
Washington, DC 20590

10. SPONSORING/MONITORING AGENCY REPORT NUMBER
DOT/FRA/ORD-17/01

11. SUPPLEMENTARY NOTES
COR: Cameron D. Stuart

12a. DISTRIBUTION/AVAILABILITY STATEMENT
This document is available to the public through the FRA Web site at http://www.fra.dot.gov.

12b. DISTRIBUTION CODE

13. ABSTRACT (Maximum 200 words)
When special trackwork contact surfaces (such as manganese-steel turnout frogs) become worn and damaged, they can be repaired to extend their lifetime, but current repair methods typically cannot return these surfaces to their original durability. Since worn or damaged frogs in freight and shared corridors have a detrimental effect on ride quality and increase life cycle costs, improved repair processes can extend the service life of frogs and improve the safety and efficiency of rail operations. In this project, EWI developed a new flux-cored arc welding (FCAW) procedure to repair manganese frogs. When EWI tested a repaired frog in simulated revenue service conditions at the Transportation Technology Center, the test results show a significant improvement in the durability of the repair as compared to traditional repair methods. Future work plans include revenue service trials, as well as refinements to weld procedures and materials.

14. SUBJECT TERMS

Reciprocating Wire Feed	Radiographic Testing
Constant Voltage	Shielded Metal Arc Welding
Flux-Cored Arc Welding	Ultimate Tensile Strength
Heat-Affected Zone	Yield Strength

15. NUMBER OF PAGES
124

16. PRICE CODE

17. SECURITY CLASSIFICATION OF REPORT	18. SECURITY CLASSIFICATION OF THIS PAGE	19. SECURITY CLASSIFICATION OF ABSTRACT	20. LIMITATION OF ABSTRACT
Unclassified	Unclassified	Unclassified	SAR

NSN 7540-01-280-5500

Standard Form 298 (Rev. 2-89)
Prescribed by ANSI Std. 239-18
298-102

METRIC/ENGLISH CONVERSION FACTORS

ENGLISH TO METRIC

LENGTH (APPROXIMATE)

1 inch (in)	=	2.5 centimeters (cm)
1 foot (ft)	=	30 centimeters (cm)
1 yard (yd)	=	0.9 meter (m)
1 mile (mi)	=	1.6 kilometers (km)

AREA (APPROXIMATE)

1 square inch (sq in, in^2)	=	6.5 square centimeters (cm^2)
1 square foot (sq ft, ft^2)	=	0.09 square meter (m^2)
1 square yard (sq yd, yd^2)	=	0.8 square meter (m^2)
1 square mile (sq mi, mi^2)	=	2.6 square kilometers (km^2)
1 acre = 0.4 hectare (he)	=	4,000 square meters (m^2)

MASS - WEIGHT (APPROXIMATE)

1 ounce (oz)	=	28 grams (gm)
1 pound (lb)	=	0.45 kilogram (kg)
1 short ton = 2,000 pounds (lb)	=	0.9 tonne (t)

VOLUME (APPROXIMATE)

1 teaspoon (tsp)	=	5 milliliters (ml)
1 tablespoon (tbsp)	=	15 milliliters (ml)
1 fluid ounce (fl oz)	=	30 milliliters (ml)
1 cup (c)	=	0.24 liter (l)
1 pint (pt)	=	0.47 liter (l)
1 quart (qt)	=	0.96 liter (l)
1 gallon (gal)	=	3.8 liters (l)
1 cubic foot (cu ft, ft^3)	=	0.03 cubic meter (m^3)
1 cubic yard (cu yd, yd^3)	=	0.76 cubic meter (m^3)

TEMPERATURE (EXACT)

[(x-32)(5/9)] °F = y °C

METRIC TO ENGLISH

LENGTH (APPROXIMATE)

1 millimeter (mm)	=	0.04 inch (in)
1 centimeter (cm)	=	0.4 inch (in)
1 meter (m)	=	3.3 feet (ft)
1 meter (m)	=	1.1 yards (yd)
1 kilometer (km)	=	0.6 mile (mi)

AREA (APPROXIMATE)

1 square centimeter (cm^2)	=	0.16 square inch (sq in, in^2)
1 square meter (m^2)	=	1.2 square yards (sq yd, yd^2)
1 square kilometer (km^2)	=	0.4 square mile (sq mi, mi^2)
10,000 square meters (m^2)	=	1 hectare (ha) = 2.5 acres

MASS - WEIGHT (APPROXIMATE)

1 gram (gm)	=	0.036 ounce (oz)
1 kilogram (kg)	=	2.2 pounds (lb)
1 tonne (t)	=	1,000 kilograms (kg)
	=	1.1 short tons

VOLUME (APPROXIMATE)

1 milliliter (ml)	=	0.03 fluid ounce (fl oz)
1 liter (l)	=	2.1 pints (pt)
1 liter (l)	=	1.06 quarts (qt)
1 liter (l)	=	0.26 gallon (gal)
1 cubic meter (m^3)	=	36 cubic feet (cu ft, ft^3)
1 cubic meter (m^3)	=	1.3 cubic yards (cu yd, yd^3)

TEMPERATURE (EXACT)

[(9/5) y + 32] °C = x °F

QUICK INCH - CENTIMETER LENGTH CONVERSION

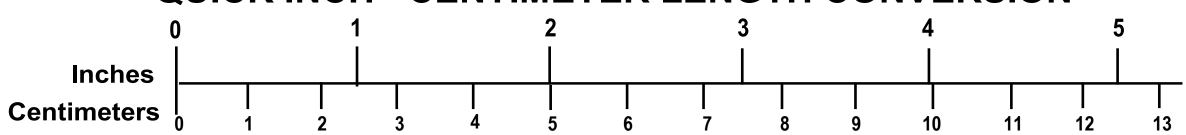

QUICK FAHRENHEIT - CELSIUS TEMPERATURE CONVERSION

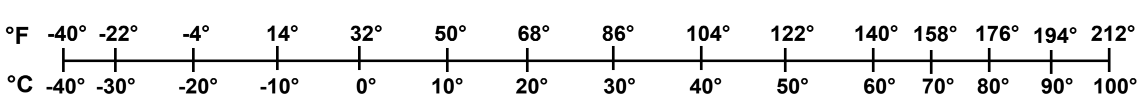

For more exact and or other conversion factors, see NIST Miscellaneous Publication 286, Units of Weights and Measures. Price $2.50 SD Catalog No. C13 10286

Updated 6/17/98

Contents

Illustrations v

Tables viii

Executive Summary 1

1. Introduction 3

1.1 Background 3
1.2 Objectives 6
1.3 Overall Approach 6
1.4 Scope 7

2. Task 1 – Process Baseline Study 10

2.1 Objectives and Approach 10
2.2 Baseline Welding 10
2.3 Evaluation of Baseline Welds 10
2.4 Interpass Temperature Trials 16

3. Task 2 – Automated Repair of Manganese Frogs Using FCAW 18

3.1 Automated FCAW Welding Trials 18
3.2 Reciprocating Wire Feed (RWF) FCAW Trials 24
3.3 Baseline Testing and Automated FCAW Development Overview 27
3.4 Field Repair Evaluation 29
3.5 Weld Repair of Partial Frog 31
3.6 Evaluation of Partial Frog Weld Repair 32
3.7 Repair of Full-Length Frogs for TTCI Testing 33

4. Track and Laboratory Testing Results 47

4.1 Track Testing Summary 52
4.2 EWI Laboratory Testing 53

5. Automation Concept 66

5.1 Automated Repair System Concept 66
5.2 Repair Approach Concept 68

6. Conclusions 69

7. References 70

Appendix. TTCI Report 71

Abbreviations and Acronyms 117

Illustrations

Figure 1: Breakout of Weld Repair 4
Figure 2: Breakout on Wing 4
Figure 3: Work Breakdown Structure 9
Figure 4: #20 Point Mock-up 11
Figure 5: Top View of #20 Point Mock-up Geometry 11
Figure 6: Side View of #20 Point Mock-up Geometry 11
Figure 7: Baseline SMAW Cross Section 12
Figure 8: Baseline FCAW Cross Section 13
Figure 9: Baseline SMAW Hardness Map 13
Figure 10: Baseline FCAW Hardness Map 14
Figure 11: Tested Sub-sized Tensile Samples 14
Figure 12: Tensile Specimen Locations 15
Figure 13: Industry-Recommended Weld Sequence 16
Figure 14: Alternate Weld Sequence 2 17
Figure 15: Alternate Weld Sequence 3 17
Figure 16: Illustration of Push and Drag Travel Angles 18
Figure 17: Weld Sequence Used for Automated Build-up Without Interpass Cleaning 19
Figure 18: Cross Section of Automated FCAW Build-up Without Interpass Cleaning 20
Figure 19: Hardness Map of Automated FCAW Build-up Without Interpass Cleaning 20
Figure 20: Corner Bead Welding 21
Figure 21: Center Bead Welding 21
Figure 22: Cross Section of Automated FCAW Build-up with Interpass Cleaning and 15-Degree Drag Angle 23
Figure 23: Hardness Map of Automated FCAW Build-up 24
Figure 24: Cross Section of Automated RWF FCAW Build-up 26
Figure 25: Hardness Map of Automated RWF FCAW Build-up 26
Figure 26: Field-Repaired Frog 29
Figure 27: Breakout on Field-Repaired Frog 30
Figure 28: Cross Section of Repaired Area Showing Use of Stainless Steel in First Two Layers 30
Figure 29: RT of Repaired Area Showing Pores at the Edges Due to Contamination from Carbon Blocks 31

Figure 30: Frog After Removal of Damaged Material with Carbon Arc Gouging and Grinding 31
Figure 31: Cross Section of Repair-welded Point 32
Figure 32: Cross Section of Repair-welded Wing 32
Figure 33: Frog #1 Marked for Carbon Arc Gouging 33
Figure 34: Frog #2 Marked for Carbon Arc Gouging 34
Figure 35: Material Removal Illustration 34
Figure 36: Carbon Arc Gouging Process 35
Figure 37: Complete Carbon Arc Gouging 35
Figure 38: Frog #1 After Grinding 36
Figure 39: Frog #1 After Grinding 36
Figure 40: Frog #1 Wing Repair Welding Sequence 38
Figure 41: Frog #1 After Wing Repair 38
Figure 42: Frog #1 After Additional "Taper" Weld Build-up 39
Figure 43: Base Material Cracking in Frog #1 at Interface with "Transition" Build-up 40
Figure 44: Removal of Cracks from Frog #1 to Allow Repair Welding 40
Figure 45: Filling of Cracks in Frog #1 41
Figure 46: Frog #1 Crack-fill Welds Ground Smooth 41
Figure 47: Weld Build-up to Complete Frog #1 Crack Repair 42
Figure 48: Illustration of Frog #1 Point Repair Sequence 43
Figure 49: Crack Found in Point of Frog #1 43
Figure 50: Frog #2 Wing Repair Welding Sequence 44
Figure 51: Frog #2 After Wing Repair 44
Figure 52: Preparation of Frog #2 Transition Area 45
Figure 53: Layer 1 Welding of Frog #2 Transition Area 45
Figure 54: Frog #2 Repair Sequence 46
Figure 55: Point Running Surface Wear Along Length of Point 48
Figure 56: Running Surface Wear 32 inches Past Frog Point 48
Figure 57: Point Running Surface Wear 32 inches from Point at 0 and 100 MGT 49
Figure 58: Point Hardness 49
Figure 59: Running Surface Wear Along Length of Wing 50
Figure 60: Wing Running Surface Wear 8 inches Past Frog Point 50
Figure 61: Wing Running Surface Wear 8 inches from Point at 0 and 100 MGT 51
Figure 62: Wing Hardness 51

Figure 63: Combined Wing and Point Running Surface Wear 52
Figure 64: Point Running Surface Spalls 52
Figure 65: Ultrasonic Testing Scan Sample 53
Figure 66: Locations from which RT Specimens were Removed 54
Figure 67: RT Image of Field-Repaired Sample 54
Figure 68: RT Image of Wing Repaired with EWI's Automated FCAW Repair Technique 55
Figure 69: AMS Frog Casting Base Material Showing Multiple Voids 55
Figure 70: Weld Metal Showing Slag Inclusion 56
Figure 71: Horizontal Cracks Likely Due to Shear Loading (1) 56
Figure 72: Horizontal Cracks Likely Due to Shear Loading (2) 57
Figure 73: Crack in Base Material Adjacent to Weld Fusion Line 57
Figure 74: Slag Inclusion and Existing Base Material Crack 58
Figure 75: Surface and Sub-surface Cracking in Point 58
Figure 76: Close-up of Sub-surface Cracking in Point 59
Figure 77: Surface Spalling 32 inches from Point 59
Figure 78: Cracking Located on Corner of Point 60
Figure 79: Cross-section Taken 9.5 inches from Point 60
Figure 80: Cross-section Taken 32 inches from Point 61
Figure 81: Cross-section Taken 42 inches from Point 61
Figure 82: Cross-section Taken 8 inches from Wing 62
Figure 83: Cross-section Taken 19 inches from Wing 62
Figure 84: Point Hardness Map 9.5 inches from Point 63
Figure 85: Wing Hardness Map 8 inches from Point 63
Figure 86: Automated FCAW Repair Microstructure – Top Layer 64
Figure 87: Automated FCAW Repair Microstructure – Second Layer 65
Figure 88: Automation Concept with Robot Cart Retracted 66
Figure 89: Automation Concept Showing Deployed Robot Cart (View 1) 66
Figure 90: Automation Concept Showing Deployed Robot Cart (View 2) 67
Figure 91: Close-up View of Robot Cart 67
Figure 92: Top View of Automation Concept 68

Tables

Table 1: Average Million Gross Tons (MGTs) until Repair is Required 3
Table 2: Average MGTs until Repair is Required – Standard vs. High-Integrity Frogs 3
Table 3: Grinding Recommendations to Avoid Breakout and Minimize Repair 5
Table 4: Process Comparison Table 7
Table 5: Major Task Milestones 8
Table 6: Baseline Welding Parameters and Productivity Data 12
Table 7: Baseline SMAW Tensile Test Results 15
Table 8: Summary of Tensile Test Data 16
Table 9: Interpass Cleaning Investigation Welding Parameters 19
Table 10: Automated FCAW Corner Bead Parameter 22
Table 11: Automated FCAW Center Bead Parameter 22
Table 12: Tensile Test Results from Automated FCAW Build-up with Interpass Cleaning and 15-Degree Drag Angle 24
Table 13: Low Heat-input Automated RWF FCAW Parameters 25
Table 14: High Deposition-rate Automated RWF FCAW Parameters 25
Table 15: Tensile Test Results from Automated RWF FCAW Build-up 27
Table 16: Overview of Tensile Testing Results for All Build-ups from Task 1 and Task 2 27
Table 17: Process Comparison Summary 28
Table 18: Automated FCAW Corner Bead Parameter 28
Table 19: Comparison of All Tensile Testing Results 33
Table 20: Charpy V-notch Toughness Properties 33
Table 21: Test Frog Welding Parameters 37
Table 22: TTCI Frog Maintenance Record 47
Table 23: RT Inspection Summary 54
Table 24: Chemical Compositions of Automated FCAW Repaired Weld 64

Executive Summary

Special trackwork components, including austenitic manganese steel (AMS) turnout frogs, are safety-critical elements in railroad track. The turnout frogs' unique construction and functional requirements subject them to high impact forces and the wear rate of these components is much higher than normal running rail surfaces. Worn or damaged frogs in freight and shared corridors can have a detrimental effect on ride quality and increase life cycle costs. Current repair methods for railroad switch frogs effectively restore the running profile of the rail, but the repaired frogs do not have the same service life as new components. Improved repair processes that can extend the service life of frogs will improve the safety and efficiency of rail operations.

Welding AMS is challenging because it requires rapid cooling rates, low heat inputs, and minimal heating of the base material to retain the mechanical properties that cause high toughness and wear resistance. Manual or semi-automatic repair of AMS frogs is challenging due to an inherent conflict between stringent limits on interpass temperature, and the level of productivity that is required to minimize track downtime. Track time is often so limited that repairs cannot be properly completed within the time allotted. In these cases, only a portion of the frog can be repaired, and the resultant height mismatch leads to further operational damage before the repair can be completed. The common repair processes are shielded metal arc welding (SMAW) and semi-automatic self-shielded flux-cored arc welding (FCAW), which is manually applied. Special techniques are used to limit heat build-up.

In this project, EWI developed a new flux-cored arc welding (FCAW) procedure that can be used to repair manganese frogs. The goal was to determine if automating FCAW process variations can increase productivity, improve weld quality, and increase the durability of repairs.

Commonly, productivity and/or reduced heat input during welding is improved by mechanizing or automating the welding process using a solid electrode. Since a solid electrode is not commercially available for welding AMS components, a self-shielded FCAW electrode was used for this project. A shielding gas blend of 75 percent Argon/25 percent CO_2 was added to improve process stability. Welding trials were conducted in constant voltage (CV) mode with a conventional power supply and a specialized system, capable of welding in short-circuit mode with reciprocating wire feed, was added to further reduce heat input, improve process stability, and minimize spatter.

Implementation of automation reduced the calculated heat input by up to 64 percent compared to baseline manual SMAW and semi-automatic FCAW techniques. This reduction minimized heating of these components during welding, minimized downtime while components were allowed to cool, and minimized local temperature spikes adjacent to the deposited weld bead. Efficiency increased significantly. The time to complete a weld layer was reduced by 30 percent compared to semi-automatic FCAW, and over 75 percent compared to SMAW. The volume of material deposited per unit time increased by 200 to 270 percent over SMAW, and was equal to that of semi-automatic FCAW.

A repaired frog was tested by EWI in simulated revenue service conditions at the US Department of Transportation (DOT) Transportation Technology Center (TTC) from Spring 2014 through Fall 2014, and the test results showed a significant improvement in the durability of the repair compared to traditional repair methods. The test frog was subjected to over 118 Million Gross Tons (MGTs) of service, and was in serviceable condition at the end of the test. The service life of the test frog was 240 percent longer than the average life of repaired frogs, and 107 percent longer than the service life of new frogs. Subsequent laboratory testing confirmed that the automated technique yields a significant increase in weld quality compared to field-repaired samples and mock baseline samples. Future work plans are to include revenue service trials as well as weld procedure and material refinements.

1. Introduction

1.1 Background

Cast austenitic manganese steel (AMS) turnout frogs and crossing diamonds are among the shortest-lived track segments. A study reported that approximately 6,800 frogs are replaced yearly at a cost of approximately $120 million(1). It also stated that another $120 million is spent on frog maintenance each year. According to this study, the average life of these cast manganese components drops sharply after the first repair:

Table 1: Average Million Gross Tons (MGTs) before Repair(1)

Frog Type	New Component	1st Repair	2nd Repair	3rd Repair	4th Repair
Manganese Turnout	57	37	33	37	32
Manganese Diamond	47	33	30	23	35
Rail-constructed Turnout	58	55	52	52	52

Another study reviewed maintenance records from the former Chicago & North Western Powder River Subdivision between Horse Creek, Nebraska, and Shawnee Junction, Wyoming, to evaluate the service lives of standard #20 AMS frogs and "high-integrity" AMS frogs(2). This line carried almost exclusively 100- and 110-ton unit coal trains. High-integrity frog castings are required to meet more stringent standards of solidity, which is accomplished with improved casting techniques (such as improved mold designs with additional risers) and by using better sand binders. The results of this study are summarized in Table 2.

Table 2: Average MGTs until Repair is Required – Standard vs. High-Integrity Frogs

Frog Type	New Component	1st Repair	Subsequent Repairs
Standard Manganese Turnout	50	20	11
High-integrity Manganese Turnout	101	39	21

Both studies show that the majority of required repairs are caused by "breakouts" or cracks. Breakouts occur when the frog casting has not been sufficiently work-hardened and plastically deforms during the beginning of its service life. The damaged material often acts as the initiation point for cracks, and can lead to the break off of large areas of material during wheel contact. Breakouts occur in new frogs as well as weld-repaired frogs; however, the reduced initial hardness of repaired frogs results in more plastic deformation, making breakouts more prevalent. Examples of breakouts are provided in Figure 1 and Figure 2.

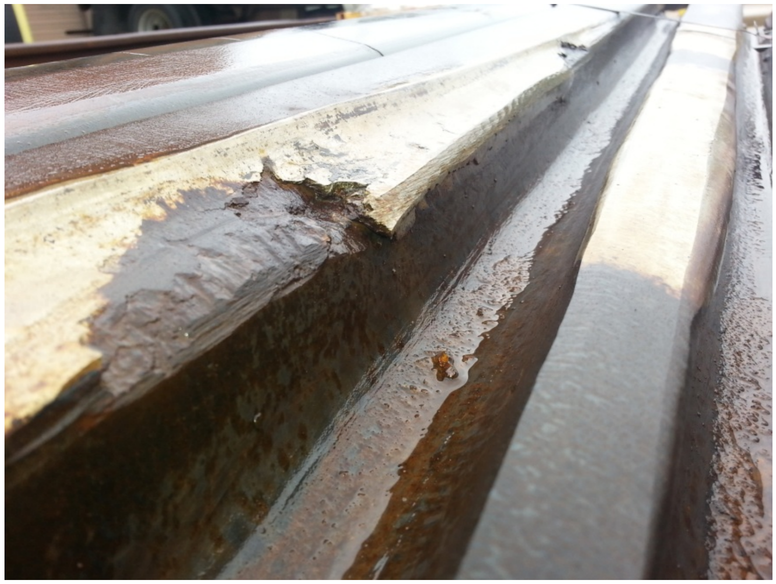

Figure 1: Breakout of Weld Repair

Figure 2: Breakout on Wing

Table 3 shows the composite frog-grinding recommendations from a survey of railroad maintenance policies. Due to track time limits, completing these procedures as recommended is challenging.

Table 3: Grinding Recommendations to Avoid Breakout and Minimize Repair

Frog Type	1st Grinding	2nd Grinding	3rd Grinding	Steady-state Interval
New AMS Frog	5 MGT	20 MGT	—	20 MGT
Repaired AMS Frog	1 Day	1 week	1 month	20 MGT

AMS has a high work-hardening capacity and resistance to wear, making it an ideal material for frogs. Though welding AMS is challenging due to temperature restrictions, it has advantageous properties when quickly cooled from welding temperatures (unlike high-carbon rail steel). Proper welding allows the wear surfaces to transform into a hard, tough structure through deformation twinning, particle precipitation, and phase change. American Welding Society (AWS) specification D15.2 states that the temperature measured 1 in (25 mm) from welding shall not exceed 500ºF (260ºC)[(3)]. Exceeding this temperature causes significant degradation of material properties, particularly the toughness and cracking resistance of hardened layers.

Repair processes for railroad manganese frogs commonly use shielded metal arc welding (SMAW) and self-shielded flux-cored arc welding (FCAW):

- SMAW employs an electrical arc between a consumable coated electrode and the base material. The molten pool is shielded by the gases created when the arc heat decomposes the electrode coating and by the slag covering that forms.
- Self-shielded FCAW uses an electrical arc between a continuously-fed cored consumable electrode and the base material. Decomposition of the electrode core produces gases and a coating to shield the weld pool.

In both processes, the slag covering must be removed via chipping or brushing to avoid slag inclusions, which negatively affect weld quality. To reduce heat build-up, both SMAW and FCAW processes call for special techniques to limit interpass temperature of AMS components, but this limits productivity.

To increase productivity and/or reduce heat input, the welding process can be mechanized or automated by using a solid electrode process known as gas metal arc welding (GMAW). GMAW is similar to FCAW because it uses an electrical arc between a continuously fed consumable electrode and the base material. Shielding gas is fed through a nozzle to shield the weld pool, and the solid electrode results in a more stable arc which can be operated in spray transition mode. This allows the use of higher currents, deposition rates and travel speeds compared to cored electrodes. Minimal interpass cleaning is required because slag coverings do not form. Solid electrodes depend on shielding gas for weld pool protection in drafty or windy environments, thus using GMAW can be problematic. This makes FCAW a common process of choice for outdoor work.

An FCAW electrode was used in all welding trials, since a solid electrode is not commercially available for welding AMS components. A 75 percent Argon/25 percent CO_2 shielding gas blend was added to improve process stability and reduce welding fumes. Welding trials were conducted in constant voltage (CV) mode with a conventional power supply and with a specialized power supply capable of welding in short circuiting mode with reciprocating wire feed to further reduce heat input, improve process stability, and minimize spatter.

1.2 Objectives

In this project, which took place from Spring 2014 through Fall 2014, AMS frogs were repaired with arc welding techniques or automated FCAW solutions and the capabilities of both solutions were compared against each other. Automated processes provide quality control and increase the deposition rate of the repair process, which results in a more durable repair. Automation also increases overall productivity, and may reduce the track time required to complete repair of a worn or damaged frog.

1.3 Overall Approach

EWI produced baseline welding samples using current industry repair techniques on "mock-ups" created to model the point of a #20 frog. EWI deposited multi-layer weld build-ups on these mock-ups using manual SMAW and semi-automatic FCAW; the completed build-ups were evaluated with radiographic testing, mechanical testing, and by examining cross sections.

EWI then automated the FCAW process and the reciprocating wire feed (RWF) FCAW process, which is a variation of the FCAW process where the wire motion is synchronized with a current waveform. EWI developed weld parameters using both FCAW process variations. These efforts were designed to improve weld quality and productivity while keeping the temperature of the base material below 500°F at a distance of 1 in from the weld. Welds were evaluated by EWI with radiographic testing (RT), tensile testing, and hardness mapping. Table 4 is a process comparison table summarizing baseline welding processes as well as both automated FCAW variations.

Table 4: Process Comparison Table

Process	Description	Advantages	Disadvantages
SMAW	- Uses "stick" electrodes - Manually applied - Decomposition of electrode coating producing gasses and slag to shield the weld puddle	- Inexpensive equipment - Welder familiarity - Works well in drafty environments	- High skill level required - High fume levels - Electrodes must be changed often, resulting in many starts/stops - Low deposition rate, resulting in low productivity
Semi-automatic FCAW	- Continuously fed cored electrode - Welding torch is manually manipulated - Decomposition of electrode coating producing gasses and slag to shield the weld puddle	- Increased deposition rate compared to SMAW - Less skill required than SMAW - Works well in drafty environments - Fewer starts/stops than SMAW - Lower heat input than SMAW	- High fume levels - Limited visibility of welding puddle - Equipment is more complex and expensive than SMAW
Automated FCAW	- Continuously fed cored electrode - Torch manipulation is automated - Decomposition of electrode coating producing gasses and slag to shield the weld puddle - In this project EWI used shielding gas to improve arc stability and reduce welding fume	- Highest deposition rate - Less skill required than SMAW and SA FCAW - Works well in drafty environments - Fewer starts/stops than SMAW - Improved welding consistency - The use of shielding gas reduces fume levels and improved visibility - Lower heat input than SA FCAW	- Welding equipment is more complex/ expensive than SMAW - Less flexibility than manual/semi-automatic processes (programming is required)
RWF FCAW	- Continuously fed cored electrode - Torch manipulation is automated - Electrode feed is synchronized with a specialized current waveform - Minimal spatter - Decomposition of electrode coating producing gasses and slag to shield the weld puddle - In this project EWI used shielding gas to improve arc stability and reduce welding fume	- Less skill required than SMAW and SA FCAW - Works well in drafty environments - Fewer starts/stops than SMAW - Improved welding consistency - The use of shielding gas reduces fume levels and improved visibility - Minimal spatter is produced - Lowest heat input level	- Welding equipment is more complex and expensive than SMAW and FCAW - Less flexibility than manual/semi-automatic processes (programming is required) - Slightly lower deposition rate than automated FCAW

EWI contracted with the Transportation Technology Center, Inc., (TTCI) to support the project with worn frogs for testing and to provide testing services at its center, TTC. EWI selected automated FCAW to repair a full-sized frog for testing, and developed the welding sequence on a partial frog section provided by TTCI. The frog was prepared in a manner representative of repairs in the field. EWI duplicated this approach on two full-length frogs and shipped them to TTCI.

TTCI performed the required finish grinding. A crack was found in the base material of the point of Frog #1. Although EWI developed a procedure capable of successfully repairing the crack, Frog #1 was not repaired due to budget and scheduling limitations. Frog #2 was ground to shape and placed in TTCI's test track for evaluation. Maintenance grinding was performed when necessary, and the frog was monitored via periodic hardness and profile measurements. Following the tests at TTCI, the frog was returned to EWI for scientific evaluation.

1.4 Scope

Major task milestones are listed in Table 5. All work was performed by EWI and TTCI, in accordance with the work breakdown structure in Figure 3.

Table 5: Major Task Milestones

WBS No.	Task Description	Milestone Completion Week
1	**Process Baseline Study/Procurement of Hardware**	**16**
1.1	Kick-off meeting at EWI	2
1.2	Procure AMS Samples	6
1.3	Procure AMS Frogs	10
1.3	Metallurgical Evaluations	14
1.4	Preliminary Report	16
2	**Automated Repair of AMS Frogs Using FCAW**	**62**
2.1	Automated FCAW Procedures Developed	22
2.2	Controlled Short Circuit FCAW Procedures Developed	36
2.3	Evaluation of Frogs at TTCI Complete	60
2.4	FCAW Automation Concepts Complete	66
3	**Reporting/Outreach**	**70**
3.1	Present at FRA Research Review	36
3.2	Present at Conference	54
3.3	Deliver Final Report	70
4	**Project Management**	**70**

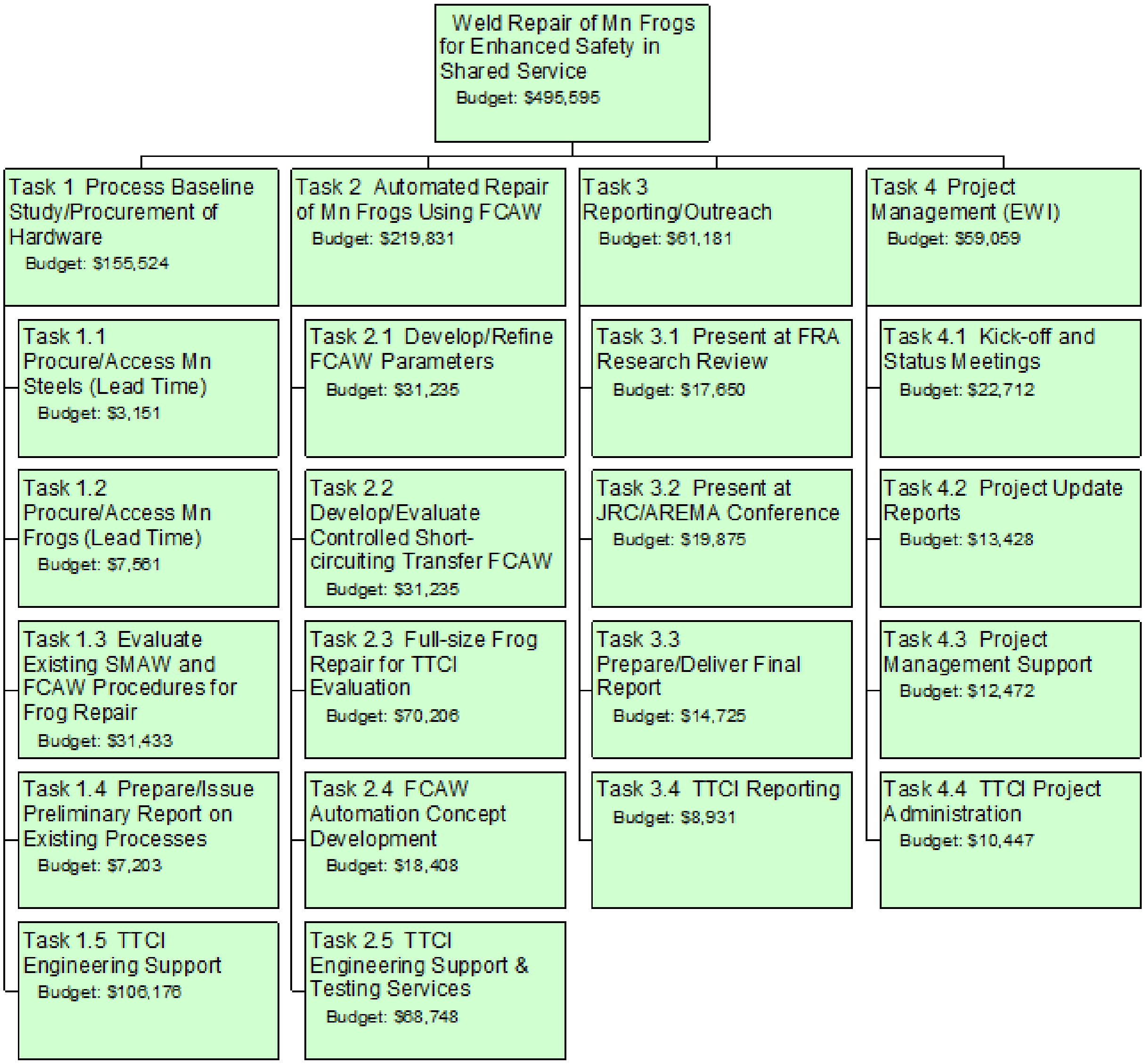

Figure 3: Work Breakdown Structure

2. Task 1 − Process Baseline Study

2.1 Objectives and Approach

In Task 1, EWI procured the required base materials and consumables to conduct welding trials, and created baseline samples with current welding processes and techniques (SMAW and semi-automatic FCAW). EWI searched the literature for an approach to creating baseline samples that represented welding completed in the field.[3-8] Based on the recommendations of AWS D15.2, railroad-supplied maintenance handbooks, and select articles, EWI conducted welding in short-circuiting transfer mode using a 35 to 50° (push) travel angle. Bead width and length were limited to 5/8 and 5.0 in, respectively.

EWI used bead sequencing to control the distribution of heat within the frog. "Skipping" sequences can effectively spread the heat from welding and prevent a relatively small area from becoming overheated. Bead sequencing also ensures adequate weld fusion by ensuring that multiple arc starts are not located adjacent to one another. This is important, as lack-of-fusion defects are most common at the start of a weld, where the welding arc has not sufficiently preheated the base material. Industry-recommended techniques included starting at the point (narrow section) and welding toward the heel (broad section), staggering weld craters, and avoiding side-by-side beads when possible. EWI filled weld craters by reversing the welding direction for approximately 0.5 in and welding back into the bead. All layers aside from the first and last were peened with a hammer to alleviate residual stresses and prevent cracking defects from forming. The maximum allowed interpass temperature was 500°F measured 1 in from the weld.

EWI cut mock-ups out of 2-in thick AMS plate to represent the geometry of a #20 frog point and welded them to a carbon-steel baseplate using 308 stainless steel electrodes (Figure 4 through Figure 6). EWI deposited multi-layer build-ups on the mock-up points to simulate repair of a worn frog point. A minimum height of 5/8 in was deposited to provide a sufficient amount of weld metal for non-destructive and mechanical testing. EWI measured the surface temperature 1 in from the weld using a contact temperature probe immediately after the termination of the welding arc to determine the maximum temperature reached by the adjacent base material during welding.

2.2 Baseline Welding

Welding parameters and productivity data are summarized in Table 6. Baseline welds created with SMAW and self-shielded FCAW were allowed to cool below 250°F between weld beads and below 100°F between layers.

2.3 Evaluation of Baseline Welds

EWI compared the weld quality and resultant mechanical properties of baseline welds to the automated FCAW and RWF FCAW welds to be produced in Task 2. RT, hardness mapping, and all-weld-metal tensile testing were performed.

Figure 4: #20 Point Mock-up

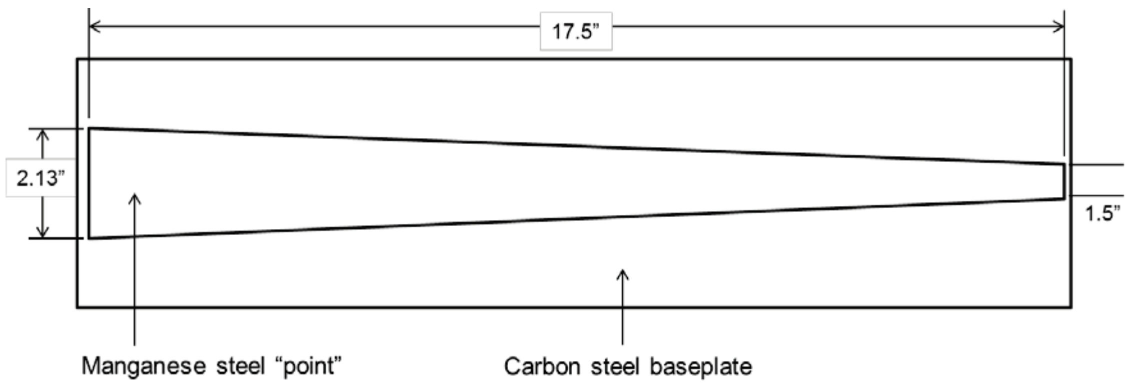

Figure 5: Top View of #20 Point Mock-up Geometry

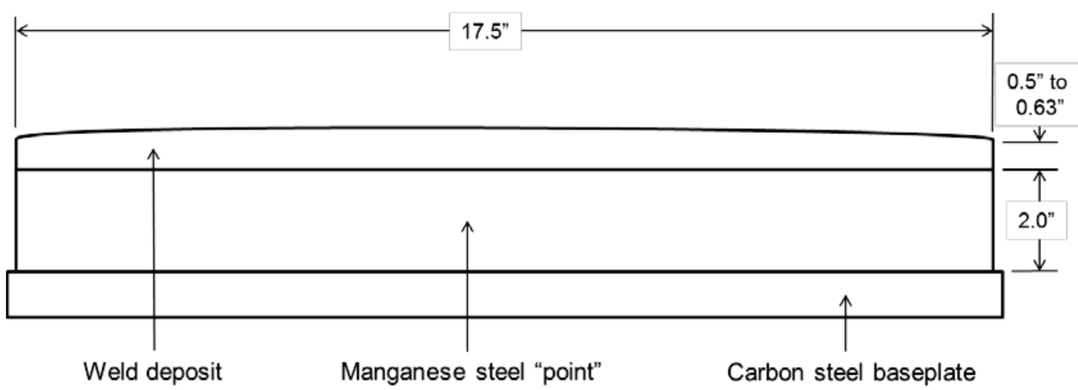

Figure 6: Side View of #20 Point Mock-up Geometry

Table 6: Baseline Welding Parameters and Productivity Data

Process	Electrode Diameter (in.)	Current (A)	Voltage (V)	Travel Speed (ipm)	Heat Input (kJ/in.)	Deposition Rate (lbs/hr.)	Time per Layer (min.)	Thickness per Layer (in.)
SMAW	5/32	180	24	4 to 6	45 to 65	3	20	0.045
FCAW	1/16	200	27	6	60	7 to 8	6.1	0.086

The cross section provided in Figure 7 shows two vertical cracks. RT of the completed baseline manual FCAW mock build-up revealed scattered porosity, which can be seen in the cross-section provided in Figure 8.

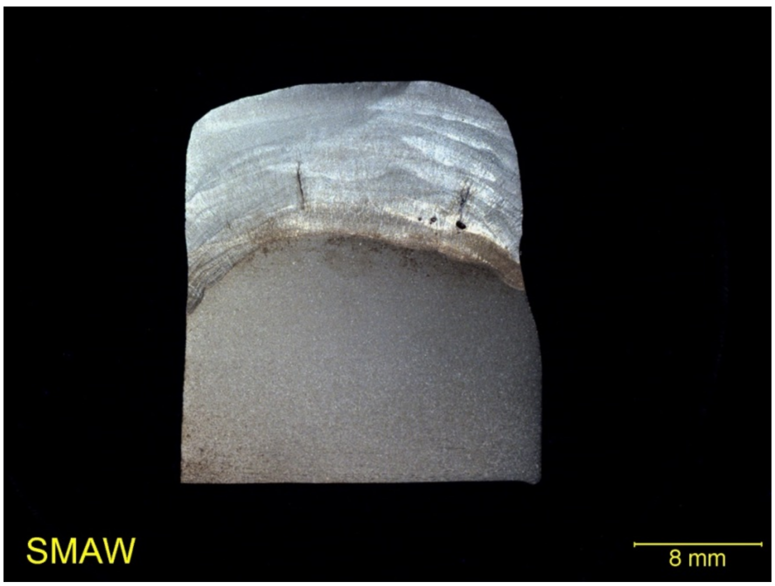

Figure 7: Baseline SMAW Cross Section

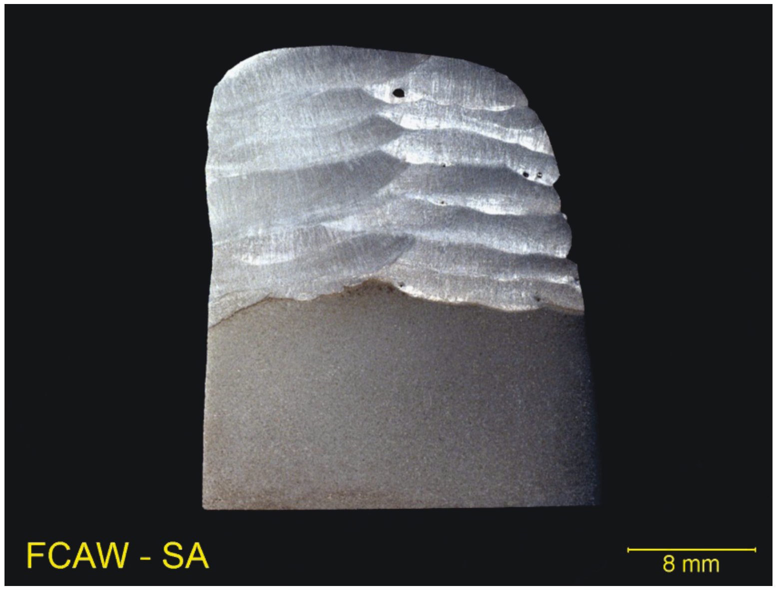

Figure 8: Baseline FCAW Cross Section

The baseline SMAW hardness map provided in Figure 9 has a weld metal hardness range of 230 to 300 Brinell, while the hardness map of the FCAW cross section provided in Figure 10 shows weld metal hardness of 220 to 300 Brinell. Data from both samples indicate that the heat from welding resulted in hardening well below the visible heat-affected zone (HAZ). AWS D15.2 states that for the grade of AMS typically used for trackwork, hardness can range from 185 to 210 Brinell in the as-cast condition, but can increase to a maximum of 550 Brinell after the work-hardening that occurs during normal operation.

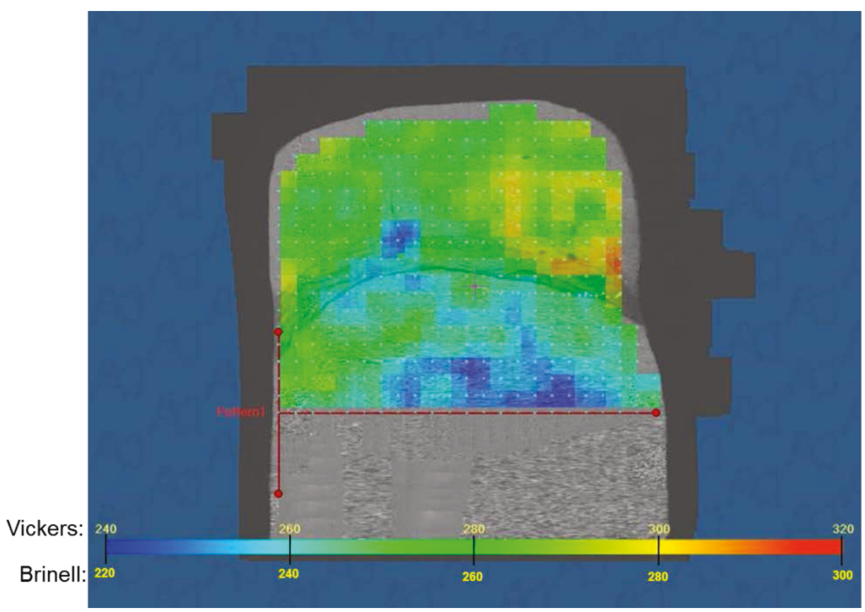

Figure 9: Baseline SMAW Hardness Map

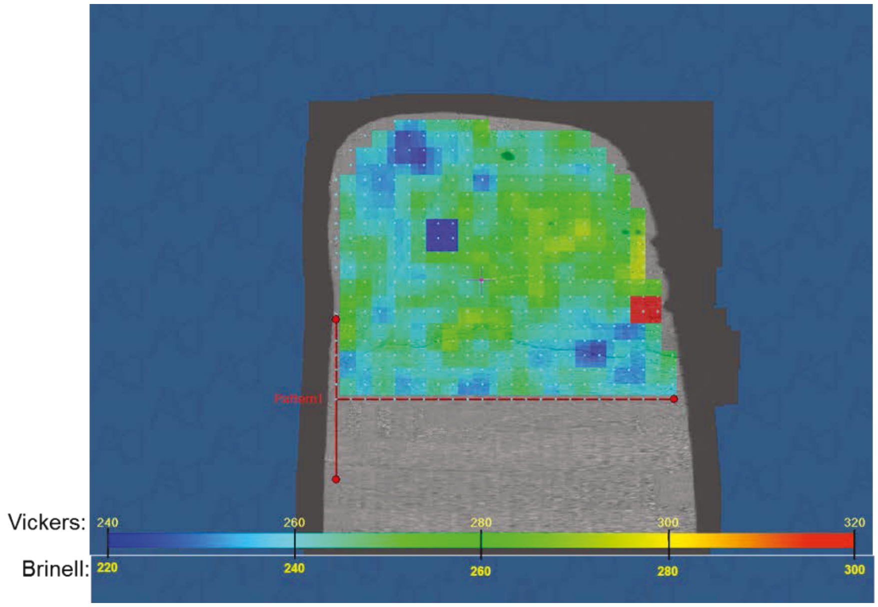

Figure 10: Baseline FCAW Hardness Map

EWI used all-weld-metal tensile specimens to determine yield strength (YS) and ultimate tensile strength (UTS) (Figure 11). Sub-sized samples were used to ensure that no base material was included in the reduced section of the tensile while the number of required passes was limited. The locations from which tensile samples were removed from the build-ups are illustrated in Figure 12, and the results of tensile testing are provided in Table 7.

Figure 11: Tested Sub-sized Tensile Samples

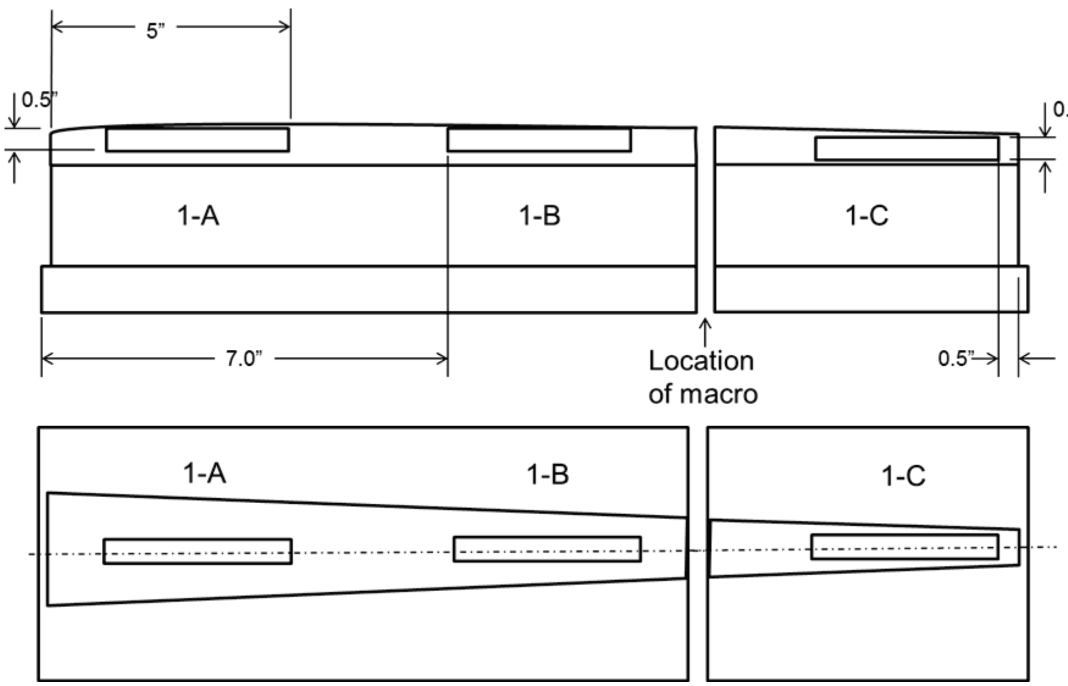

Figure 12: Tensile Specimen Locations

Table 7: Baseline SMAW Tensile Test Results

Specimen I.D.	Specimen Diameter		Test Temperature		Ultimate Strength		0.2% Yield Strength		Elongation	Area Reduction
	(mm)	(in)	(°C)	(°F)	(MPa)	(ksi)	(MPa)	(ksi)	(%)	(%)
SAW-A	8.99	0.354	24	75.2	821.4	119.1	609.0	88.3	15.4	25.8
SAW-B	8.94	0.352	24	75.2	789.0	114.4	562.8	81.6	17.3	11.0
SAW-C	8.94	0.352	24	75.2	801.4	116.2	552.4	80.1	17.2	23.9
FCAW-A	8.94	0.352	24	75.2	618.6	89.7	501.4	72.7	13.0	35.4
FCAW-B	8.94	0.352	24	75.2	695.2	100.8	506.2	73.4	17.9	30.7
FCAW-C	8.94	0.352	24	75.2	671.7	97.4	520.7	75.5	12.9	18.4

A summary of this data is provided in Table 8, along with typical tensile and YS ranges provided in AWS D15.2. While the ultimate strength (UTS) of the SMAW mock build-up was within the range for the grade of AMS typically used for special trackwork specified by AWS D15.2, the yield strength (YS) is significantly higher. The average UTS of the FCAW mock build-up is below the range for the grade of AMS that is typically used for trackwork; however, the YS was above the range. The higher average YS of both baseline samples may reduce plastic deformation. Since the majority of AMS frog repairs are due to damage that occurs when plastically deformed material is torn off, this has the potential to positively impact overall durability while reducing required grinding.

Table 8: Summary of Tensile Test Data

Material Property	AWS D15.2 Range (ksi)	SMAW Baseline Average (ksi)	FCAW Baseline Average (ksi)
YS	50 - 57	83.3	73.87
UTS	100 - 145	116.57	95.97

2.4 Interpass Temperature Trials

EWI conducted trials to determine how weld sequence and bead length affected the interpass temperature of mock-up samples. EWI kept all other welding variables (current, voltage, travel speed, and travel angle) constant, and evaluated three sequences using SMAW. Mock-ups were welded with minimal delay between passes to represent a worst-case scenario regarding overheating of the base material.

The baseline weld sequence employed the same welding parameters and guidelines used in baseline SMAW trials. EWI removed slag via wire brushing and performed peening after each weld pass. Subsequent weld passes were then deposited without delay. As shown by the color-coding in Figure 13, the temperature exceeded 500°F in six of the eleven deposited weld beads, and in one of these beads, exceeded 600°F.

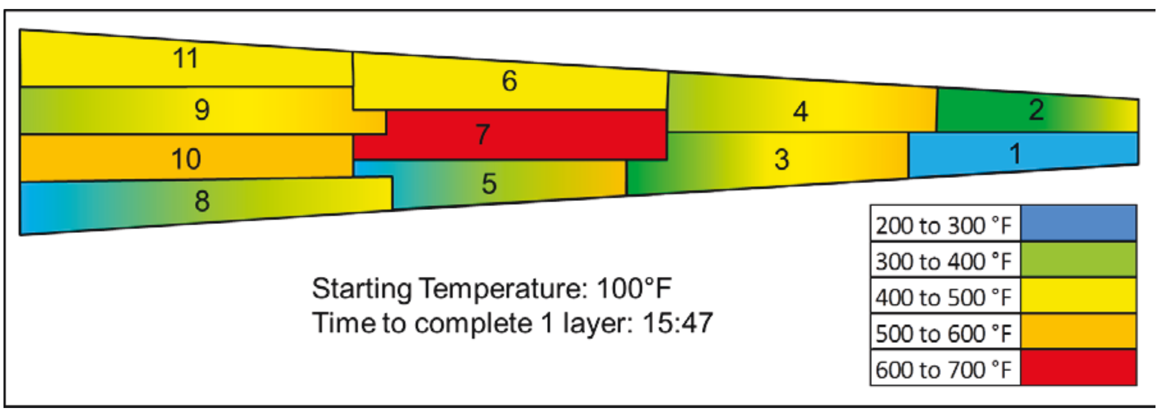

Figure 13: Industry-Recommended Weld Sequence

EWI evaluated a second weld sequence which used an alternate intermittent welding sequence in an attempt to avoid heat build-up; however, the temperature exceeded 500°F in four of the fifteen deposited weld beads, and in three of these beads, exceeded 600°F (Figure 14).

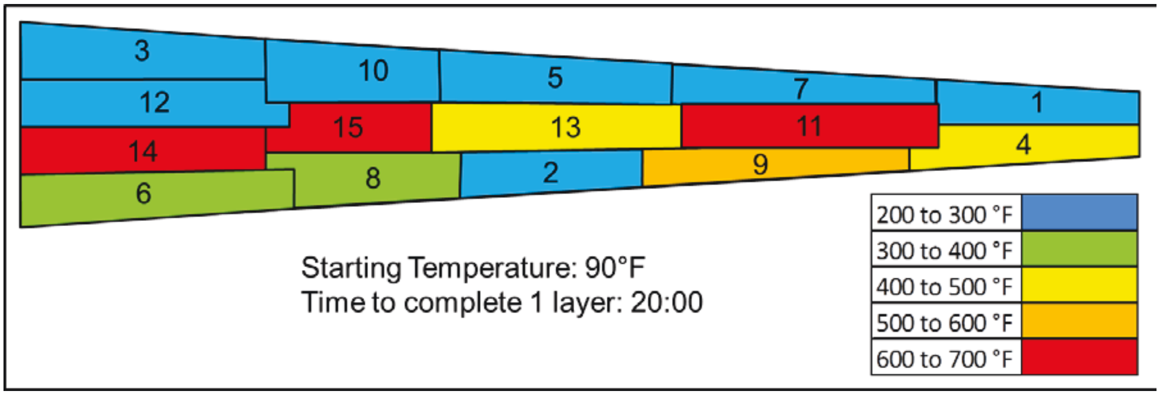

Figure 14: Alternate Weld Sequence 2

A third weld sequence used longer welds and a diagonal placement pattern for the first three weld beads (Figure 15). The temperature did not exceed 500°F in any of the five beads, which reveals the impact that weld sequencing can have on heat build-up. Based on these findings, the team's subsequent FCAW development used a welding sequence with long, continuous beads at a high travel speed to decrease heat input and minimize heat build-up in the component.

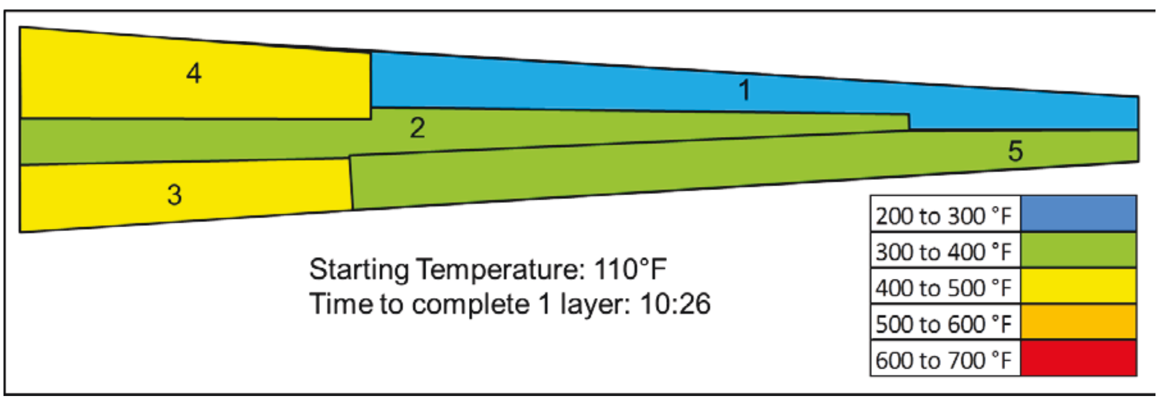

Figure 15: Alternate Weld Sequence 3

3. Task 2 – Automated Repair of Manganese Frogs Using FCAW

3.1 Automated FCAW Welding Trials

EWI developed automated FCAW parameters by performing a series of welding trials. These trials had the following goals:

- Evaluate the need for interpass cleaning
- Determine the effect of travel angle on weld quality
- Develop welding parameters to avoid corner roll-off
- Create a mock build-up
- Test the mock build-up with RT, hardness mapping, and mechanical testing

EWI conducted all automated FCAW trials using a 6-axis welding robot with a 0.045-in self-shielded FCAW electrode. A shielding gas mix of 75 percent Argon and 25 percent CO_2 was used to improve arc stability, decrease fume generation, and improve visibility. Figure 16 illustrates the difference between push (+) and drag (-) travel angles.

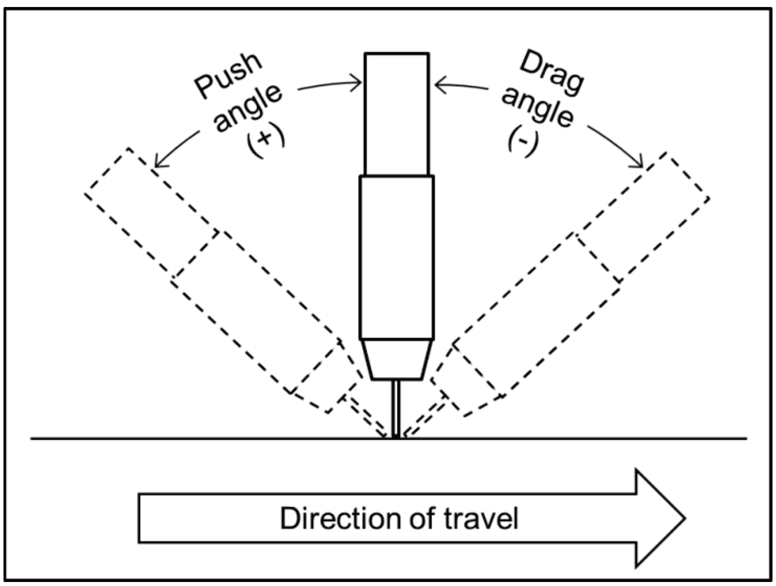

Figure 16: Illustration of Push and Drag Travel Angles

3.1.1 Interpass Cleaning Investigation

In FCAW, the molten weld pool is protected by a slag coating. This coating is typically chipped or brushed off after each individual weld bead to prevent slag inclusions. While automated brush cleaning systems are commercially available and could be integrated into a final automated solution, minimizing inter-bead cleaning requirements is important because it would allow a less complex system to make repair welds in the field. EWI created a mock build-up removing slag only upon completion of each layer to determine the viability of this approach. Subsequent passes in a given layer were completed without delay, weld beads were not peened, and slag was removed only upon the completion of each multi-bead layer. The build-up was welded one layer at a time and allowed to cool to approximately 100°F before welding of the subsequent layer began. The welding parameters and welding sequence are provided in Table 9 and Figure 17, respectively.

Table 9: Interpass Cleaning Investigation Welding Parameters

Current (A)	200
Voltage (V)	30
Travel Speed (ipm)	20
Deposition rate (lbs/hr)	7 to 8
Heat Input (kJ/in)	18
Travel Angle (°)	15

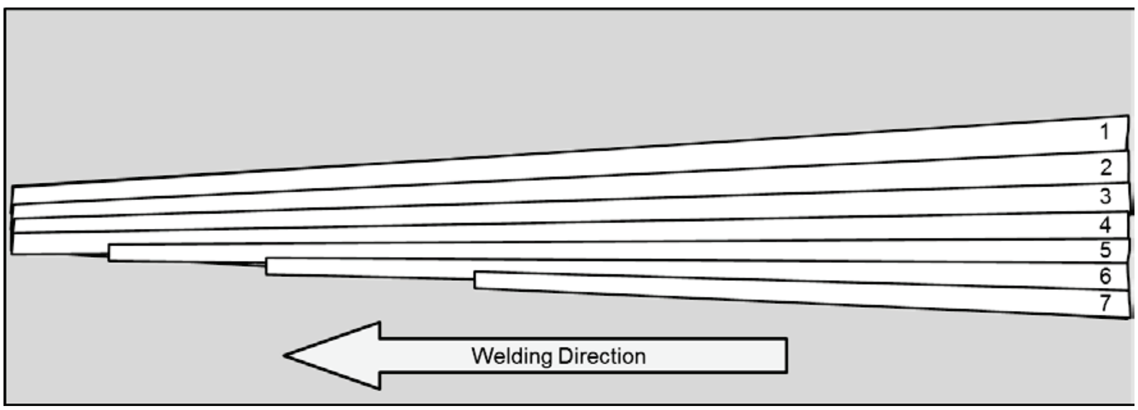

Figure 17: Weld Sequence Used for Automated Build-up Without Interpass Cleaning

EWI evaluated the build-up using RT. Linear slag inclusions were found throughout, which indicated a need for interpass cleaning. The photo-macrograph of a cross section (provided in Figure 18) shows adequate penetration and fusion with the base material and previously deposited weld beads; however, a large slag inclusion is visible in the center of the build-up. The hardness matrix provided in Figure 19 indicates that the hardness of the weld metal ranged from 230 to 300 Brinell, and hardness data from the base metal indicates that the heat from welding resulted in hardening well below the visible HAZ. Due to the number of slag inclusions found, EWI did not perform tensile testing.

Figure 18: Cross Section of Automated FCAW Build-up Without Interpass Cleaning

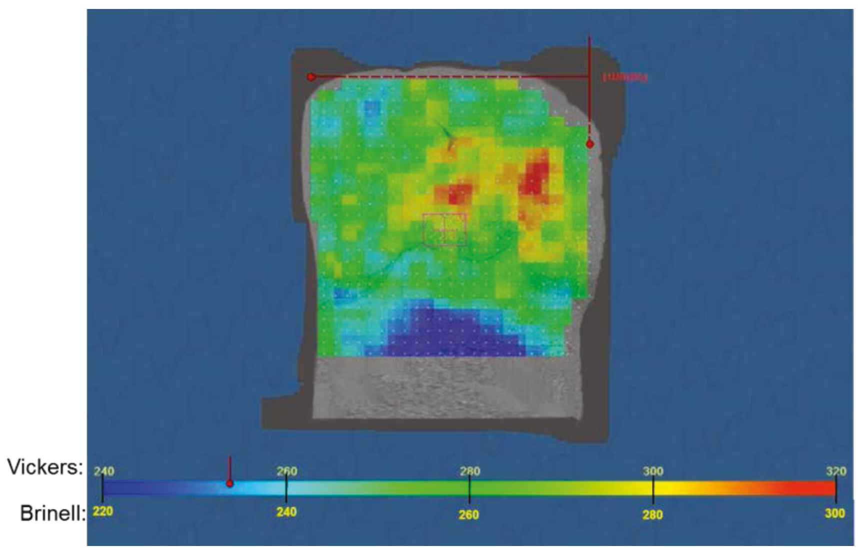

Figure 19: Hardness Map of Automated FCAW Build-up Without Interpass Cleaning

3.1.2 Effect of Travel Angle on Weld Quality

EWI created another mock build-up with interpass cleaning using a "+15-degree" travel angle and examined it with RT. While the number of slag inclusions was reduced, they were not eliminated. EWI welded another mock build-up with a "-15 degree" angle to evaluate whether slag inclusions could be further reduced or eliminated by directing the arc force and molten slag backwards. This technique avoids "running over" the slag and trapping it at the bottom of the weld bead. The RT examination revealed a significant reduction in slag inclusions. As a result, a drag angle was used in all subsequent welds.

3.1.3 Automated FCAW Welding Parameter Development

When a frog is repaired, weld beads must be deposited on the corner of the point as well as in the middle. These two scenarios present different welding challenges. As illustrated in Figure 20, welds placed on the corner of the point are at risk of "drooping" due to the force of gravity. After the two corner beads are deposited, center beads can be deposited without fear of drooping (Figure 21). In this case, a higher heat input parameter can be used for increased productivity.

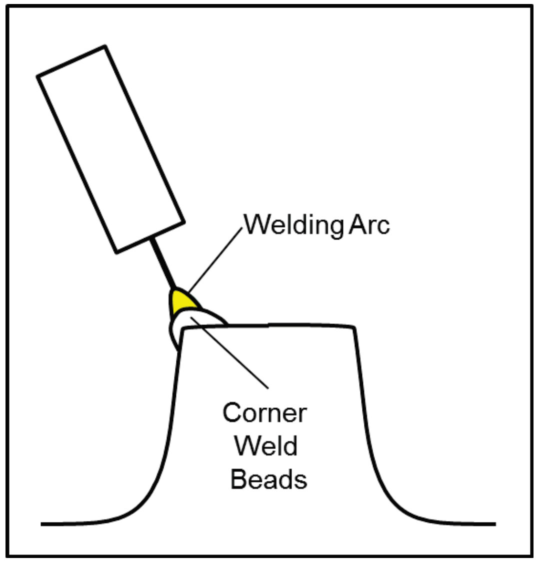

Figure 20: Corner Bead Welding

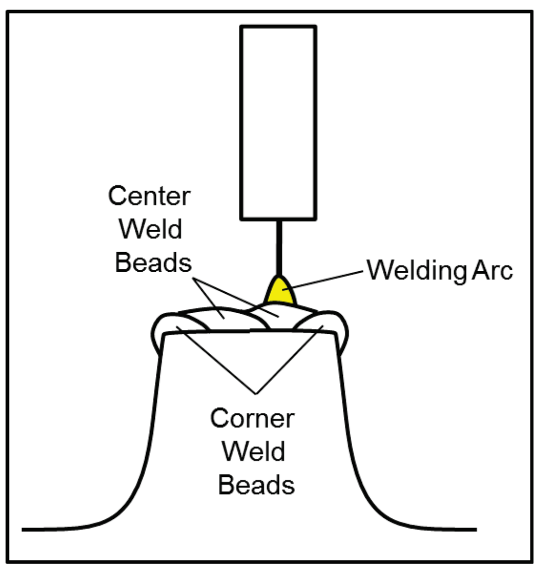

Figure 21: Center Bead Welding

EWI developed two welding parameter sets to address these different scenarios. A lower heat-input parameter was developed to allow weld beads to be deposited on a corner without drooping (Table 10). EWI developed a higher heat input parameter for use on center beads to create a flat weld bead that allows for adequate tie-in when welding in the middle of the mock-up, and provides adequate heat to reduce slag inclusions (Table 11).

Table 10: Automated FCAW Corner Bead Parameter

Current (A)	140
Voltage (V)	21
Travel Speed (ipm)	15
Deposition rate (lbs/hr)	6
Heat Input (kJ/in)	12
Travel Angle (°)	-15

Table 11: Automated FCAW Center Bead Parameter

Current (A)	200
Voltage (V)	28
Travel Speed (ipm)	15
Deposition rate (lbs/hr)	10
Heat Input (kJ/in)	23.5
Travel Angle (°)	-15

3.1.4 Automated FCAW Mock Build-up Creation and Testing

EWI created a build-up using the parameters described above. The photo-macrograph of a cross-section (provided in Figure 22) shows adequate penetration and fusion with the base material and previously deposited weld beads.

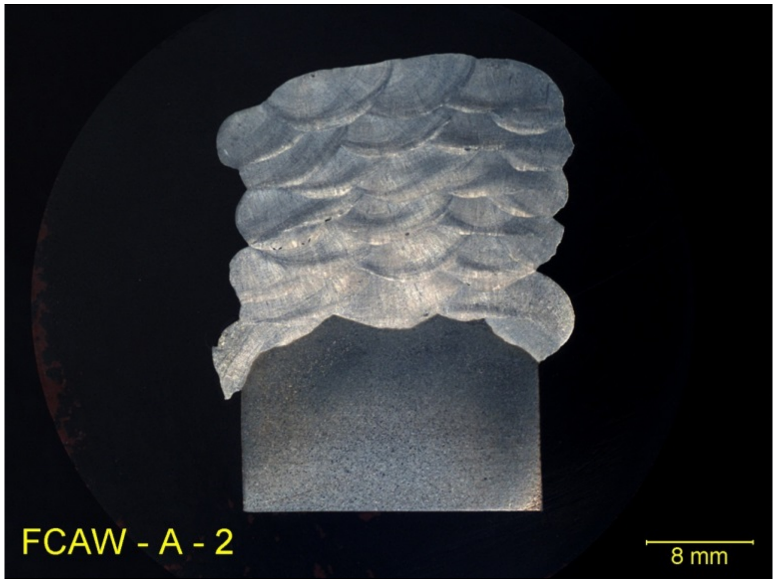

Figure 22: Cross Section of Automated FCAW Build-up with Interpass Cleaning and 15-Degree Drag Angle

EWI performed an RT inspection of the automated FCAW mock build-up. The number of slag inclusions found in the mock build-up was significantly less than in previous automated FCAW build-ups and no porosity was observed. The hardness matrix provided in Figure 23 indicates that the hardness of the weld metal ranged from 250 to 320 Brinell, with hardening below the visible HAZ. The area of higher hardness in the center suggests higher core temperatures during welding, which may be due to the fact that minimal time elapsed between welding passes (since the surface temperature did not exceed the limit of 500°F).

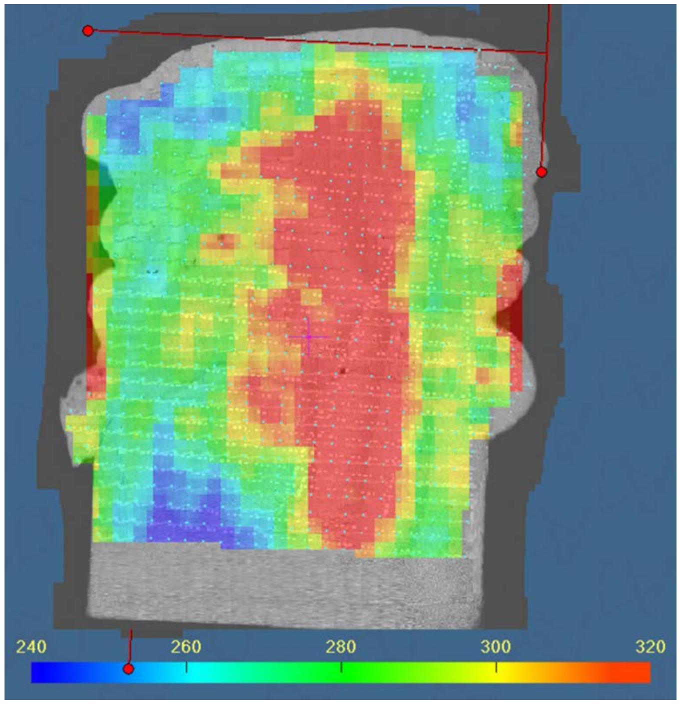

Figure 23: Hardness Map of Automated FCAW Build-up

Tensile testing results are provided in Table 12. The reported tensile strengths are within the AWS-supplied range for as-cast AMS components, and are similar to the baseline SMAW data. The higher average YS may reduce plastic deformation and positively impact overall durability while reducing the grinding required.

Table 12: Tensile Test Results from Automated FCAW Build-up with Interpass Cleaning and 15-Degree Drag Angle

Specimen Identification	Specimen Diameter		Test Temperature		Ultimate Strength		0.2% Yield Strength		Elongation	Reduction of Area
	(mm)	(in)	(^oC)	(^oF)	(MPa)	(ksi)	(MPa)	(ksi)	(%)	(%)
4-A	8.92	0.351	23	73	860.7	124.8	575.2	83.4	25.4	12.7
4-B	8.94	0.352	23	73	866.9	125.7	569.0	82.5	24.1	14.8
4-C	8.86	0.349	23	73	855.9	124.1	575.9	83.5	25.3	17.0

3.2 Reciprocating Wire Feed (RWF) FCAW Trials

RWF GMAW is a variation of the GMAW process in which the wire motion is synchronized with a current waveform. When the electrode is being fed toward the weld pool, the current is at its peak and a ball is formed at its end. When the electrode contacts the weld pool, the current is decreased, and the ball detaches due to the combination of surface tension forces and retraction of the wire. Since no electrical shorting occurs, minimal spatter is produced. Another advantage of RWF GMAW is that it can be operated at low voltages, which results in low heat input levels. Although the process is designed to be used with a solid electrode, EWI combined it with the previously evaluated commercially available flux cored electrode as a method of decreasing heat input and improving process consistency. Per AWS, the use of a flux-cored electrode in place of a solid electrode necessitates a process designation change from GMAW to FCAW. As a result, this EWI-modified process is herein referred to as RWF FCAW.

3.2.1 FCAW Welding Parameter Development

EWI conducted parameter development trials using a 0.045-in diameter electrode and 75 percent Argon/25 percent CO_2 shielding gas. A 15-degree drag angle was used to improve arc stability and decrease the risk of slag entrapment in the weld. EWI developed two welding parameter sets. The lower heat input parameter is shown in Table 13, and the higher heat input parameter set is shown in Table 14. A weave was added to the higher heat input parameter set to promote improved wetting and tie-in. This parameter set was designed to create a flat weld bead that reduced slag inclusions and allowed for adequate tie-in when welding in the middle of the mock-up.

Table 13: Low Heat-input Automated RWF FCAW Parameters

Current (A)	150
Voltage (V)	17.5
Travel Speed (ipm)	24
Heat Input (kJ/in)	7
Travel Angle (°)	-15

Table 14: High Deposition-rate Automated RWF FCAW Parameters

Current (A)	195
Voltage (V)	18.5
Travel Speed (ipm)	13
Heat Input (kJ/in)	15.7
Travel Angle (°)	-15

3.2.2 FCAW Mock Build-up Creation and Testing

EWI created a build-up and evaluated it using RT. As they did in the automated FCAW build-up, EWI used the lower heat input parameters on the corners and the higher heat input parameters in the center. No porosity was found; however, more slag inclusions were found than in the build-up generated by automated FCAW. The photo-macrograph of the cross section in Figure 24 shows adequate penetration and fusion with the base material and previously deposited weld beads.

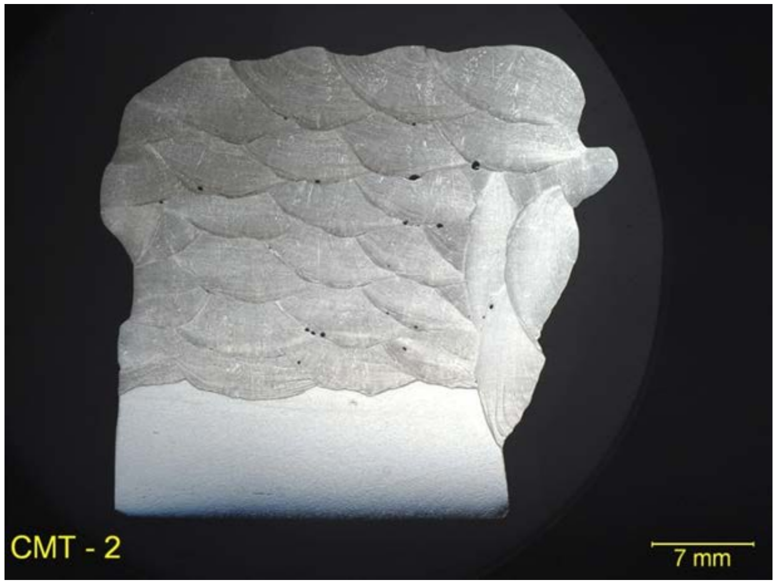

Figure 24: Cross Section of Automated RWF FCAW Build-up

The hardness matrix (see Figure 25) indicates that the hardness of the weld metal ranges from 250 to 320 Brinell. This hardness matrix is dissimilar from Figure 23, in that areas of peak hardness are spread throughout the cross section. The beads on the right side, which were primarily low heat input beads, have lower hardness. Tensile testing results are provided in Table 15. The reported tensile strengths are within AWS-supplied range for as-cast AMS components and are similar to the baseline SMAW data. The higher average YS may reduce plastic deformation with the potential to positively impact overall durability while reducing required grinding.

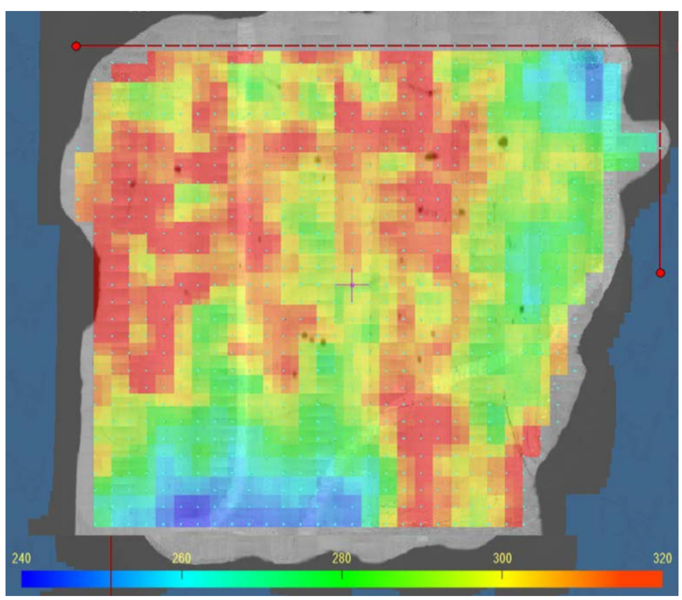

Figure 25: Hardness Map of Automated RWF FCAW Build-up

Table 15: Tensile Test Results from Automated RWF FCAW Build-up

Specimen Identification	Specimen Diameter		Test Temperature		Ultimate Strength		0.2% Yield Strength		Elongation	Reduction of Area
	(mm)	(in)	(^oC)	(^oF)	(MPa)	(ksi)	(MPa)	(ksi)	(%)	(%)
5A	8.94	0.352	24	75	846.2	122.7	584.8	84.8	20.9	13.7
5B	8.94	0.352	24	75	816.6	118.4	597.2	86.6	17.4	15.3
5C	8.94	0.352	24	75	839.3	121.7	589.7	85.5	20.3	16.8

3.3 Baseline Testing and Automated FCAW Development Overview

Table 16 compares tensile testing from baseline mock build-ups created in Task 1 to the FCAW-A and RWF FCAW mock build-ups created in Task 2.

Table 16: Overview of Tensile Testing Results for All Build-ups from Task 1 and Task 2

Property	Typical Casting Properties	Mock-up Material	Baseline SMAW	Baseline SA FCAW	FCAW-A	RWF FCAW
Tensile Strength (ksi)	100 to 145	142	117	96	125	121
Yield Strength (ksi)	50 to 57	59	83	74	83	86

Table 17 summarizes the welding processes. For the purposes of this overview, productivity is rated by considering both deposition rate and the required interpass cooling time. For a given deposition rate, processes with a shorter interpass cooling time are considered to have a higher productivity than those with longer interpass cooling times. In the chart provided, the degree to which the ball is colored in black represents the rating for that category. A ball with a quarter colored black represents the lowest rating, while a ball that is completely black represents the highest rating.

Based on Table 17 and the testing results, automated FCAW was selected for all subsequent welding. A final automated FCAW procedure summary is provided in Table 18.

Table 17: Process Comparison Summary

Process	Heat Input	Deposition Rate	Weld Quality	Productivity	Yield Strength*	Tensile Strength	Average
Base Material (non-cast)	N/A	N/A	N/A	N/A	◑	●	●
Shielded Metal Arc Welding (SMAW)	◑	◔	◔	◔	●	●	◑
Flux Cored Arc Welding (FCAW)	◔	●	◕	◑	◕	◕	◕
Automated FCAW	◕	◕	●	●	●	●	●
Reciprocating Wire Feed Speed FCAW	●	◑	◑	◕	●	●	◕

*Yield strength ranking based on assumption that higher yield will result on decreased flow without a reduction in toughness

Table 18: Automated FCAW Corner Bead Parameter

Automated FCAW	
Common Parameters	
Electrode Diameter (in)	0.045
Electrode Type	Flux-cored
Polarity	Direct Current, Electrode Positive
Shielding Gas	75 percent Argon/25 percent CO_2
Travel Angle (°)	-15 (drag)
Travel Speed (ipm)	15
Max Interpass Temp. (°F)	500°F 1-in from the weld
Corner Weld Parameters	
Current (A)	140
Voltage (V)	21
Deposition rate (lbs/hr)	6
Heat Input (kJ/in)	12
Center Weld Parameters	
Current (A)	200
Voltage (V)	28
Deposition rate (lbs/hr)	10
Heat Input (kJ/in)	23.5

3.4 Field Repair Evaluation

TTCI supplied a worn partial AMS frog section that had been field-repaired. EWI used this section to evaluate weld quality and to develop the welding sequence on the actual frog geometry prior to welding the full-size frogs for in-track testing at TTCI. While TTCI did not know the number of repairs that had been performed, a CSX railroad representative verified that the level of wear and the quality of the repair were typical of what is seen in the field. Images of the supplied frog are provided in Figure 26 and Figure 27. A typical “breakout” which is caused by lack of maintenance grinding is shown in Figure 27.

EWI removed the field-repaired area towards the heel of the frog section (located at the top of Figure 26), examined it using RT, and cross-sectioned it to evaluate weld quality. The photo-macrograph provided in Figure 28 shows that stainless steel was used as a “butter” layer between the base material and the manganese alloy repair weld, which is common practice when welding over a crack. Stainless steel has been shown to retard crack growth; however, due to its significantly decreased hardness compared to AMS, railroads require that the stainless steel deposit be at least 0.75 in below the running surface.

Figure 26: Field-Repaired Frog

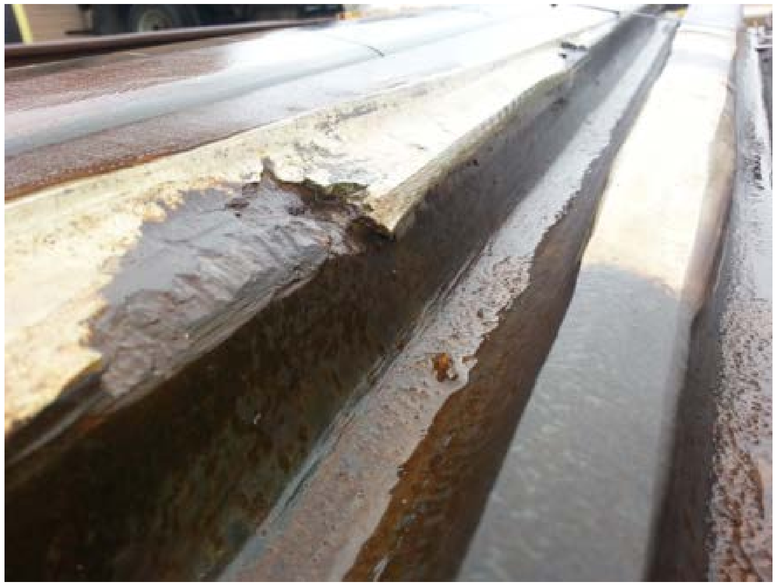

Figure 27: Breakout on Field-Repaired Frog

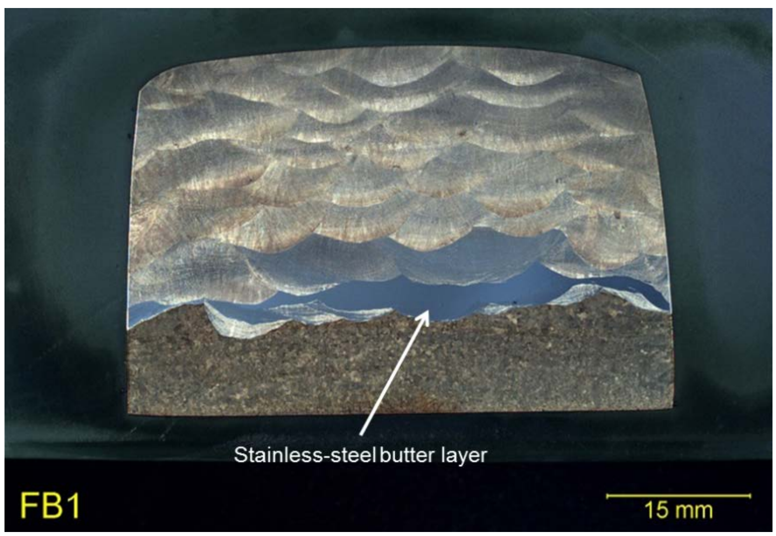

Figure 28: Cross Section of Repaired Area Showing Use of Stainless Steel in First Two Layers

EWI performed RT on the section as shown in Figure 29. This film was shot from above and revealed significant porosity at both sides of the weld. According to a railroad representative, this is a common discontinuity associated with the improper use of carbon blocks. Carbon blocks are used to provide a surface for edge beads to "roll" against. Some welders wedge the carbon block to fit it tight against the corner being welded and minimize post-weld finish grinding. As a result, the welding arc contacts the carbon block, contaminating the weld and causing porosity. The railroad representative added that breakout failures often reveal large pores, suggesting that these pores significantly weaken the weld repair.

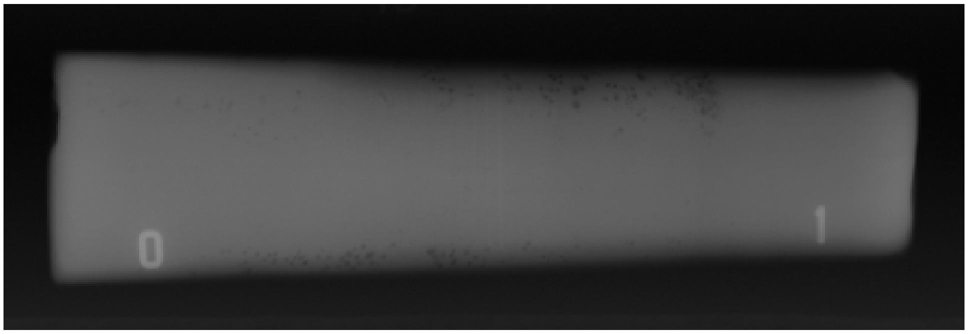

Figure 29: RT of Repaired Area Showing Pores at the Edges Due to Contamination from Carbon Blocks

3.5 Weld Repair of Partial Frog

The uncut portions of the field-repaired frog were used to develop the welding sequence for the wing and point. A railroad representative taught EWI personnel how to remove the damaged sections of the frog and prepare it for repair welding using carbon arc gouging. EWI then smoothed the surfaces by grinding. Figure 30 shows the frog section after carbon arc gouging and grinding. EWI documented the locations where material was removed as well as the geometry to allow the same joint preparation to be used on subsequently welded frogs.

Figure 30: Frog After Removal of Damaged Material with Carbon Arc Gouging and Grinding

EWI used two parameter sets to complete welding on the frog section. EWI used the lower heat input parameters on the corners of the point, and the higher heat input parameters when welding in the center of the point and on the wing (parameters described in Section 3.2). Photo-macrographs of cross sections taken from the point and the wing after weld repair are provided in Figure 31 and Figure 32, respectively.

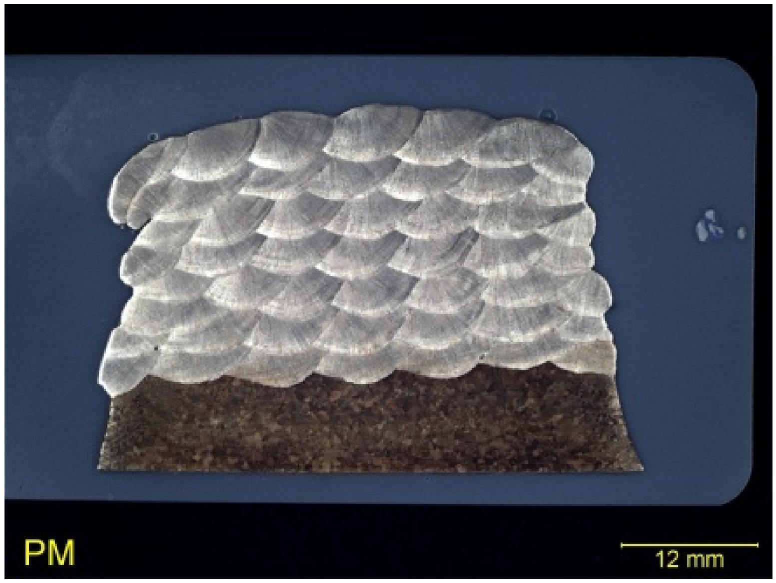

Figure 31: Cross Section of Repair-welded Point

Figure 32: Cross Section of Repair-welded Wing

3.6 Evaluation of Partial Frog Weld Repair

EWI used RT to assess the weld quality of the repaired wing and point. Weld quality was comparable to that of the FCAW-A mock build-ups, and no lack-of-fusion discontinuities were found. EWI performed tensile testing on both the point and wing repair and Table 19 provides a comparison with previous tensile testing results. While the yield strength was lower than that of the FCAW-A mock build-up repair, it was still within typical range of casting properties. The UTS dropped as well, but it was still higher than the typical range.

EWI also performed Charpy V-notch testing to evaluate toughness at room temperature and at -30°F (Table 20). As expected, toughness decreased significantly with the decrease in temperature.

Table 19: Comparison of All Tensile Testing Results

Property	Typical Casting Properties	Mock-up Material	Baseline SMAW	Baseline SA FCAW	FCAW-A	RWF-FCAW	FCAW-A on Partial Frog (point)	FCAW-A on Partial Frog (wing)
Tensile Strength (ksi)	100 to 145	142	117	96	125	121	112.1	109.5
Yield Strength (ksi)	50 to 57	59	83	74	83	86	73.7	74.7

Table 20: Charpy V-notch Toughness Properties

Location	Test Temp. (°F)	Absorbed Energy (J)	Absorbed Energy (ft-lbs)	Lateral Expansion (mm)	Lateral Expansion (mils)	Shear (%)
Point	-30.28	40.67	30	0.6	23.62	100
Point	-30.28	43.39	32	0.68	26.77	100
Point	-30.28	44.74	33	0.44	17.32	100
Wing	73.4	84.06	62	1.25	49.21	100
Wing	73.4	115.24	85	1.41	55.51	100
Wing	73.4	90.84	67	1.34	52.76	100

EWI concluded that the developed FCAW-A parameters could be used to effectively repair the removed sections.

3.7 Repair of Full-Length Frogs for TTCI Testing

TTCI also supplied EWI with two full-length frogs (Frog #1 and Frog #2) for repair and subsequent placement in the test track for evaluation. Frog #1 was a conformal frog, and had more wear, namely "breakouts" on both wings (Figure 33). A conformal frog has an improved geometry that more evenly distributes wheel loads to minimize contact stresses and resultant plastic deformation. Frog #2 was a standard flat frog, and had minimal wear from 6.8 MGTs of traffic (Figure 34).

Figure 33: Frog #1 Marked for Carbon Arc Gouging

Figure 34: Frog #2 Marked for Carbon Arc Gouging

3.7.1 Preparation of Frogs for Weld Repair

EWI repaired the point and the "point facing left" wing of each frog. The "point facing right" wings were not repaired since TTCI's plan was to test only one wing in-track. EWI removed material to mimic a field repair, which was based on the amount of material that was removed from the partial frog for welding sequence development. Since neither Frog #1 nor Frog #2 required the same level of repair as the partial frog, this meant that excess material was removed to create a "typical" repair scenario. The repaired point sections of both frogs were extended toward the heel to simulate a repair of the area that was cut out for RT cross-sectioning as illustrated in Figure 35.

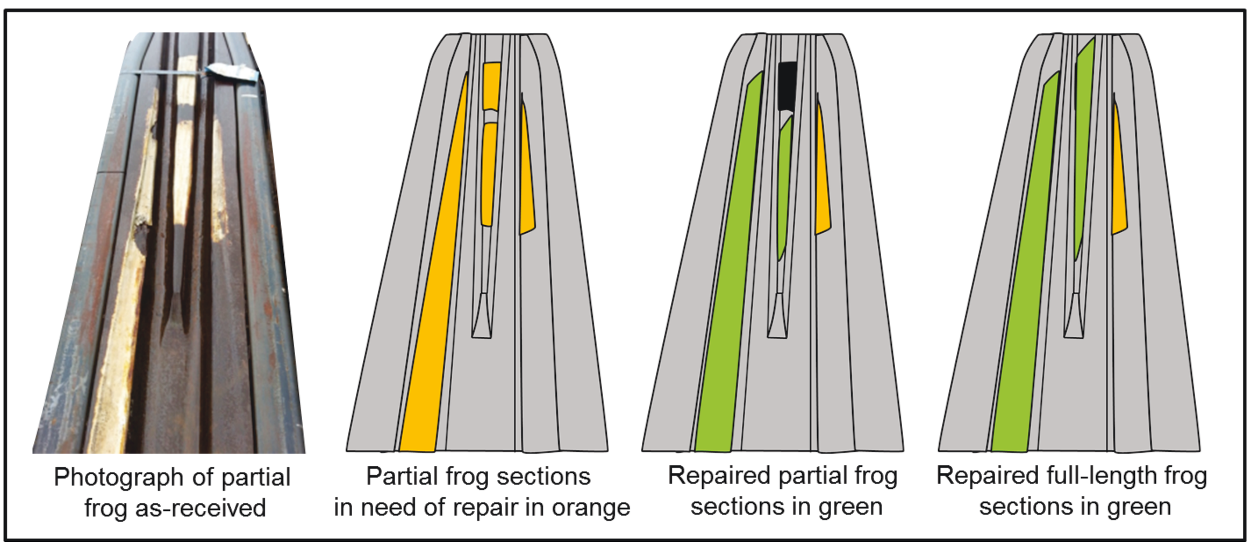

Figure 35: Material Removal Illustration

As with the partial frog, EWI used carbon arc gouging to complete the bulk of the required material removal. Figure 36 shows the carbon arc gouging process, while Figure 37 shows Frog #1 after the completion of carbon arc gouging. EWI then ground both frogs smooth to prepare for weld repair (Figure 38 and Figure 39).

Figure 36: Carbon Arc Gouging Process

Figure 37: Complete Carbon Arc Gouging

Figure 38: Frog #1 After Grinding

Figure 39: Frog #1 After Grinding

3.7.2 Weld Repair of Frog #1

EWI completed welding of Frog #1 using the procedure developed on the field-repaired frog (Table 21). Six layers were required to build-up the wing of Frog #1. The number of beads per layer decreased with successive weld layers, as shown in Figure 40. The maximum recorded interpass temperature of the wing repair, as measured 1 in from the weld, was 219°F. A photograph of the completed wing repair is provided in Figure 41. The maximum interpass temperature reached during welding of the point was 228°F.

Seven layers were required to build the point up to the required height. Upon the recommendation of railroad welding supervisors, EWI deposited additional material at the heel of the frog to ensure a smooth transition between the weld repaired area and the unwelded area. Prior to depositing this material, EWI removed 0.125 in of adjacent material to ensure that welds were not deposited on work-hardened material which would be more prone to cracking. Four layers were required to build up this area to allow for a smooth transition (Figure 42). The maximum interpass temperature reached during the deposition of these additional layers was 235°F.

Table 21: Test Frog Welding Parameters

Automated FCAW	
Common Parameters	
Electrode Diameter (in)	0.045
Electrode Type	Flux-cored
Polarity	Direct Current, Electrode Positive
Shielding Gas	75 percent Argon/25 percent CO_2
Travel Angle (°)	-15 (drag)
Travel Speed (ipm)	15
Max Interpass Temp. (°F)	500°F 1-in from the weld
Corner Weld Parameters	
Current (A)	140
Voltage (V)	21
Deposition rate (lbs/hr)	6
Heat Input (kJ/in)	12
Center Weld Parameters	
Current (A)	200
Voltage (V)	28
Deposition rate (lbs/hr)	10
Heat Input (kJ/in)	23.5

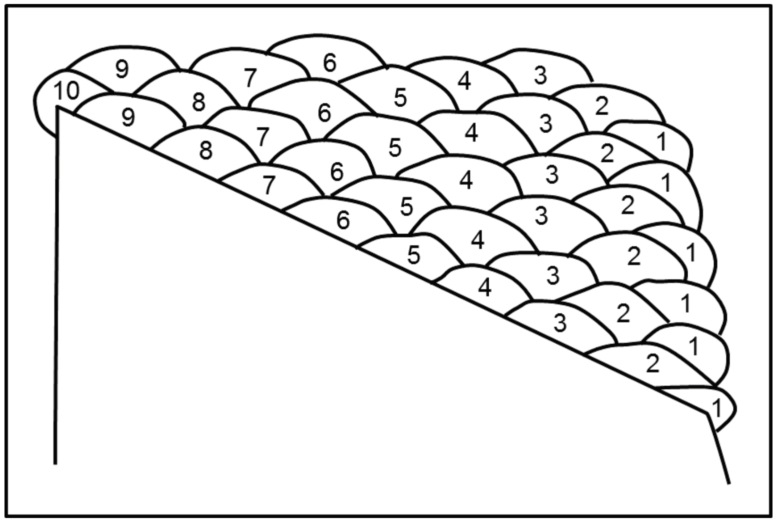

Figure 40: Frog #1 Wing Repair Welding Sequence

Figure 41: Frog #1 After Wing Repair

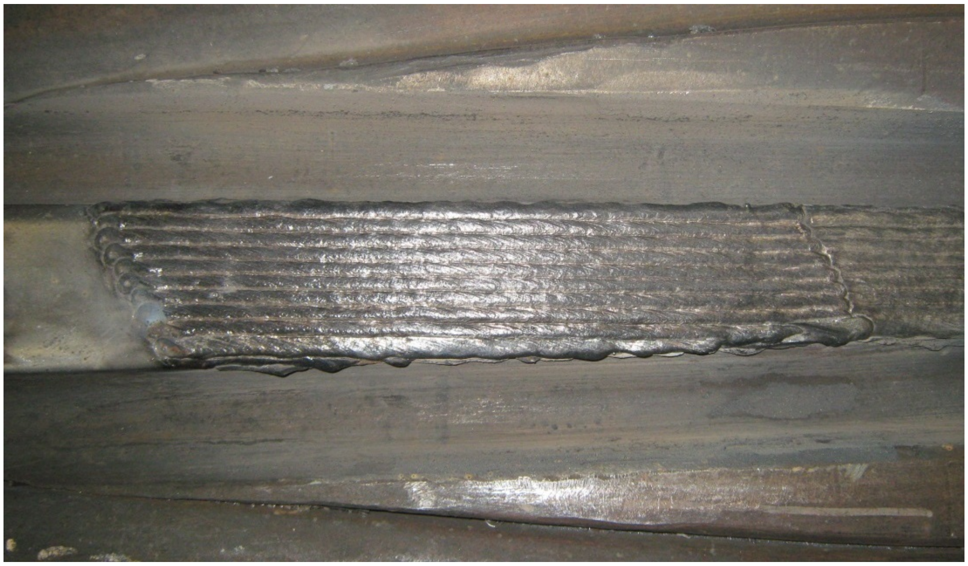

Figure 42: Frog #1 After Additional "Taper" Weld Build-up

3.7.2.1 Frog #1 Weld Cracking

EWI observed cracks oriented transverse to the welding direction in the base material during welding of the transition area (Figure 43). EWI ground these cracks out and removed 0.125 in of material from the adjacent area to avoid welding on work-hardened material (Figure 44). Since the cracks extended 0.25 in deep, EWI filled these areas and ground the surface smooth before depositing subsequent layers (Figure 45 and Figure 46). EWI extended the grinding into the previously welded area to determine if cracks extended into the weld; however, no additional cracks were found using dye-penetrant testing.

Figure 43: Base Material Cracking in Frog #1 at Interface with "Transition" Build-up

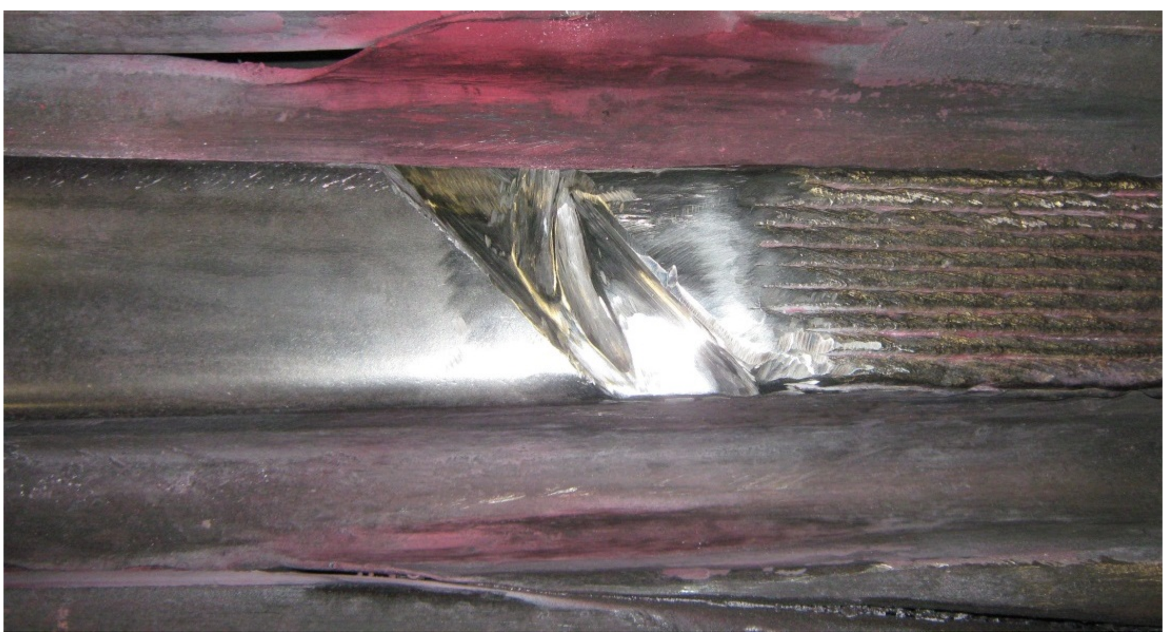

Figure 44: Removal of Cracks from Frog #1 to Allow Repair Welding

Figure 45: Filling of Cracks in Frog #1

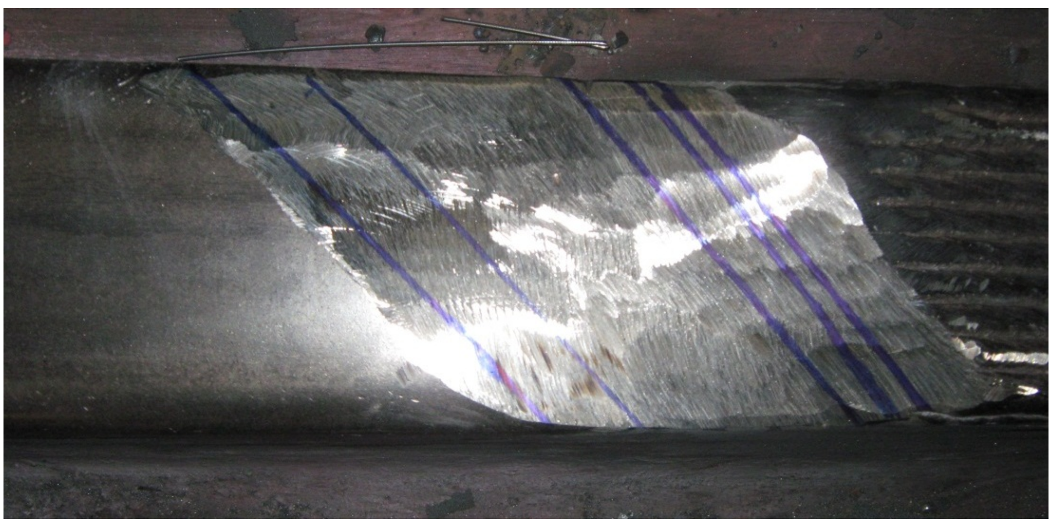

Figure 46: Frog #1 Crack-fill Welds Ground Smooth

EWI concluded that the cracking of the base material was caused by a combination of two factors. The first factor was the high hardness and relatively low ductility of the work-hardened base material adjacent to the weld. The second factor was the high residual stresses associated with multiple overlapping weld craters adjacent to the work-hardened base material, which is significant because the weld crater is typically hotter than the start of the weld. The increased heat leads to increased penetration and higher residual stresses than at the start of the weld. Since the base material cannot be altered to alleviate the problem, EWI developed a new welding sequence to relocate the weld craters away from the interface with the work-hardened base material, reducing residual weld stresses and successfully eliminating cracking of the base material. The modified procedure does not add any additional time to the repair process, and therefore will have no effect on productivity.

EWI deposited a third layer in the original welding direction to even out the build-up and ensure the proper height; however, this layer did not extend to the interface between the weld repair and the work-hardened base material (Figure 47).

Figure 47: Weld Build-up to Complete Frog #1 Crack Repair

The repair sequence used on the point of Frog #1 is summarized below (and illustrated in Figure 48).

(1) Original point geometry.

(2) EWI removed material to simulate a worst-case scenario field repair using carbon arc gouging and grinding.

(3) EWI deposited seven layers to build up the removed material. Layers were nine to ten beads wide.

(4) EWI removed additional material toward the heel of the point to create a smooth transition in accordance with the recommendation of CSX personnel.

(5) EWI deposited four layers to build up the removed material in the transition area. Two cracks were found in the base material adjacent to the weld craters during dye-penetrant testing.

(6) EWI removed the cracks by grinding, and removed 0.125 in of material from the adjacent surface area.

(7) After filling the deep area where the cracks were removed and grinding the area flush, EWI deposited two layers in the opposite direction of all other welding passes to minimize heating of the unground, work-hardened base material. An additional layer was deposited in the original direction to even out the height of the build-up.

(8) TTCI ground the frog to final shape.

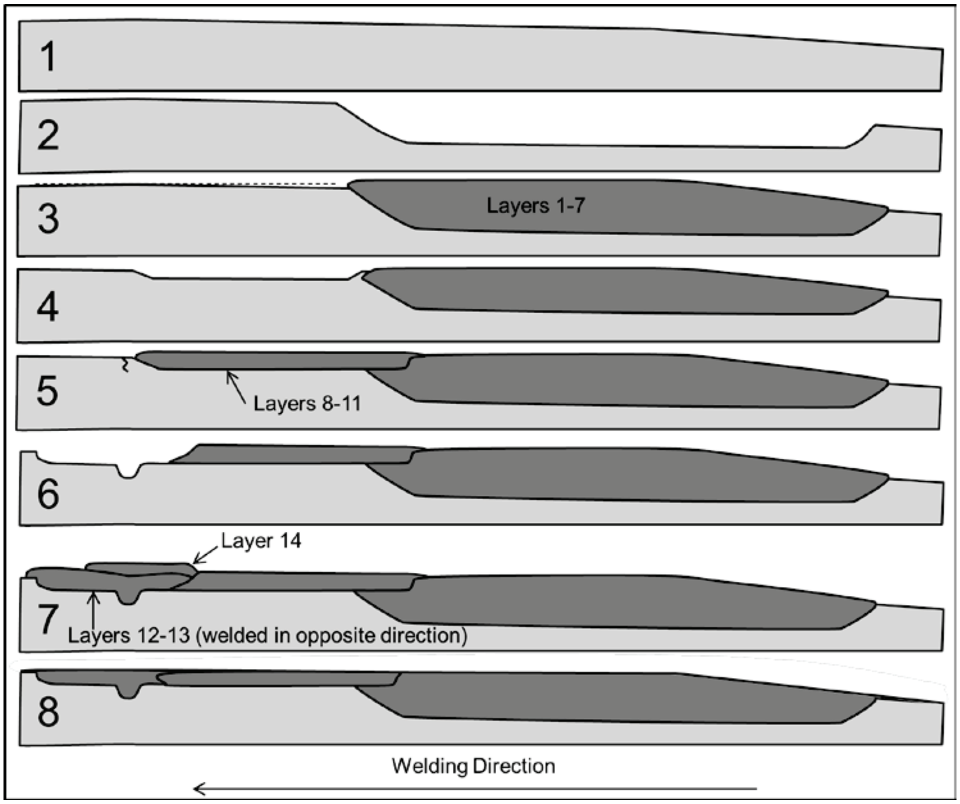

Figure 48: Illustration of Frog #1 Point Repair Sequence

EWI sent the repaired frog to TTCI to be ground to shape and inspected in preparation for installation in track. After grinding the frog to shape, TTCI found a crack in the point of Frog #1, as shown in Figure 49. As in the crack found in the heel of Frog #1, the crack was located in the base material adjacent to the weld-repaired area. Due to project budget and schedule constraints, this crack was not repaired with the weld sequencing repair method (described above).

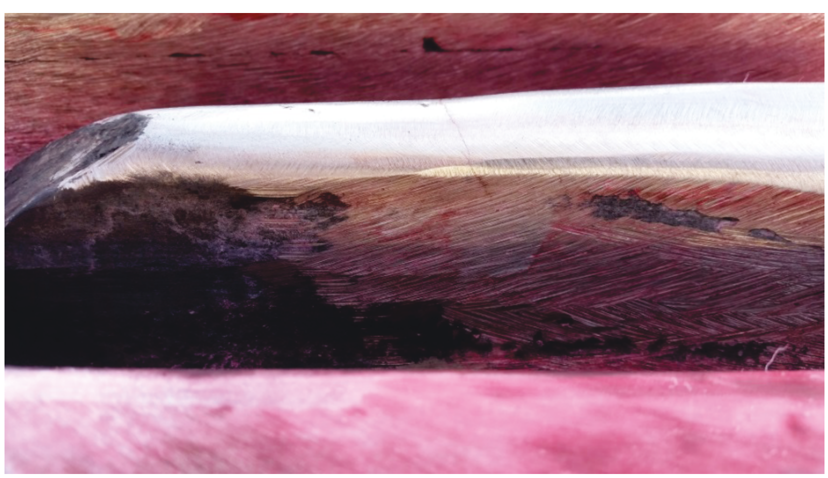

Figure 49: Crack Found in Point of Frog #1

3.7.3 Frog #2

EWI used the same approach to weld Frog #2 that was used on Frog #1. Throughout welding of the wing, the maximum interpass temperature reached as measured 1 in from the weld was 219°F. Figure 50 illustrates the welding sequence used to repair the wing. Six layers were required to build up the wing to the required height. A photograph of the completed wing repair is provided in Figure 51.

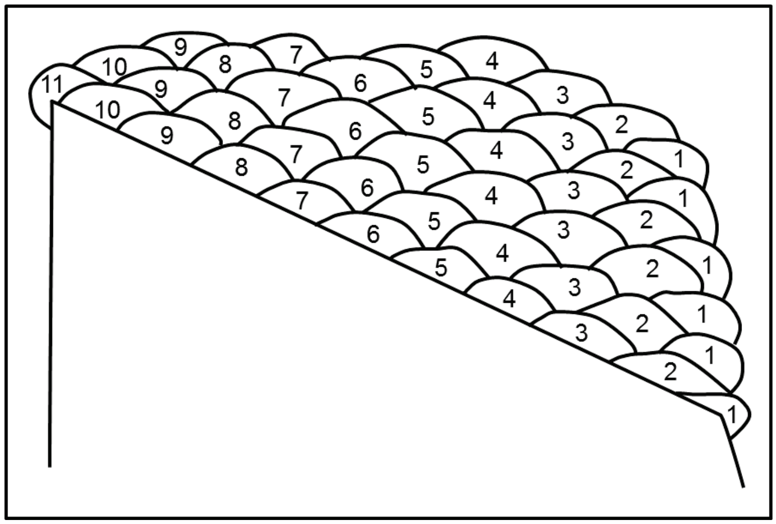

Figure 50: Frog #2 Wing Repair Welding Sequence

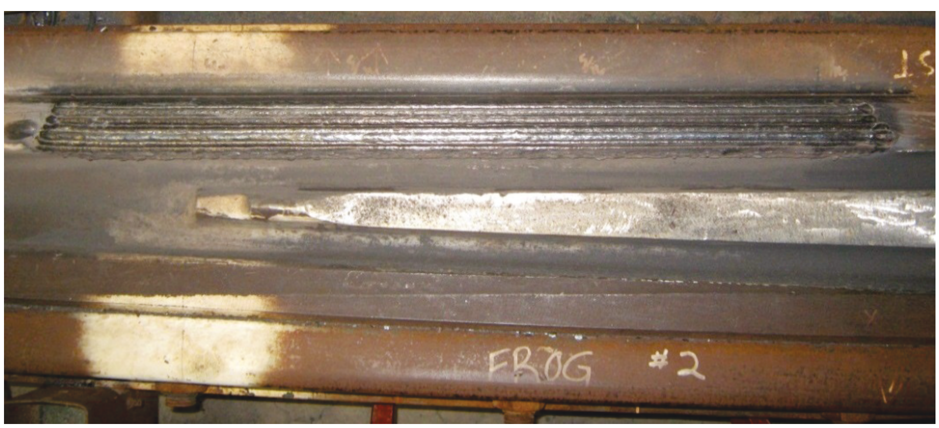

Figure 51: Frog #2 After Wing Repair

EWI deposited eight layers on the point to build up the removed material. The maximum interpass temperature measured 1 in from the weld was 242°F. Upon the recommendation of railroad welding supervisors, EWI deposited additional material at the heel of the frog to ensure a smooth transition between the weld-repaired area and the unwelded area. EWI ground the surface to a depth of 0.125 in to ensure that welds were not deposited on work-hardened material which would be more prone to cracking (Figure 52). Two layers were required to build up this area to match the height of the previously welded section (Figure 53). The maximum interpass temperature reached during the deposition of these layers was 220°F.

Figure 52: Preparation of Frog #2 Transition Area

Figure 53: Layer 1 Welding of Frog #2 Transition Area

Three additional layers were deposited to ensure that sufficient material was deposited in order to allow EWI to finish grinding. The maximum interpass temperature reached during the deposition of these three layers was 239°F.

No cracking occurred during the welding of Frog #2. The repair sequence used on the point is summarized below and illustrated in Figure 54.

(1) Original frog geometry.

(2) EWI removed material from the point to simulate a worst-case scenario field repair using carbon arc gouging and grinding.

(3) EWI deposited eight layers to build-up the removed material. Layers were nine to ten beads wide.

(4) EWI removed additional material toward the heel of the point according to the recommendation of CSX personnel.

(5) EWI deposited two layers to build up the removed material.

(6) EWI deposited two additional layers that were nearly the full length of the repair to build the height of the point to match the height of the wings. EWI also deposited one additional, shorter layer to build up a "dip" in the repaired area.

(7) TTCI ground the frog to final shape.

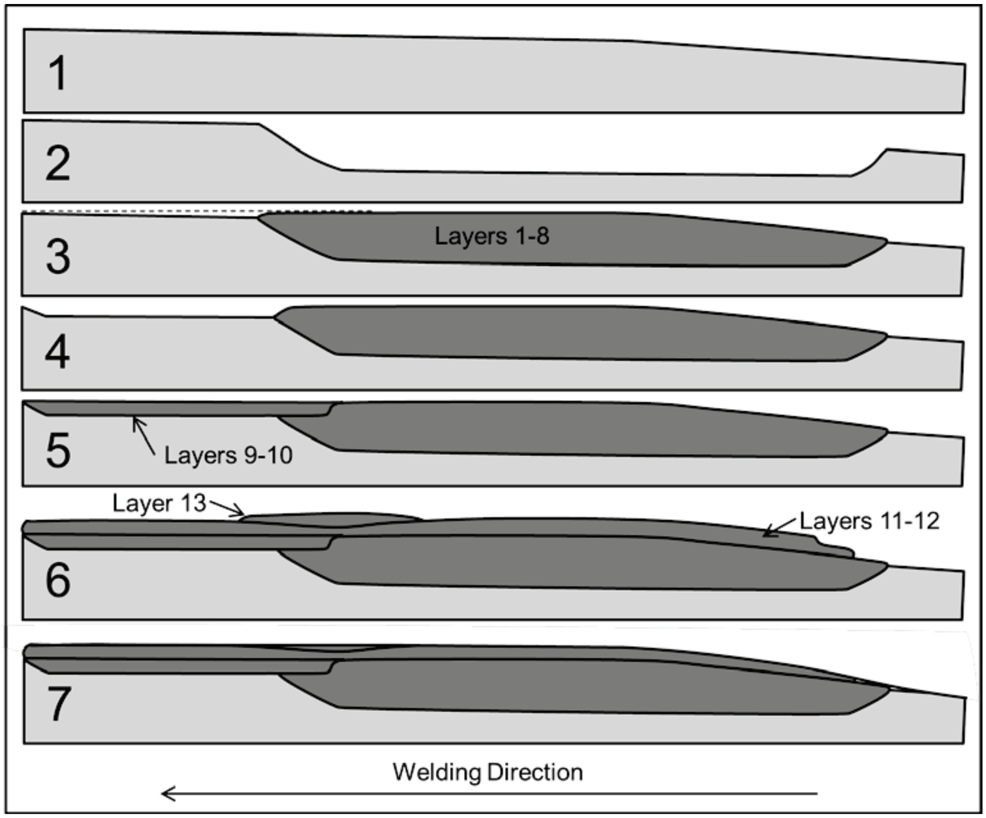

Figure 54: Frog #2 Repair Sequence

Due to the presence of an unrepaired crack in the base material adjacent to the weld repair, Frog #1 was not tested. Frog #2 was placed in TTC's high-tonnage loop (HTL), where it was tested and monitored. At the conclusion of testing, the frog was removed and returned to EWI for post-test laboratory evaluation.

4. Track and Laboratory Testing Results

TTCI monitored the performance of Frog #2 under 40 mph heavy axle load traffic, consisting of approximately 110 cars with a gross rail load of 315,000 pounds. Traffic was run in both directions. Since TTCI installed the frog in open track (not in a turnout) the frog point and only one wing rail were subjected to the heavy axle load (HAL) traffic. TTCI performed the following performance measurements:

- Profile and hardness measurement intervals: 0, 2, 5, 10, 20, 40, 70 and 100 MGTs
- Profile measurements were taken at the following locations with respect to the point
  - Point measurements (inches): +2, +4, +6, +8 . . . +36
  - Wing measurements (inches): -16, -8, 0.5, +2, +4, +6, +8 . . . +26
- Running surface hardness measurements taken at the following locations with respect to the point: -16, -8, 0.5, +2, +8, +16 and +22
- Maintenance performed in accordance with the policy and procedures established for TTCI's HTL

After the maintenance grinding performed at 10.15 and 17.53 MGTs, no further maintenance was required. The frog was removed from track after accumulating 118.16 MGTs. This is a significant improvement over the typical maintenance intervals shown in Table 1, as it represents over 100 MGTs of maintenance-free operation. A record of all performed maintenance is provided in Table 22. In this table, Item 1 and 2 pertain to inspection and installation, while Item 3 through Item 6 pertain to in-track maintenance.

Table 22: TTCI Frog Maintenance Record

<table>
<tr><th colspan="6">Test Frog No. 2</th></tr>
<tr><th>Item</th><th>Date</th><th>Tonnage (MGT)</th><th>Description</th><th>Component</th><th>Measurements</th></tr>
<tr><td>1</td><td>4/21/14</td><td>0</td><td>Weld Repair Flaw Inspection</td><td>Test Frog</td><td>Ultrasonic and Dye Pen</td></tr>
<tr><td>2</td><td>4/22/14</td><td>0</td><td>Installed in HTL Section 27</td><td>Test Frog</td><td>Profiles and Hardness</td></tr>
<tr><td>3</td><td rowspan="2">5/8/14</td><td rowspan="2">10.15</td><td>• Slight Vertical Dip on the tread running surface
• Ground Slight Bulge at Gage Face</td><td>Wing Rail</td><td rowspan="2">Pre- and Post-Grind Profiles</td></tr>
<tr><td>4</td><td>Ground Metal Flow, Gage Corner, Entire Length of Frog Point</td><td>Frog Point</td></tr>
<tr><td>5</td><td rowspan="2">5/15/14</td><td rowspan="2">17.53</td><td rowspan="2">Ground Metal Flow, Gage Corner, Entire Length of Frog Point and Wing Rail</td><td>Wing Rail</td><td rowspan="2">Post-Grind Profiles</td></tr>
<tr><td>6</td><td>Frog Point</td></tr>
</table>

TTCI measured the running surface wear at multiple locations along the length of the point and wing throughout the duration of the test. Figure 55 shows the running surface wear along the length of the point at approximately 100 MGT. An increase in running surface wear is indicated approximately 32 inches from the point. At this location the load that was once "shared" by the wing and point is completely transferred to the point. Figure 56 shows the area loss at this location at different intervals throughout the service life of the frog. Profile measurements of this location taken at 0 and 100 MGT are provided in Figure 57. The dotted line represents the wear limit, indicating that significant additional running surface wear is available.

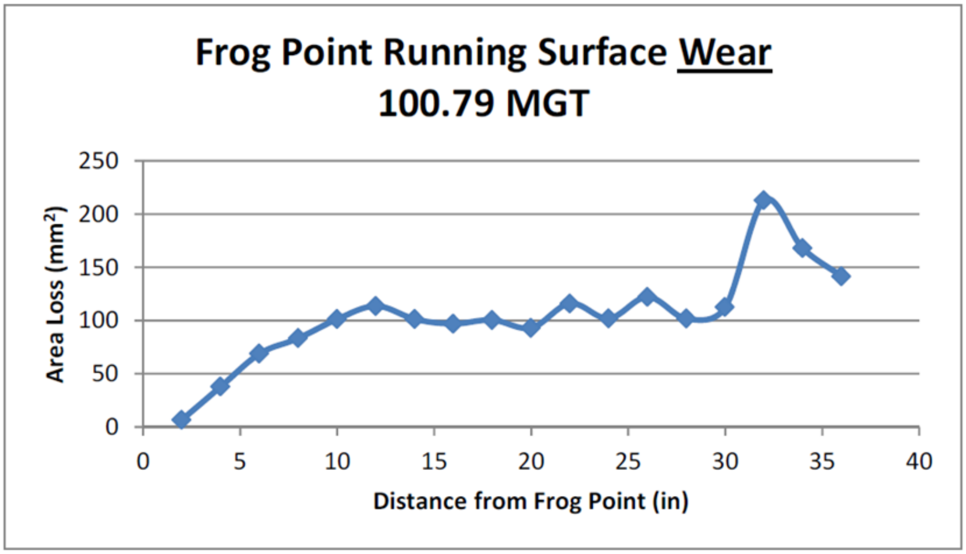

Figure 55: Point Running Surface Wear Along Length of Point

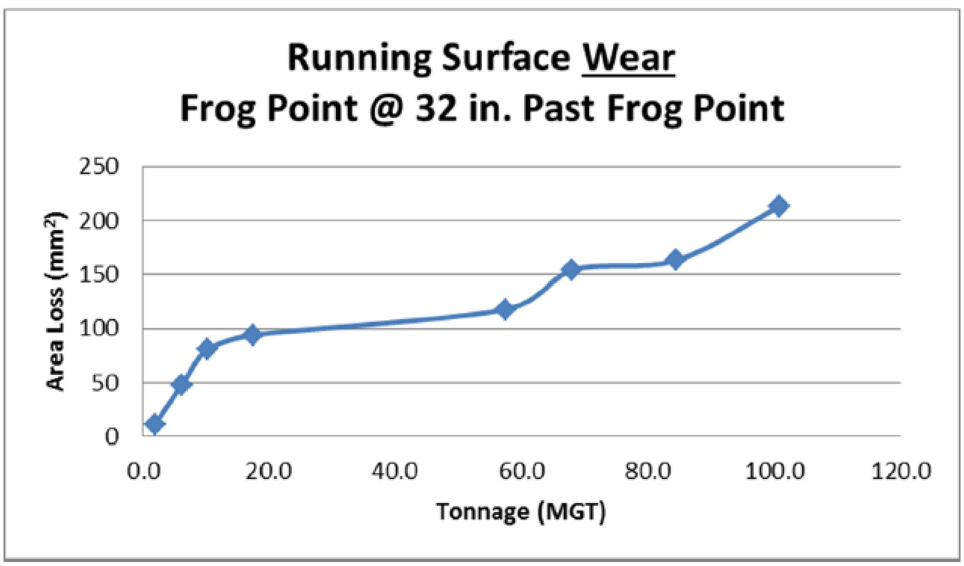

Figure 56: Running Surface Wear 32 inches Past Frog Point

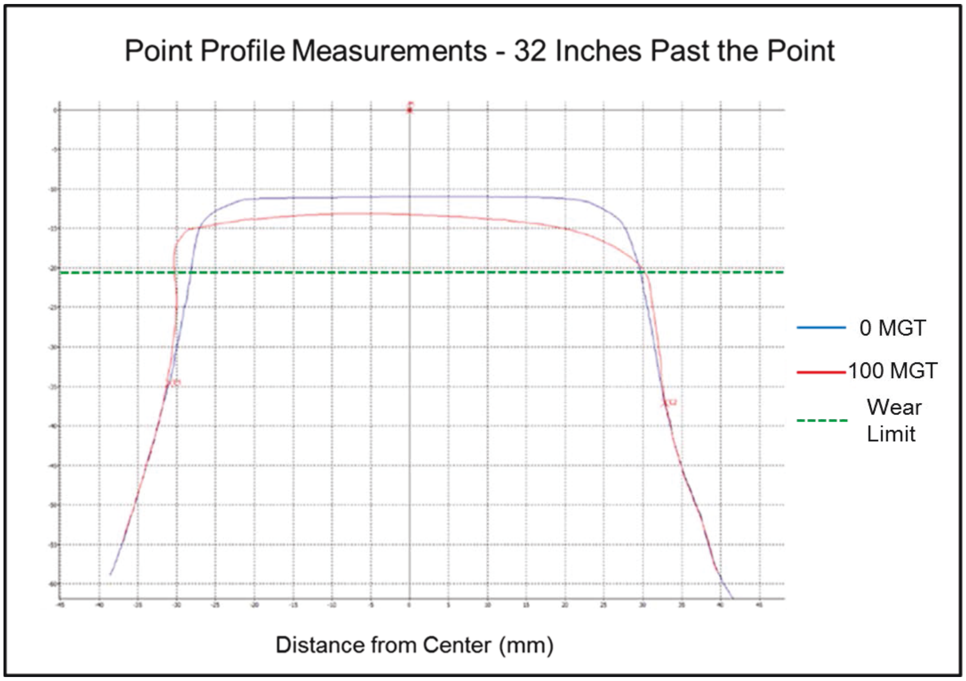

Figure 57: Point Running Surface Wear 32 inches from Point at 0 and 100 MGT

TTCI took periodic hardness measurements at three different locations on the running surface. As shown in Figure 58, hardness increased quickly over the interval from 0 to 2 MGT, then again over the interval from 2 to 6.17 MGT. After 10.15 MGT the hardness dropped, and then dropped again after 17.53 MGT. These hardness drops coincide with the occurrence of maintenance grinding, where TTCI removed work-hardened material. Since only a portion of the work-hardened material was removed, the hardness did not drop down to level of the as-welded repair.

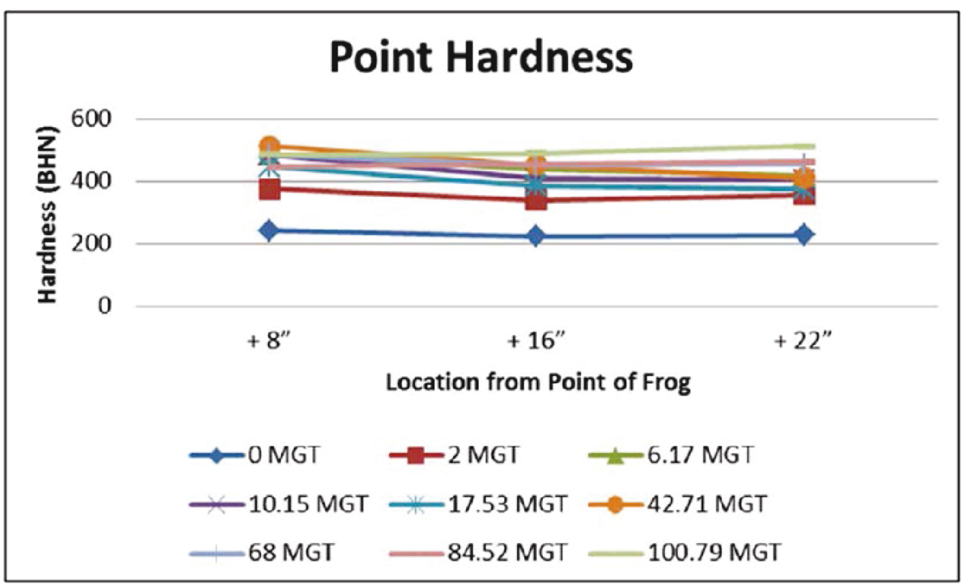

Figure 58: Point Hardness

TTCI measured the running surface wear at multiple locations along the length of the wing (Figure 59). Figure 60 shows the area loss 8 inches past the point throughout the service life of the frog. Profile measurements taken at 0 and 100 MGT are provided in Figure 61. The dotted line represents the wear limit, indicating that significant additional running surface wear would have to take place before a repair would be required. TTCI took periodic hardness measurements at three different locations on the running surface (Figure 62). As with the point, hardness increased significantly after just 2 MGTs.

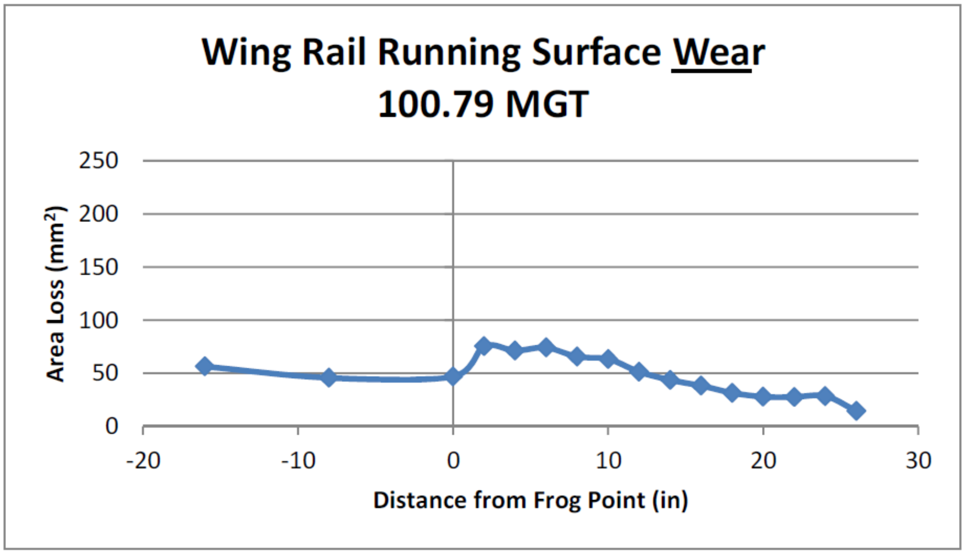

Figure 59: Running Surface Wear Along Length of Wing

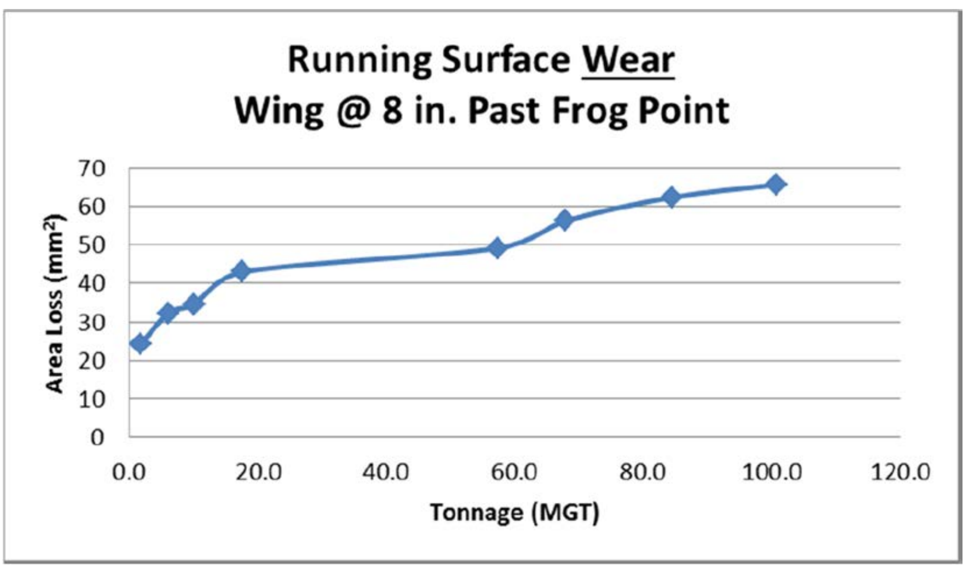

Figure 60: Wing Running Surface Wear 8 inches Past Frog Point

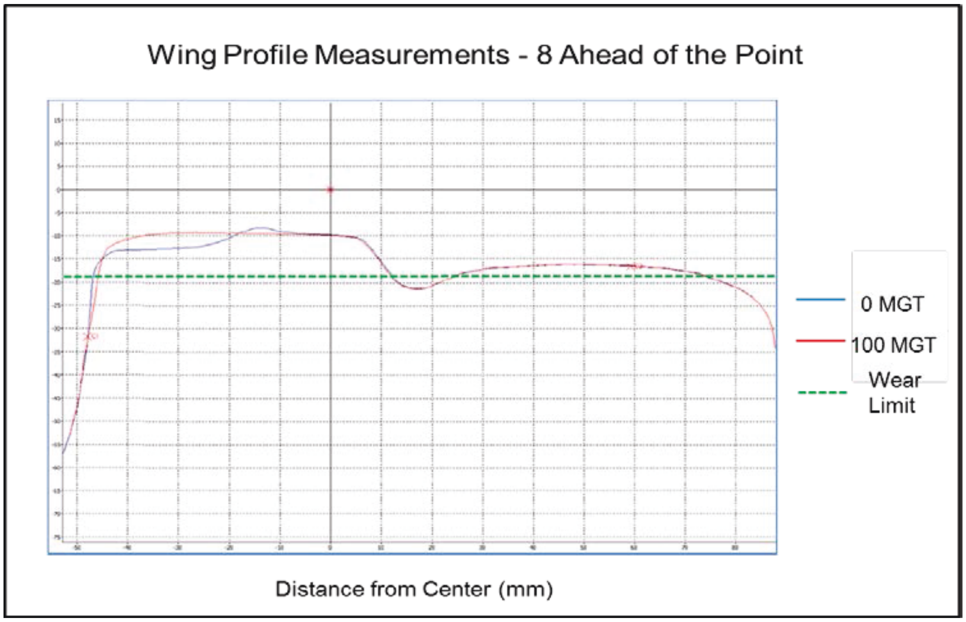

Figure 61: Wing Running Surface Wear 8 inches from Point at 0 and 100 MGT

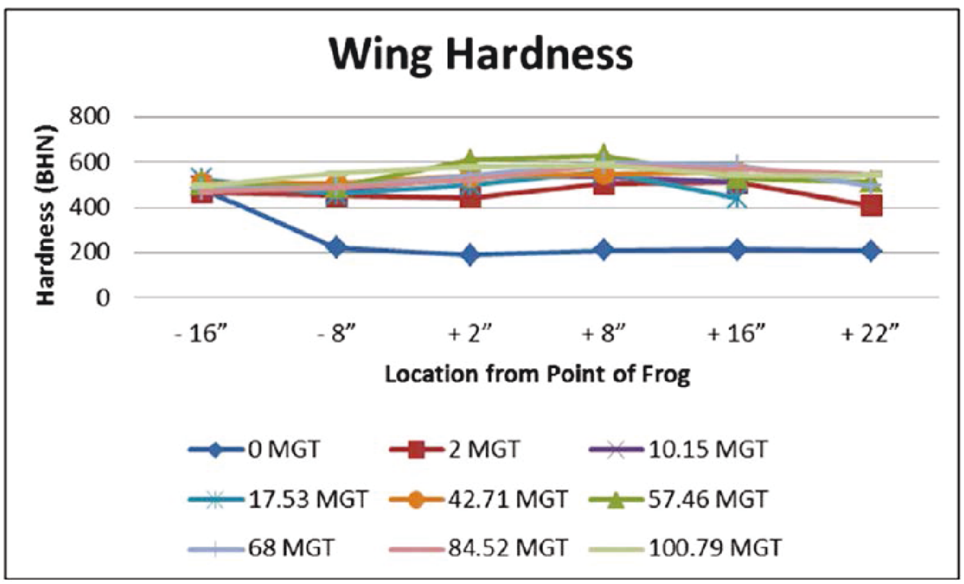

Figure 62: Wing Hardness

Figure 63 is an overlay of running surface wear data along the length of the frog. As the wheel starts to move towards the edge of the running surface of the wing (progressing from left to right), the reduction in contact area results in a sudden increase in area loss approximately 2 in past the point. As a greater portion of the load is carried by the point, the wing wear is gradually reduced until the entire load is located on the point (at approximately 32 in past the point).

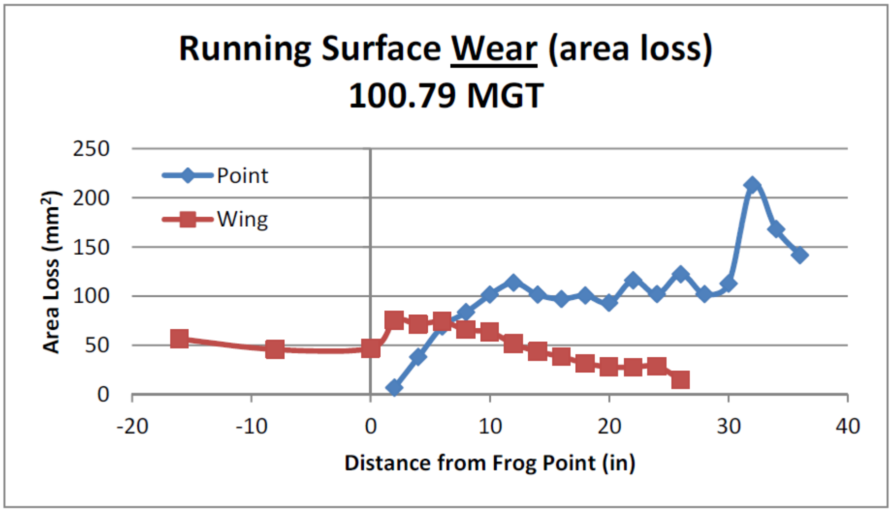

Figure 63: Combined Wing and Point Running Surface Wear

Spalling occurred at two locations on the frog point; however, this is a discontinuity commonly found on worn AMS frogs and the spalling was not significant enough to remove the frog from service (Figure 64). Termination of the in-track test after 118.16 MGTs was not due to wear, but rather to the scheduled conclusion of the test according to the project plan. In their testing summary report, TTCI stated that "based on visual inspection at the time it was removed from track, the frog could have remained in service."

Figure 64: Point Running Surface Spalls

4.1 Track Testing Summary

Frog #2 accumulated 118.16 MGTs before TTCI removed it from track and shipped it back to EWI for evaluation. Based on the average frog life data presented in Table 1, the overall time in testing represents a 240 percent increase in service life compared to the average life of repaired frogs, and a 107 percent increase over the service life of new frogs. Decreased plastic deformation led to a significant decrease in required maintenance, and after over 118 MGTs, the running surface wear of the point and wing was less than 25 and 40 percent of the maximum allowable, respectively.

4.2 EWI Laboratory Testing

EWI performed the following laboratory tests to evaluate Frog #2, after the conclusion of in-track testing at TTCI:

- Ultrasonic testing (UT)
- Radiographic testing (RT)
- Cracking Analysis
- Metallurgical Examination
- Hardness Mapping

After the conclusion of in-track testing, EWI examined the repaired surfaces via UT and RT. EWI used both of these methods because UT is a more effective method of detecting cracks, while RT is better at detecting porosity. Phased array UT scans were performed from the running surfaces using -30 to +30 degree refracted longitudinal waves and 35 to 70 degree shear waves. All discontinuity indications were detected with the refracted longitudinal scan. Ten discontinuities were found, and all indications were isolated to the weld overlay. An example of a UT scan image is provided in Figure 65.

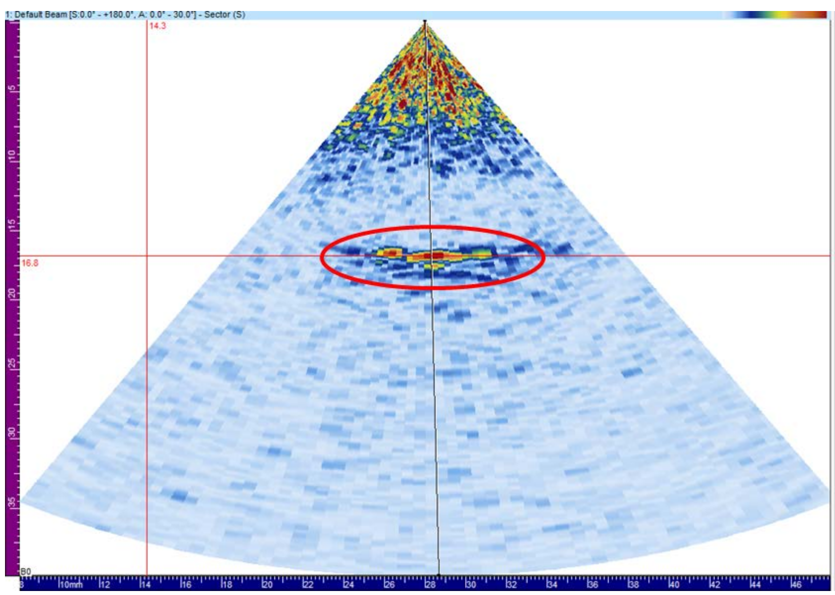

Figure 65: Ultrasonic Testing Scan Sample

EWI cut the repaired sections out of the frog (Figure 66) and inspected them using RT. RT images were compared to the RT image of the field-repaired sample. An inspection summary report is provided in Table 23. In this table, "Rail Number" FB1-1 refers to the field-repaired sample; those beginning with "WX" designate sections of the wing; and, those beginning with "PX" designate sections of the point. As noted in the report, over 120 pores were found in the 8-in long field-repaired sample, while only 10 total pores were found in the combined linear 61 inches of the full-thickness automated weld repairs (this number does not include the taper section towards the heel). This is a reduction from 15 pores per linear inch of repair to 0.16 pores per inch of linear repair. Images of RT films provided in Figure 67 and Figure 68 provide a visual comparison of weld quality. In Figure 67, large densely packed areas of porosity are located near the edges of the longitudinal surfaces. In Figure 68 (Section W2), no indications are visible.

Figure 66: Locations from which RT Specimens were Removed

Table 23: RT Inspection Summary

Rail Number	Radiography Location	Comments
FB1-1	0-1	Shot from top of rail shows severe clusters of porosity, approx. 120 pores within 6" length. Nominal pore diameter approximately 1/16"
FB1-1	0-1	Shot from side of rail shows cracking and scattered pores approx. 3/64" in diameter
WX1	0-1	3 pores approx. 3/64" to 1/16" in diameter
WX2	0-1	no reportable indications
WX3	0-1	Transverse crack approximately 12.5" from "0" end of rail segment
WX3	1-2	2 pores approximately 3/64" diameter
PX1	0-1	no reportable indications. Sawcut / flame cut marks observed on film
PX2	0-1	Transverse crack approximately 10" from "0" end of rail segment
PX2	1-2	3 pores approx. 3/64" to 1/16" in diameter
PX3	0-1	2 pores approximately 3/64" diameter
PX4	0-1	no reportable indications. Isolated spawling noted on film
PX4	1-2	no reportable indications. Sawcut / flame cut marks observed on film

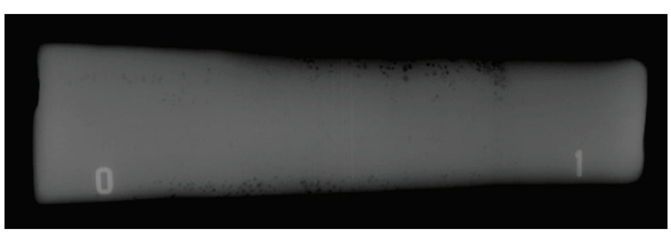

Figure 67: RT Image of Field-Repaired Sample

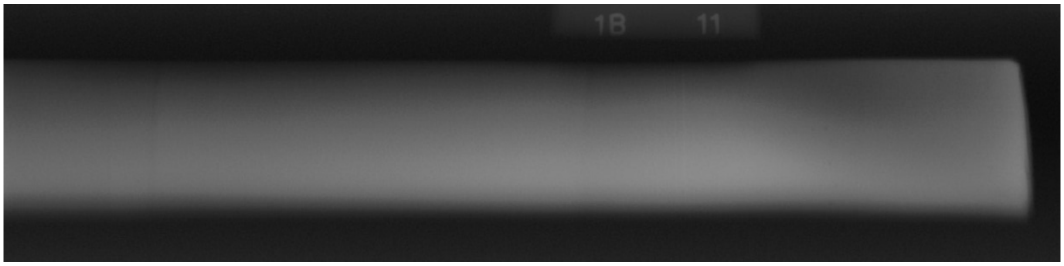

Figure 68: RT Image of Wing Repaired with EWI's Automated FCAW Repair Technique

EWI cut cross-sections of the weld-repaired areas of the point and wing to understand the reason(s) for its improved performance over current industry repair techniques by evaluating weld quality, investigating cracking discontinuities, and studying its microstructure. Casting voids present in the AMS base material are shown in Figure 69. As shown in Figure 70, fewer discontinuities were found in automated FCAW welds compared to the base material, although they are larger. Those that are present are isolated slag inclusions, and EWI's examination indicates that these inclusions are typically not correlated with the presence of cracks. Groups of horizontal cracks likely due to shear loading were found (Figure 71 and Figure 72). These cracks were not associated with any particular microstructure, grain boundaries, or discontinuity.

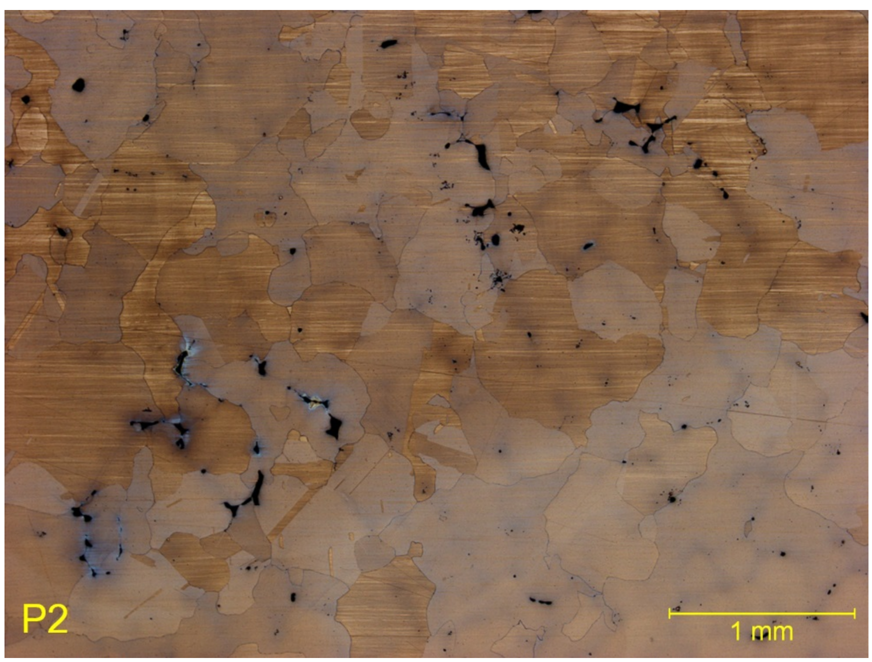

Figure 69: AMS Frog Casting Base Material Showing Multiple Voids

Figure 70: Weld Metal Showing Slag Inclusion

Figure 71: Horizontal Cracks Likely Due to Shear Loading [1]

Figure 72: Horizontal Cracks Likely Due to Shear Loading [(2)]

Figure 73 shows a crack in the base material adjacent to the fusion line of a weld pass from the first layer of the build-up repair. It is unclear whether this crack was present prior to welding, or it was induced by residual weld stresses in combination with base material discontinuities. Figure 74 shows a slag inclusion, as well as a base material crack. Since this crack does not extend into the weld, it can be concluded that this crack was present prior to welding. In both examples, the crack has not propagated to failure after over 118 MGTs, indicating good toughness of the base material and weld metal.

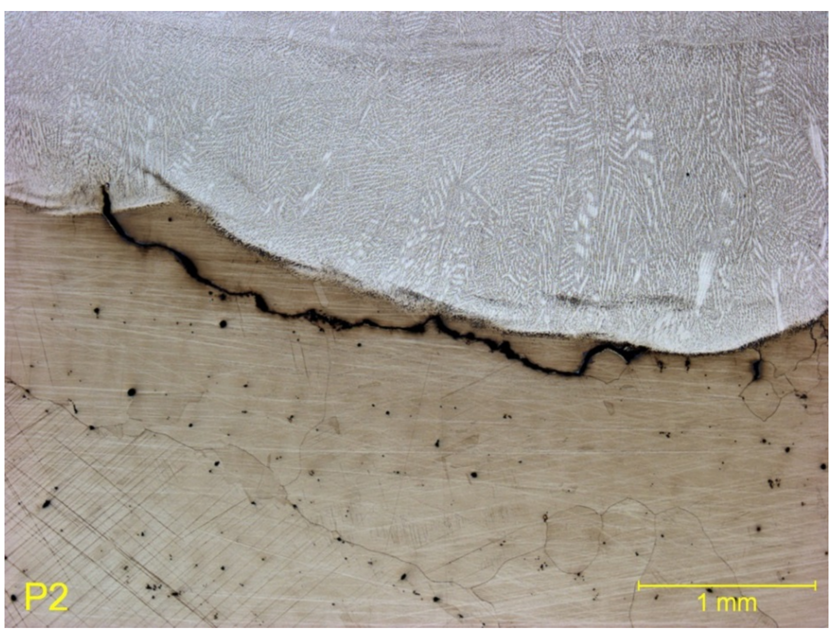

Figure 73: Crack in Base Material Adjacent to Weld Fusion Line

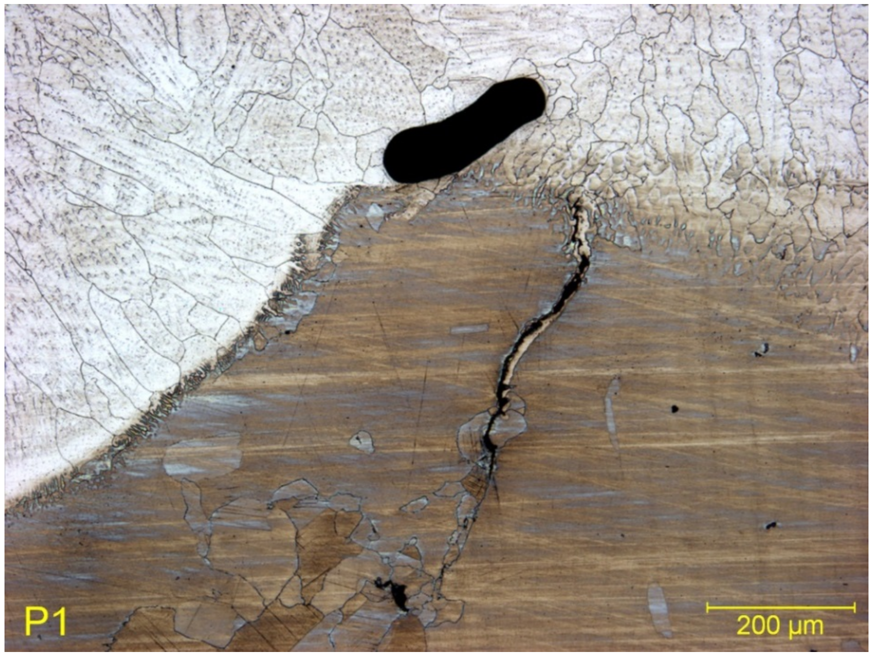

Figure 74: Slag Inclusion and Existing Base Material Crack

Surface cracks found in a cross-section of the point indicate significant shear loading. As shown in Figure 75, larger cracks were present at the surface, while a series of smaller, stacked horizontal cracks extended into the next weld layer. Figure 76 shows a close-up of these cracks, which were found in other cross sections from the point as well. These subsurface cracks are similar to those shown in Figure 71 and Figure 72.

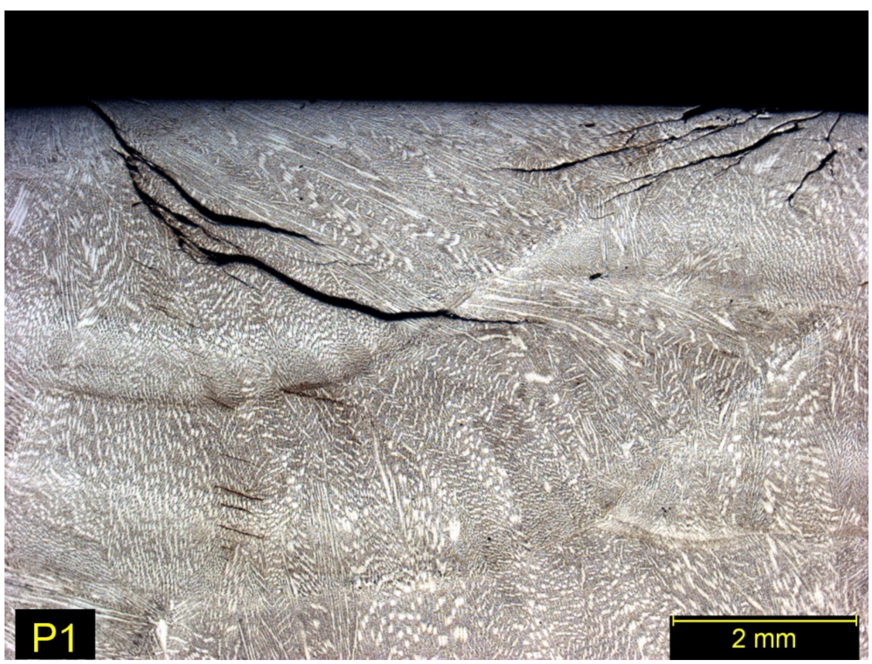

Figure 75: Surface and Sub-surface Cracking in Point

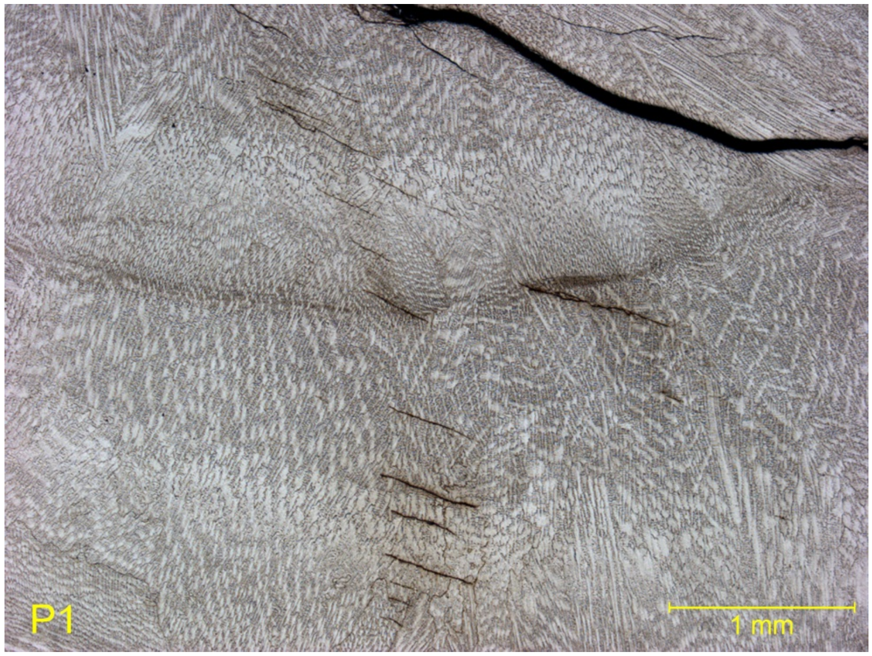

Figure 76: Close-up of Sub-surface Cracking in Point

As shown in Figure 64, surface spalling was observed at two locations on the point. The cross-section provided in Figure 77 shows the spalling located approximately 32 in past the point, at the location of complete load transfer from the wing to the point. Figure 78 shows corner cracking at the same location along the length of the point.

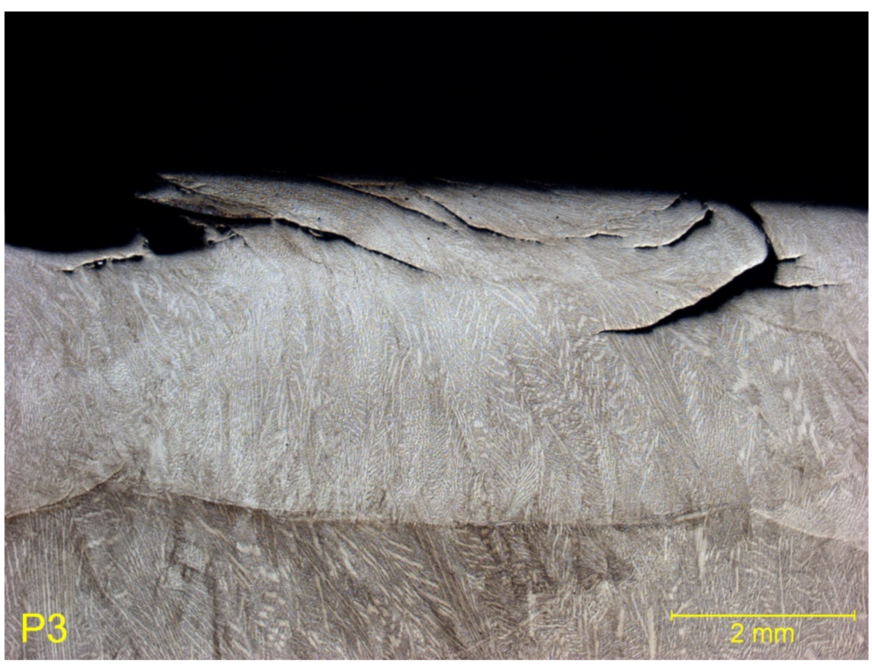

Figure 77: Surface Spalling 32 inches from Point

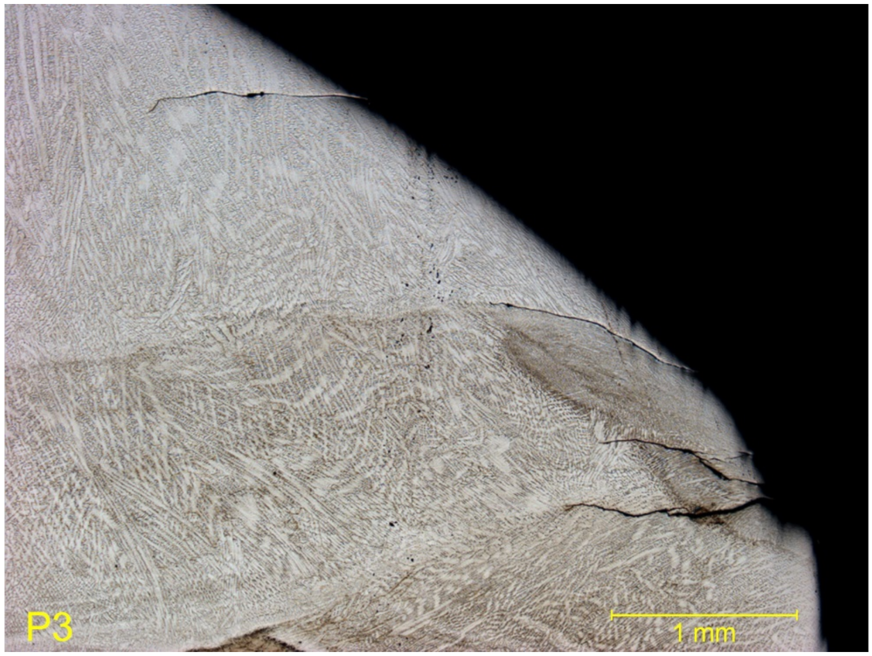

Figure 78: Cracking Located on Corner of Point

Photo-macrographs taken 9.5, 32 and 42 inches from the point are provided in Figure 79, Figure 80, and Figure 81, respectively. The weld deposit in Figure 81 is significantly shallower than the others because this area was welded to provide a smooth taper towards the heel of the point.

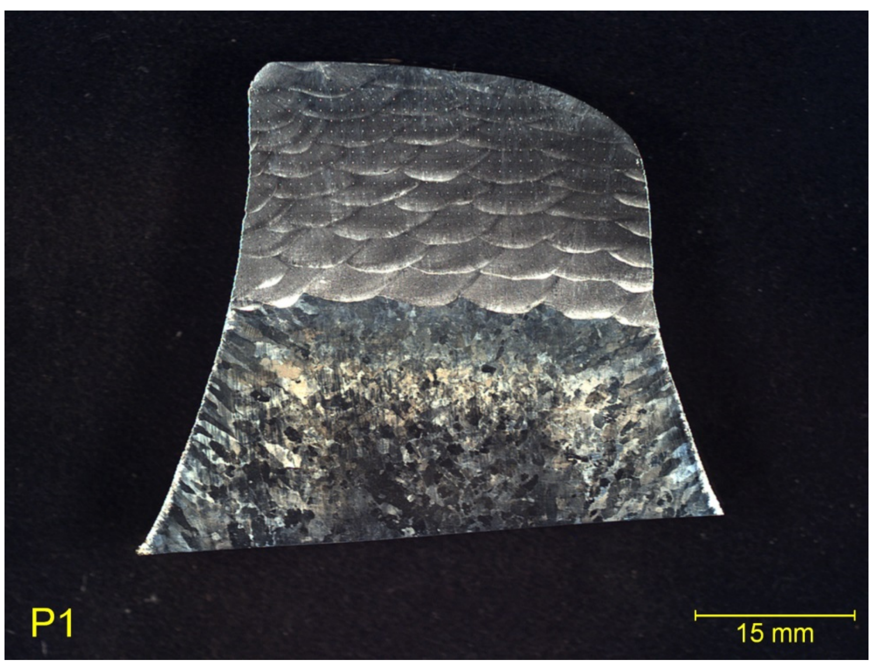

Figure 79: Cross-section Taken 9.5 inches from Point

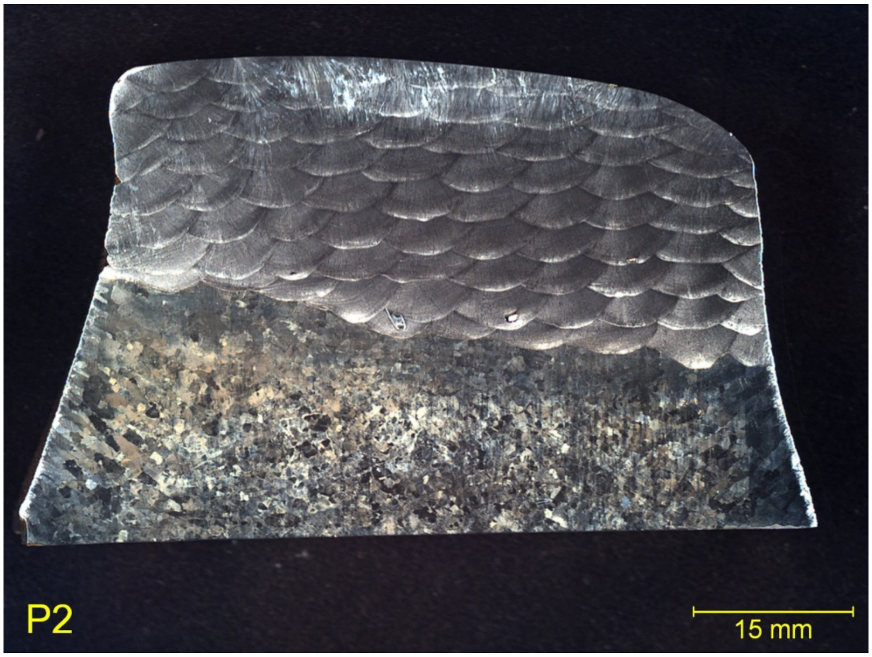

Figure 80: Cross-section Taken 32 inches from Point

Figure 81: Cross-section Taken 42 inches from Point

Photo-macrographs taken 8 and 19 inches from the wing are provided in Figure 82 and Figure 83, respectively. The increased deformation seen in Figure 82 is the result of a reduced contact patch created when the wheel moves towards the edge of the running surface. Deformation is reduced in Figure 83, since a greater portion of the load was carried by the point at that location along the length of the frog.

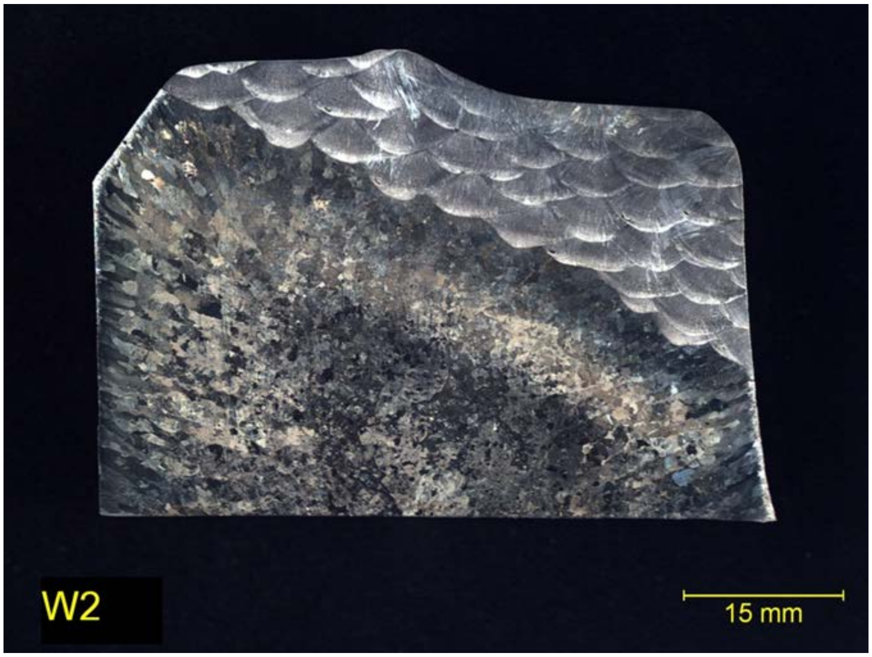

Figure 82: Cross-section Taken 8 inches from Wing

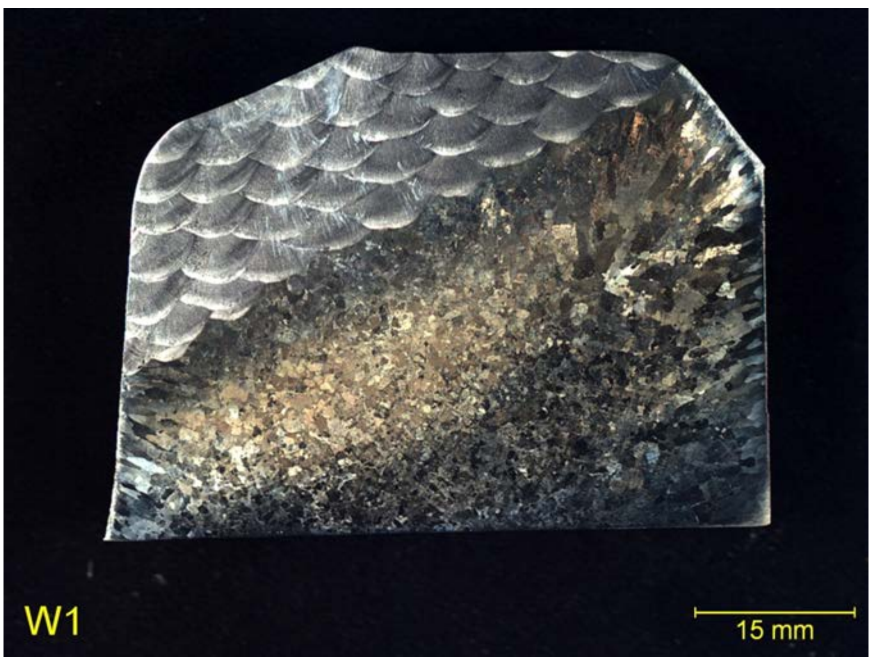

Figure 83: Cross-section Taken 19 inches from Wing

Figure 84 provides a hardness map of the point cross section shown in Figure 79. While the hardness of the base material and first layers was approximately the same, the layers above have been work-hardened with the hardest regions closest to the running surface. Figure 85 provides a hardness map of the cross section shown in Figure 82. The top layers of the reduced-contact-patch area have been work-hardened, with the hardest regions closest to the running surface.

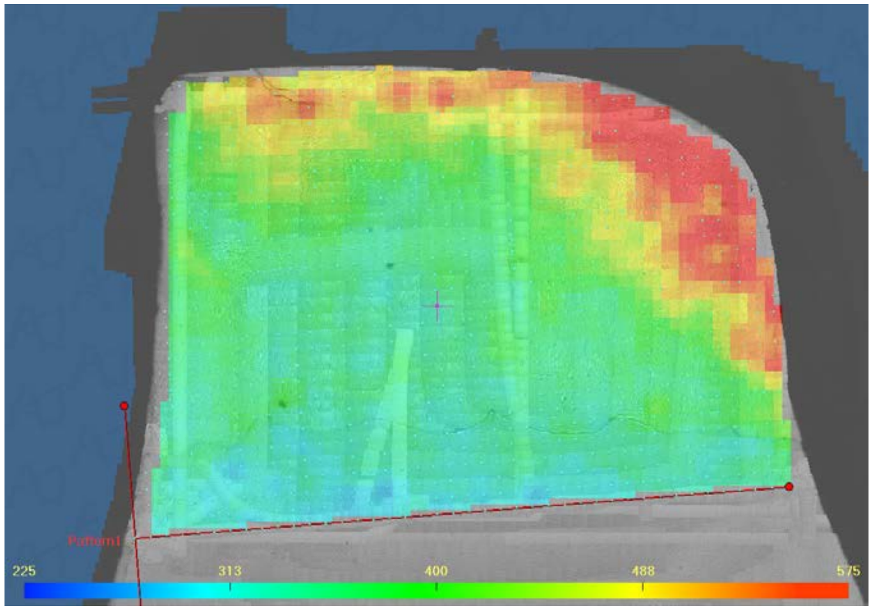

Figure 84: Point Hardness Map 9.5 inches from Point

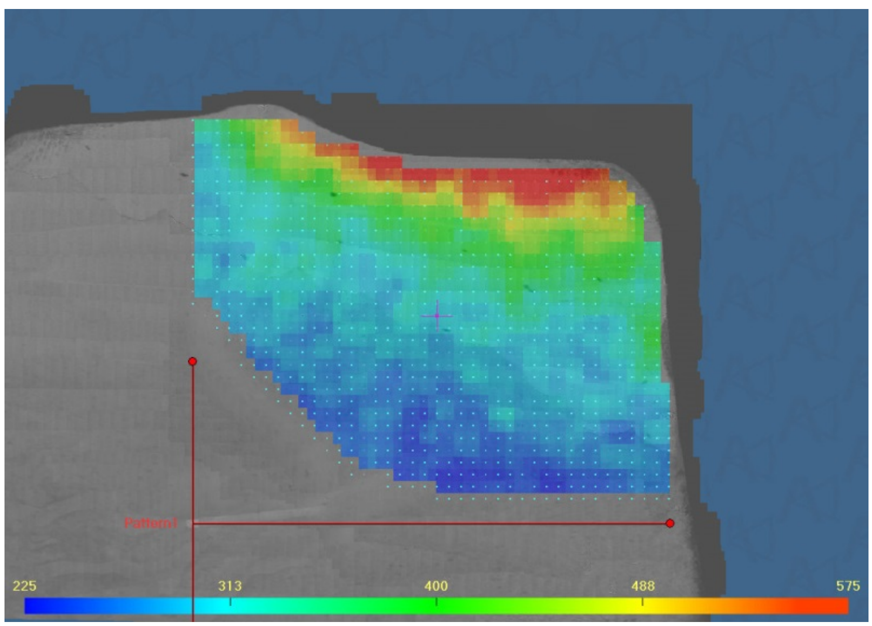

Figure 85: Wing Hardness Map 8 inches from Point

Table 24 provides results from a chemical analysis of the Frog #2 weld repair. In addition, the cross-sections provided in Figure 86 and Figure 87 were examined to identify the microstructures present. The eutectoid structure of the automated FCAW repair weld is associated with increased yield strength and is expected to reduce the "flow," which should lead to better durability.

Table 24: Chemical Compositions of Automated FCAW Repaired Weld

`1	FCAW-A Repair
Aluminum	0.003
Carbon	0.82
Chromium	3.92
Cobalt	—
Copper	0.039
Iron	Balance
Manganese	14.6
Molybdenum	—
Nickel	0.60
Niobium	—
Phosphorus	0.015
Silicon	0.004
Sulfur	0.010
Titanium	0.003
Tungsten	0.008
Vanadium	0.009

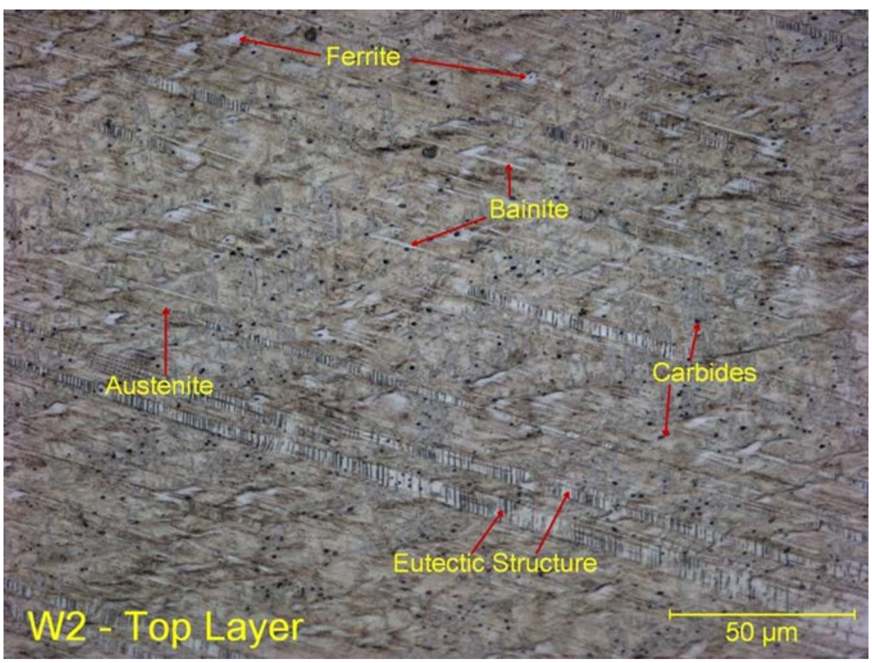

Figure 86: Automated FCAW Repair Microstructure – Top Layer

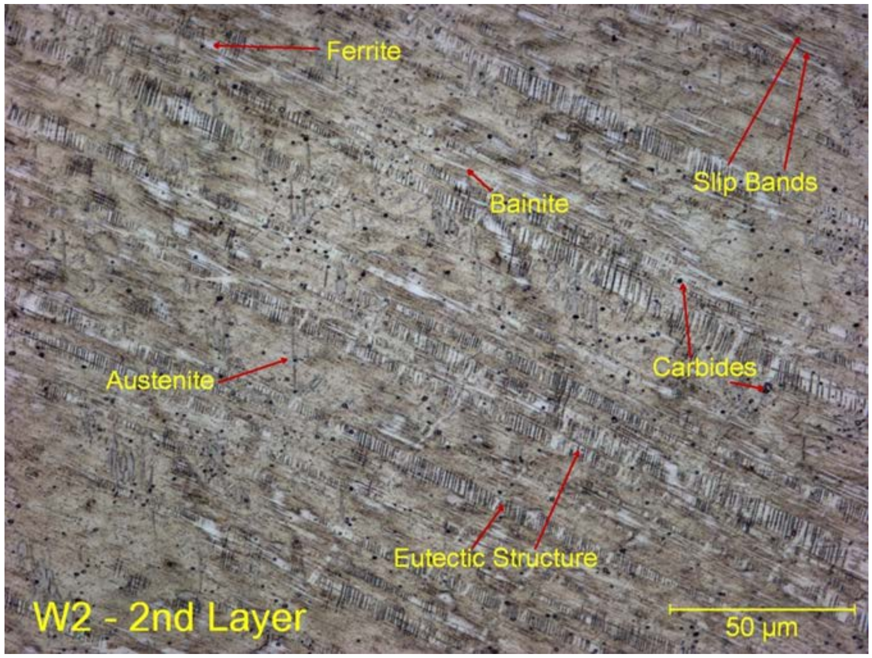

Figure 87: Automated FCAW Repair Microstructure – Second Layer

4.2.1 EWI Laboratory Testing Summary

The results of EWI's post-test investigation indicate that the repair weld is of higher quality than repairs made with current techniques. EWI's examination of observed cracks indicates good toughness, which corresponds to the results of TTCI's in-track testing. No correlation was found between weld discontinuities and weld defects, indicating that no significant benefit would be realized by an increase in weld quality alone. The presence of pre-existing base material cracks indicated that there was resistance to crack propagation, which further increases durability.

5. Automation Concept

5.1 Automated Repair System Concept

EWI created an in-track repair automation concept, illustrated in Figure 88 through Figure 92. In this concept, two 6-axis robots are housed in a box truck, along with the required robot power supplies, and a welding power supply (Figure 88). This concept includes a water tank mounted on the underside of the truck (not pictured) as well as a supply of abrasive required for water-jet cutting. Linkage would be included to allow the robot cart to be lowered onto the track (Figure 89).

The robot cart is designed with a cutaway on either side to allow frog repair regardless of the direction of the truck. The water-jet cutting robot would be used to prepare the frog for welding by removing defective material. Welding would then be completed by the arc welding robot. It may be possible to complete post-weld preparation using the water-jet cutting robot instead of grinding. If not, post-weld grinding would be completed using existing methods.

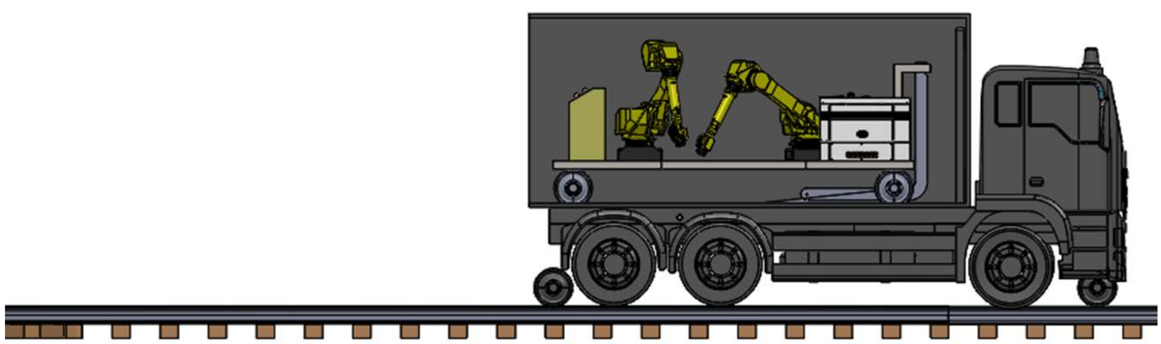

Figure 88: Automation Concept with Robot Cart Retracted

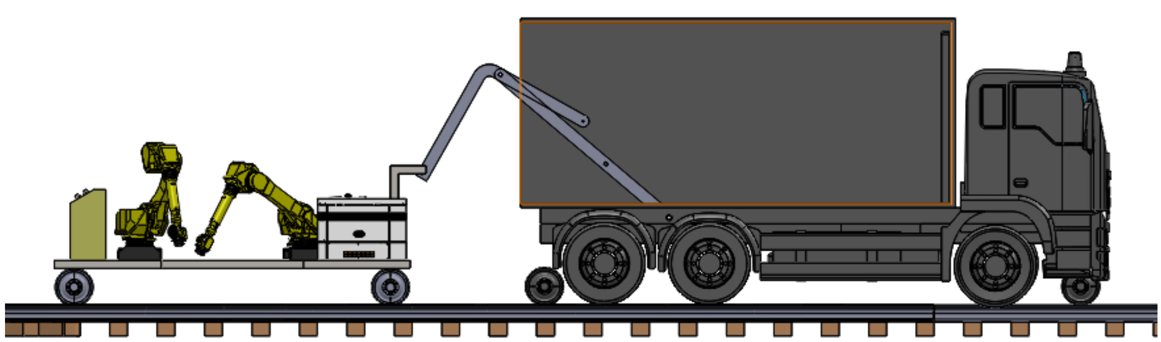

Figure 89: Automation Concept Showing Deployed Robot Cart (View 1)

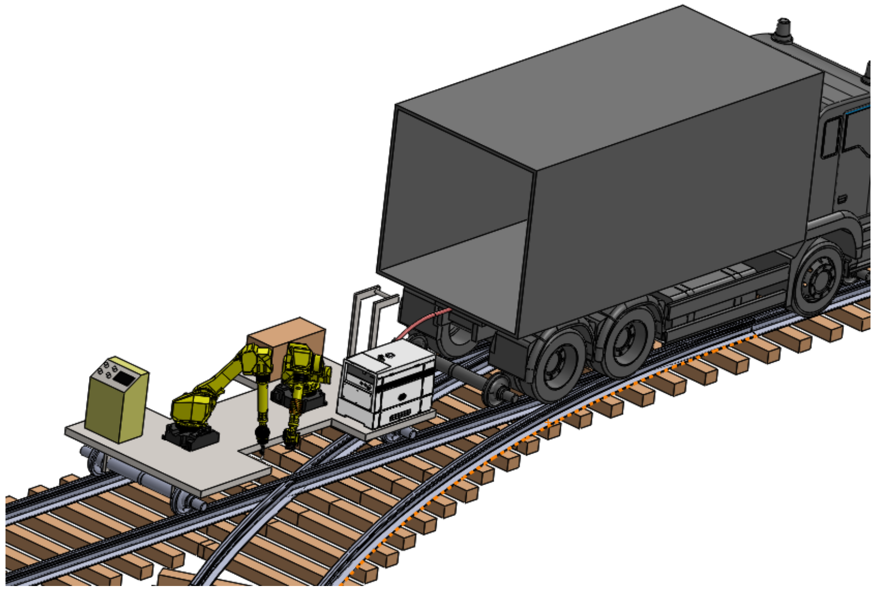

Figure 90: Automation Concept Showing Deployed Robot Cart (View 2)

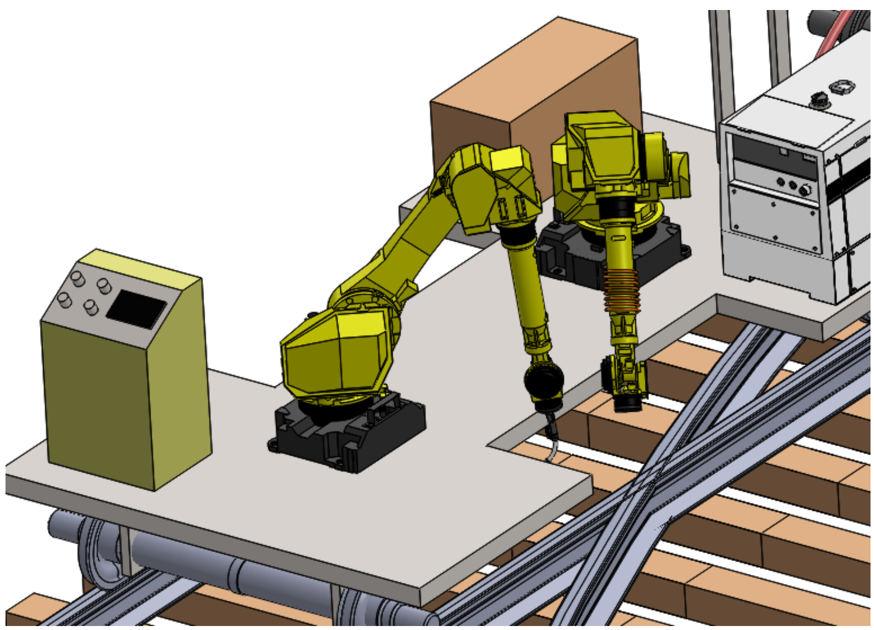

Figure 91: Close-up View of Robot Cart

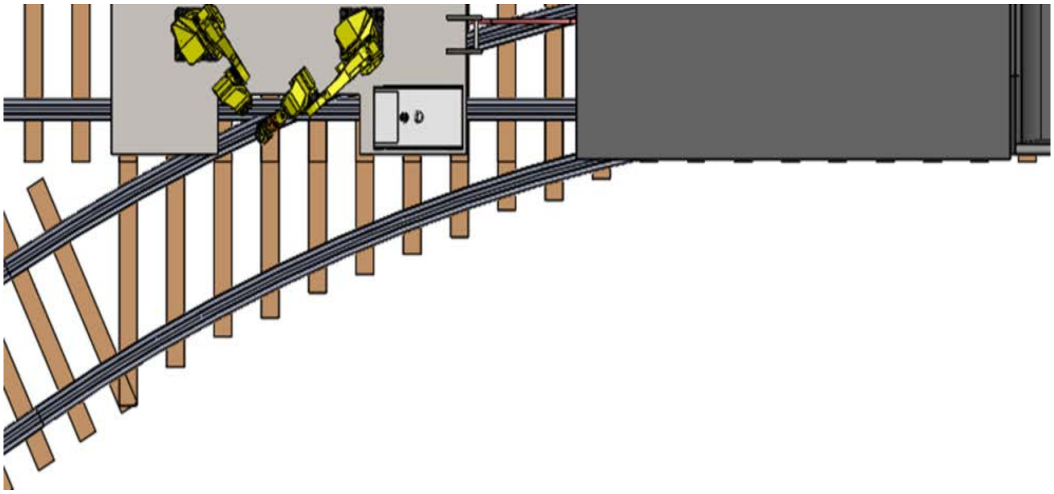

Figure 92: Top View of Automation Concept

5.2 Repair Approach Concept

The level of wear/damage and the resultant level of repair required can vary significantly between frogs. Technology to address these variations exists, but can add significantly to the cost and complexity of the repair solution. An alternate option is to create a known geometry in the most commonly damaged areas and to preprogram the corresponding robot paths to complete the repair of that geometry. This system proposes to use the latter of these two solutions. Since the level of wear can vary from frog to frog, operators will be able to choose between a number of different "wear levels". The intent of this strategy is to limit excess material removal while still standardizing the geometry. In addition to variations in the level of repair required, railroads use a number of different frog geometries. These geometries vary with the frog number (indicative of the angle of the frog) or the frog type (flat versus conformal). The most commonly used frogs would be included in the program list. Operators would then choose a frog type and level of wear to select the correct repair sequence.

6. Conclusions

EWI has successfully used automated FCAW to significantly improve the durability of repaired AMS railroad frogs compared to currently used processes and techniques:

- Multiple parameter sets produced a weld repair requiring the minimum amount of post-weld grinding to increase overall efficiency.
- Significant decrease in heat input reduced heating of the frog, which shortens the waiting time required for the frog to cool to an acceptable temperature before resuming welding.
- A specialized crack mitigation technique allowed welds to be placed adjacent to work-hardened material without base material cracking. The modified procedure does not add additional time to the repair process, and therefore will have no effect on productivity.

The use of automated FCAW resulted in a significant increase in weld quality compared to field-repaired samples and mock baseline samples created in the field and in EWI's lab. An AMS frog repaired using EWI's technique was subjected to over 118 MGTs in TTC's test track. This represented a 240 percent increase in service life compared to the average life of repaired frogs, and a 107 percent increase over the service life of new frogs.

At the time that the test frog was removed from the track, the running surface wear was significantly below the maximum, which indicated that the frog could have remained in track. Good weld quality can be seen in the ultrasound testing (UT) results, RT results, and in cross sections taken from the completed weld after the conclusion of testing. EWI's evaluation of cross-sections taken from the wing and point indicates good toughness and increased weld quality over baseline and field-repaired samples.

As a result of these significant gains, EWI has proposed a follow-up project to place frogs that have been repaired with this technique into revenue service so they can be tested in the field. In addition, EWI has identified the following areas for future research:

- UT evaluation of current weld quality, to create a baseline against which frogs repaired using automation can be compared.
- Use of metal-cored wire to improve weld quality and eliminate the need for time-consuming interpass cleaning required by the current FCAW consumable.
- Use of ultrasonic machining to prepare frogs for welding by removing damaged base material and/or previous repairs, and to complete final machining. Railroads that have participated in Phase I and Phase II have identified this topic as an area of significant concern.
- Create an automation demonstration that showcases the technologies, techniques, and concepts that will be incorporated into the final integrated solution.

7. References

(1) Davis, D., Sun, J., Terrill, V., and Hansen, B., "Industry Survey of Frog Weld Repair Best Practices," Association of American Railroads Research and Test Department Technology Digest, 1997.

(2) Davis, D. D. and Rogers, P. D., "Comparison of Weld Repairs for Standard and High-Integrity Rail Bound Manganese Frogs in Heavy Haul Service," Association of American Railroads Research and Test Department Technology Digest, 1996.

(3) Subramanyam, D. K., Swansiger, A. E., Avery, H. S., "Austenitic AMSs," ASM Handbook Volume 1, Properties and Selection: Irons, Steels, and High-Performance Alloys, pp. 822-840, 1990.

(4) Handbook for Track Welders: MW&S Standard Procedure for Welding Repairs to Rail and Track Fixtures and Grinding", Norfolk Southern Corporation, December 1992.

(5) "How to Repair AMS Castings," Abex Corporation Amsco Division, Bulletin WB-873.

(6) "Instructions Governing the Inspection, Welding, Grinding and Heat Treatment of Track Components," Union Pacific Railroad Company Engineering Services, November 1990.

(7) "Recommended Practices for the Welding of Rails and Rail Related Components for Use By Rail Vehicles," American Welding Society AWS D15.2, pp. 21-23, 2003.

(8) "Welding Alloys for Railroad Track Maintenance," McKay Technical Report.

FROG WELD REPAIR: AN IN-TRACK TEST AT THE FACILITY FOR ACCELERATED SERVICE TESTING

Letter Report No. P14-14-042
Prepared for Edison Welding Institute
by Rafael Jimenez and David Davis
Transportation Technology Center, Inc.

...a subsidiary of the Association of American Railroads
P. O. Box 11130, Pueblo, Colorado 81001 USA December 9, 2014

Disclaimer: This report was prepared for Edison Welding Institute (EWI), by Transportation Technology Center, Inc. (TTCI), a subsidiary of the Association of American Railroads, Pueblo, Colorado. It is based on investigations and tests conducted by TTCI with the direct participation of EWI to criteria approved by them. The contents of this report imply no endorsements whatsoever by TTCI of products, services or procedures, nor are they intended to suggest the applicability of the test results under circumstances other than those described in this report. The results and findings contained in this report are the sole property of EWO. They may not be released by anyone to any party other than EWI without the written permission of EWI. TTCI is not a source of information with respect to these tests, nor is it a source of copies of this report. TTCI makes no representations or warranties, either expressed or implied, with respect to this report or its contents. TTCI assumes no liability to anyone for special, collateral, exemplary, indirect, incidental, consequential, or any other kind of damages resulting from the use or application of this report or its contents.

Table of Contents

1.0 INTRODUCTION 1
2.0 PROCEDURES 1
  2.1 Test Frogs 1
  2.2 Test Environment 4
3.0 MEASUREMENTS 5
  3.1 Running-Surface Wear Performance 5
    3.1.1 Running-Surface Wear Results 6
  3.2 Running-Surface Hardness 12
    3.2.1 Running-Surface Hardness Results 13
  3.3 Track Geometry 14
  3.4 Frog Components Maintenance 14
4.0 FINAL INSPECTION 15
5.0 TEST TERMINATION 17
  5.1 Disposition of Test Frogs 17
Attachment 1: Profiles A-1
Attachment 2: Running Surface Wear Data Tables A-2
Attachment 3: Hardness Data Table A-3
Attachment 4: Updates submitted to EWI during Period of Performance A-4

List of Figures

Figure 1. Frog 1: Wing rail repair about 36 inches long; point repair about 48 inches long 1

Figure 2. Frog 2: Wing rail repair about 36 inches long; point repair about 43 inches long 2

Figure 3. Weld repaired Frog 2 after grinding excess weld material 3

Figure 4. Frog 1: Transverse crack near the point of the frog visible with dye penetrant 4

Figure 5. Frog 2 installed in Section 27 of the High Tonnage Loop 4

Figure 6. Frog Point: Measurement location 16, 32 inches past the POF — overlay of the newly ground (0 MGT) weld repaired frog point profile and the final profile (100 MGT) 7

Figure 7. Frog Point: Cumulative wear on the frog point at measurement location 16, 32 inches past the POF 7

Figure 8. Frog Point: Measurement interval wear rate on the frog point at measurement location 16, 32 inches past the POF 8

Figure 9. Frog Wing Rail: Measurement location 25, 8 inches ahead the POF — overlay of the newly ground (0 MGT) weld repaired frog wing rail profile and the final profile (100 MGT) 9

Figure 10. Frog Wing Rail: Wear on the frog point at measurement location 25, 8 inches ahead the POF 9

Figure 11. Frog Wing Rail: Measurement interval wear rate on the frog point at measurement location 25, 8 inches ahead the POF 10

Figure 12. Frog Point: Total running surface wear at each measurement location on the frog point 10

Figure 13. Wing Rail: Total running surface wear at each measurement location on the wing rail 11

Figure 14. Test-total wear (area loss) of the wing rail and the frog point at each measurement location 11

Figure 15. Test-total wear (height loss) of the wing rail and the frog point at each measurement location 12

Figure 16. Frog point running surface hardness 13

Figure 17. Wing rail running surface hardness 13

Figure 18. Final inspection: running surface spalls developing on the frog point 15

Figure 19. Final inspection: close-up of running surface spalls developing on the frog point 15

Figure 20. Final inspection: close-up running surface spalls developing on the frog point 16
Figure 21. Final inspection: minor running surface pitting on the wing rail 16
Figure 22. Test Frog 2 cut and ready for return shipping to EWI 17

List of Tables

Table 1. Running-surface profile measurement locations 5
Table 2. Profile locations used to represent wear and plastic flow on the point and on the wing rail 6
Table 3. Running-surface hardness measurement locations 12

1.0 INTRODUCTION

At the request of Edison Welding Institute (EWI), Transportation Technology Center, Inc. (TTCI) conducted a weld repaired frog performance test under heavy axle loads (HAL) at the Facility for Accelerated Service Testing (FAST) in Pueblo, Colorado.

2.0 PROCEDURES

2.1 Test Frogs

TTCI provided and shipped two No. 20 railbound manganese (RBM) frogs to EWI's facility for weld repairs. Frog 1 (Figure 1) had been removed from the High Tonnage Loop (HTL) at FAST because of running surface wear and damage. Frog 2 (Figure 2) had been in HTL service briefly for about 6 million gross tons (MGT) of HAL traffic.

EWI returned the frogs to TTCI after the weld repairs had been completed (Figures 1 and 2) and asked TTCI to perform the grinding work (Figure 3).

TTCI welders ground the excess weld repair material from both test frogs. Figure 3 shows Frog 2 ready for installation on the HTL after grinding was completed.

Figure 1. Frog 1: Wing rail repair about 36 inches long; point repair about 48 inches long

Figure 2. Frog 2: Wing rail repair about 36 inches long; point repair about 43 inches long

Figure 3. Weld repaired Frog 2 after grinding excess weld material

Nondestructive testing (dye penetrant and ultrasonic) was performed on the two frogs after grinding was completed. The results indicated that Frog 1 had a transverse crack near the point of frog at the interface of the weld repair material and the original frog casting material (Figure 4). TTCI's track engineering group decided that Frog 1 would not be installed in track.

Figure 4. Frog 1: Transverse crack near the point of the frog visible with dye penetrant

2.2 Test Environment

Frog 2, with its corresponding plate work and guardrail, was installed on new 9-foot ties and ultimately welded in place on tangent track in Section 27 of the HTL, as Figure 5 shows.

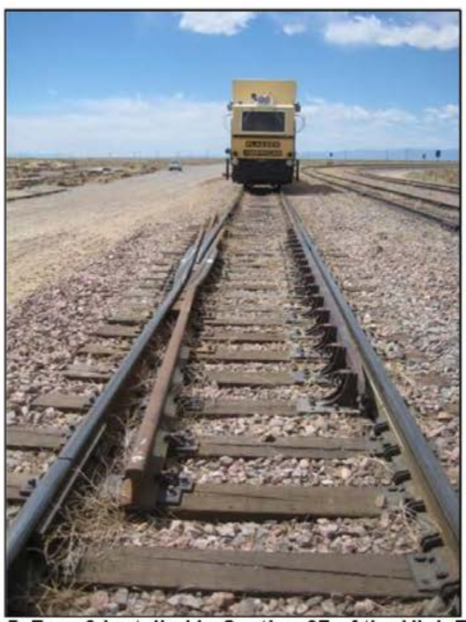

Figure 5. Frog 2 installed in Section 27 of the High Tonnage Loop

The 39-ton HAL train that operated over the test frog at 40 MPH consisted of about 110 cars. The frog was in service for 118.16 MGT of HAL traffic.

Given that the frog was installed in open track, not in a turnout, the frog point and one wing rail were subjected to the HAL traffic.

3.0 MEASUREMENTS

3.1 Running-Surface Wear Performance

TTCI measured the running-surface profile of the frog using MiniProf™ at the locations listed in Table 1. The measurements were taken at the following nominal tonnage (MGT) intervals: baseline (0), 2, 5, 10, 20, 40, 85, and 100.

Table 1. Running-surface profile measurement locations

Measurement Location on the Frog	Mainline Wing Rail (Measurement Location Number)	Frog Point (Measurement Location Number)
-16"	19	N/A
-8"	20	N/A
Point	21	N/A
+2"	22	1
+4"	23	2
+6"	24	3
+8"	25	4
+10"	26	5
+12"	27	6
+14"	28	7
+16"	29	8
+18"	30	9
+20"	31	10
+22"	32	11
+24"	33	12
+26"	34	13
+28"	N/A	14
+30"	N/A	15
+32"	N/A	16
+34"	N/A	17
+36"	N/A	18

3.1.1 Running-Surface Wear Results

Table 2 lists the two locations selected to represent the wear and plastic flow measured on Frog 2 in the periodic updates sent to EWI and in this final report. These include one location on the point at 32 inches past the point of frog (POF) and one location on the wing rail at 8 inches ahead of the POF.

Table 2. Profile locations used to represent wear and plastic flow on the point and on the wing rail

Location on Frog	Location Relative to POF	Test Frog 2 Measurement Number
Point	32 in. past POF	16
Wing Rail	8 in. ahead of POF	25

MiniProf™ software was used to calculate area loss (wear) and area gain (plastic flow) in terms of mm^2 at each of the measurement locations.

Figure 6 is an overlay of the newly ground (0 MGT) frog profile (blue line) and the final profile (red line) at location 16, 32 inches past the POF. Material wear is the area below the blue line and above the red line. Material plastic flow is the sum of the areas right of the blue line to the red line on the right side of the overlay (traffic side) and left of the blue line to the red line on the left side of the overlay (non-traffic side).

The total wear measured was 213.00 mm^2, as Figure 7 shows, and the final flow measured was 27.07 mm^2. Grinding was done to remove some of the material flow on the traffic side of the point when the frog had been in service 18 MGT. The result of this grinding reduced the material flow from 31.65 mm^2 to 13.63 mm^2. The material flow on the non-traffic side of the frog point was not ground during the test; some of this material would have been removed by wheels in a turnout operation. Figure 8 shows that the wear rate, calculated for each measurement interval reached a steady state after 60 MGT.

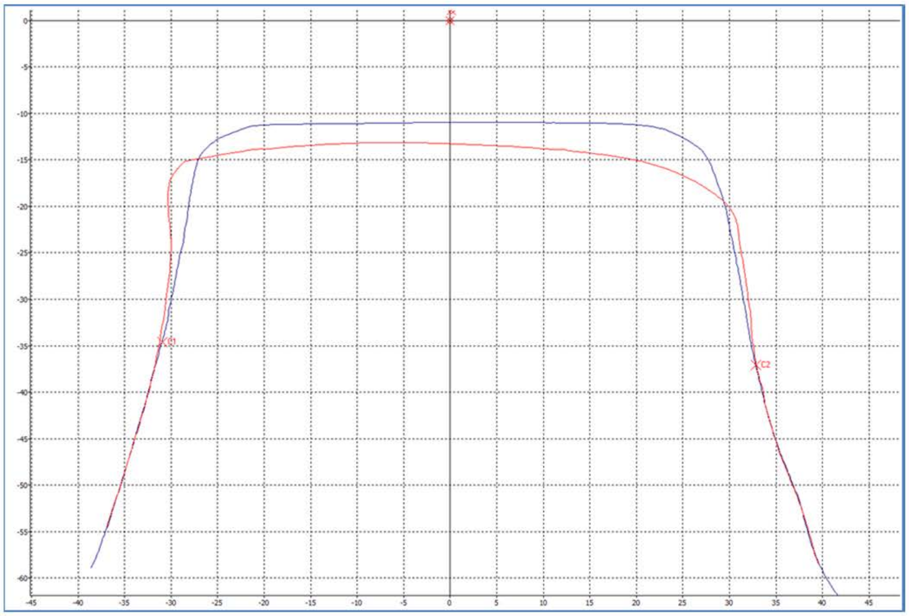

Figure 6. Frog Point: Measurement location 16, 32 inches past the POF — overlay of the newly ground (0 MGT) weld repaired frog point profile and the final profile (100 MGT)

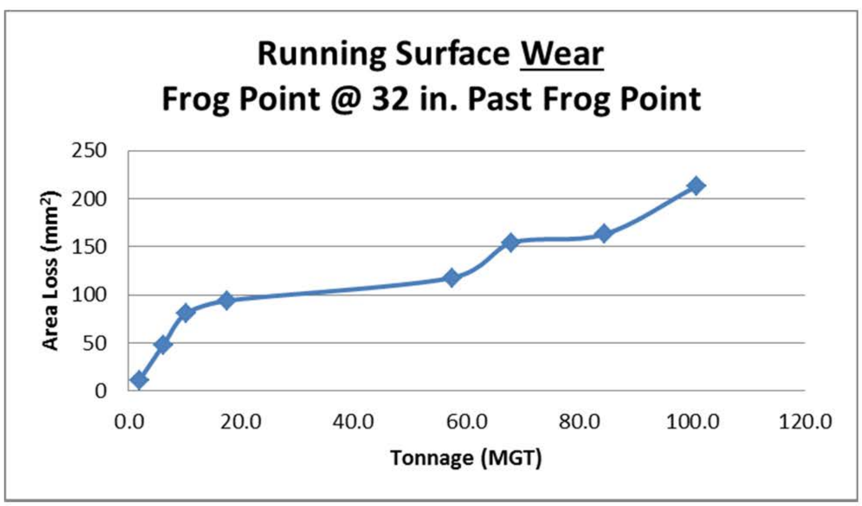

Figure 7. Frog Point: Cumulative wear on the frog point at measurement location 16, 32 inches past the POF

7

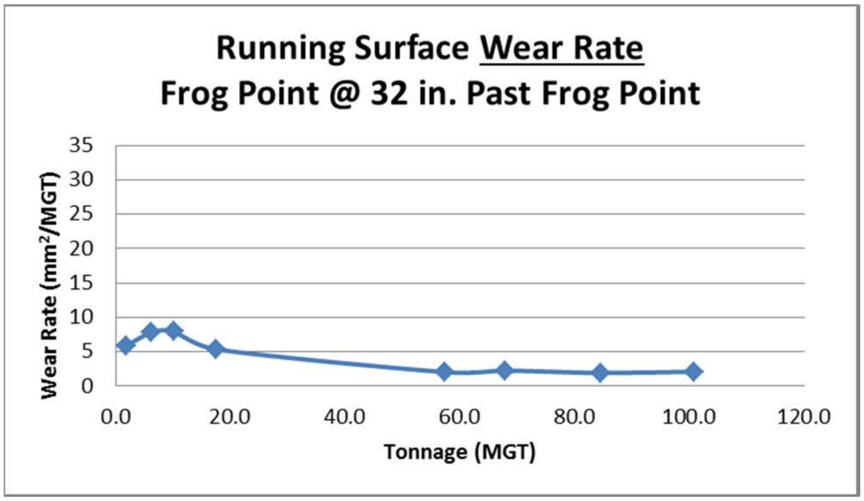

Figure 8. Frog Point: Measurement interval wear rate on the frog point at measurement location 16, 32 inches past the POF

Figure 9 is an overlay of the newly ground (0 MGT) wing rail profile (blue line) and the final profile (red line) at location 25, 8 inches ahead the POF. Material wear is the area below the blue line and above the red line. Material plastic flow is the sum of the areas where the blue line is beyond the red line.

The total wear measured was 65.67 mm^2, as Figure 10 shows, and the final flow measured was 19.43 mm^2. Grinding was done to remove some of the material flow on the gage side of the wing rail when the frog had been in service 18 MGT. The result of this grinding reduced the material flow from 33.63 mm^2 to 12.78 mm^2. The material flow on the top of the wing rail was not ground during the test. Figure 11 shows that the wear rate, calculated for each measurement interval, reached a steady state after 60 MGT.

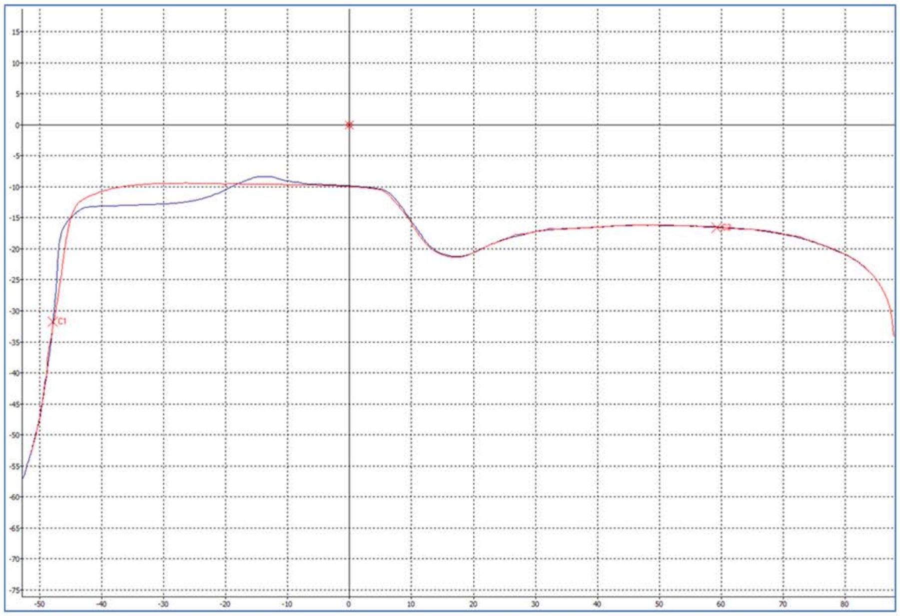

Figure 9. Frog Wing Rail: Measurement location 25, 8 inches ahead the POF — overlay of the newly ground (0 MGT) weld repaired frog wing rail profile and the final profile (100 MGT)

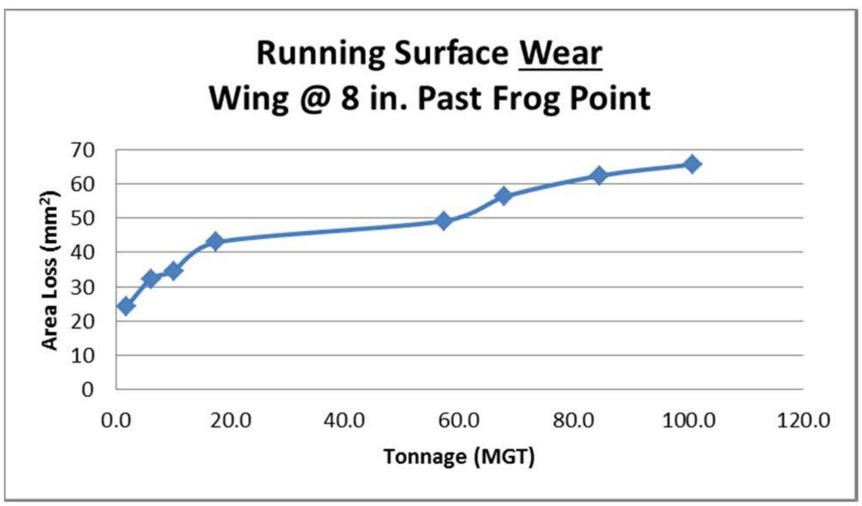

Figure 10. Frog Wing Rail: Wear on the frog point at measurement location 25, 8 inches ahead the POF

9

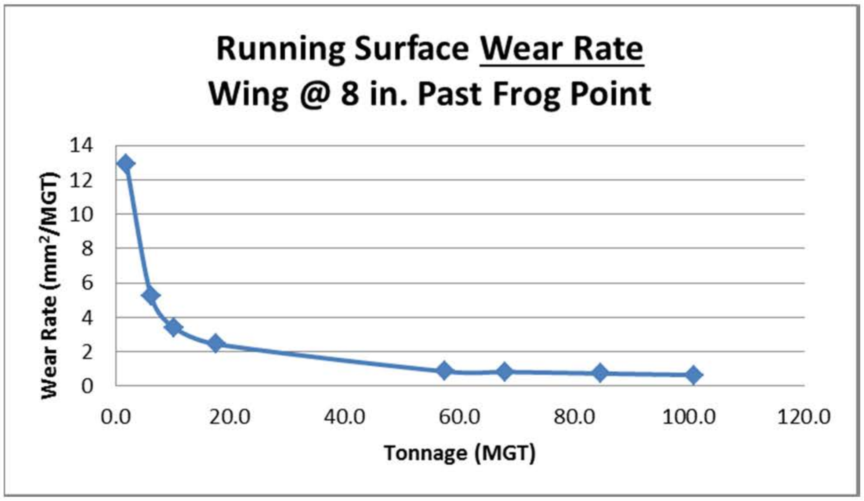

Figure 11. Frog Wing Rail: Measurement interval wear rate on the frog point at measurement location 25, 8 inches ahead the POF

Figures 12 and 13 show the test-total running surface wear (area loss) at each of the measurement locations on the frog point and the wing rail, respectively.

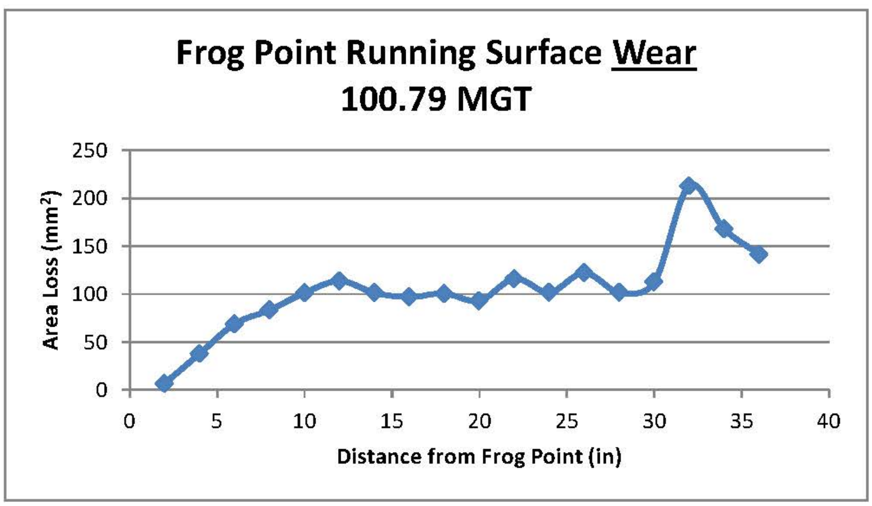

Figure 12. Frog Point: Total running surface wear at each measurement location on the frog point

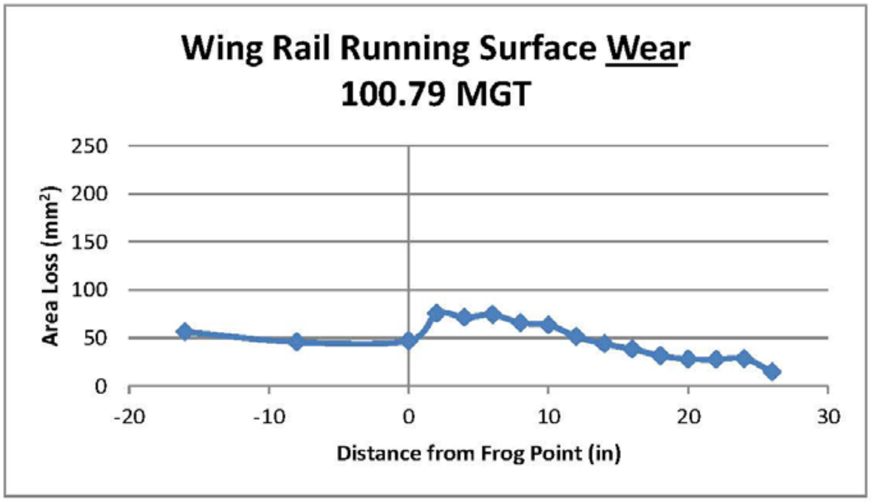

Figure 13. Wing Rail: Total running surface wear at each measurement location on the wing rail

Figure 14 combines the data presented in Figures 12 and 13 to show the relative wear (area loss) of the wing rail and the frog point. Figure 15 shows the total-test relative wear (height loss) of the same two components.

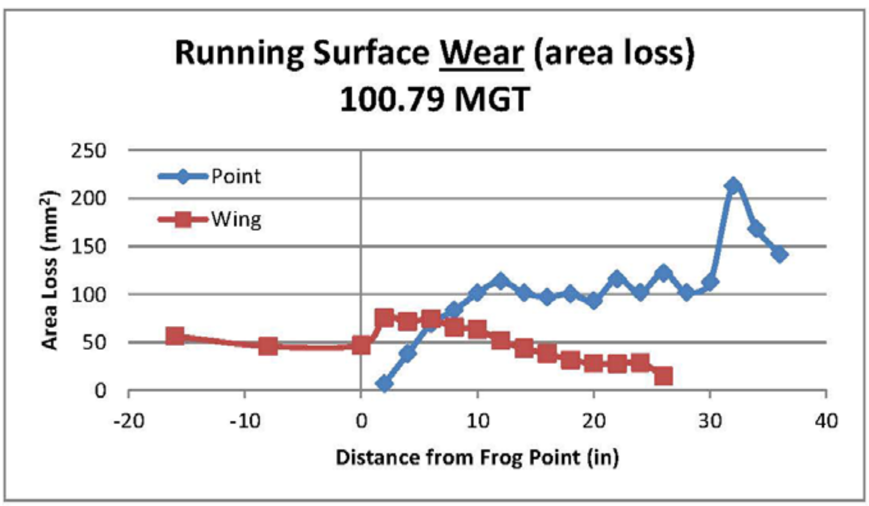

Figure 14. Test-total wear (area loss) of the wing rail and the frog point at each measurement location

11

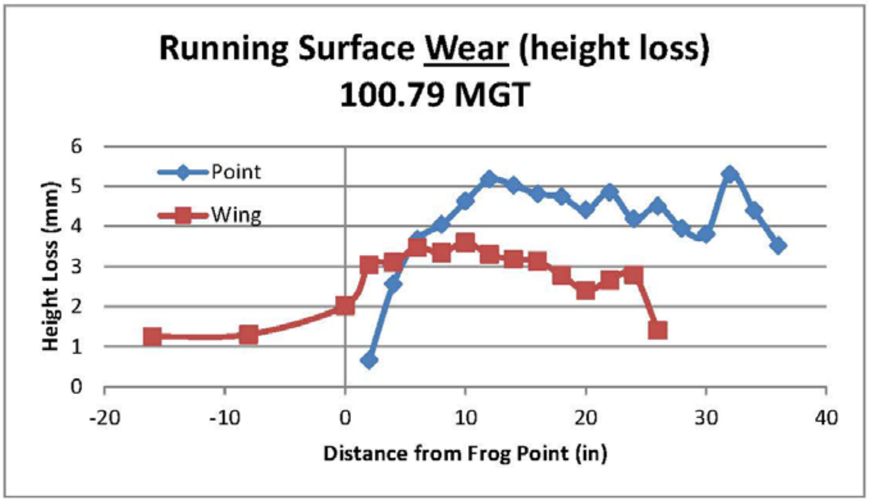

Figure 15. Test-total wear (height loss) of the wing rail and the frog point at each measurement location

3.2 Running-Surface Hardness

The running-surface hardness (BHN) was measured using a Proceq EquoTip portable hardness testing device at the same MGT intervals as the profiles at the locations shown in Table 3.

Table 3. Running-surface hardness measurement locations

Distance Relative to POF	Measurements Taken on the Wing Rail	Measurements Taken on the Frog Point
-16"	√	N/A
-8"	√	N/A
+2	√	N/A
+8"	√	√
+16"	√	√
+22	√	√

3.2.1 Running-Surface Hardness Results

Figures 16 and 17 show the running surface hardness measured on the frog point and the wing rail.

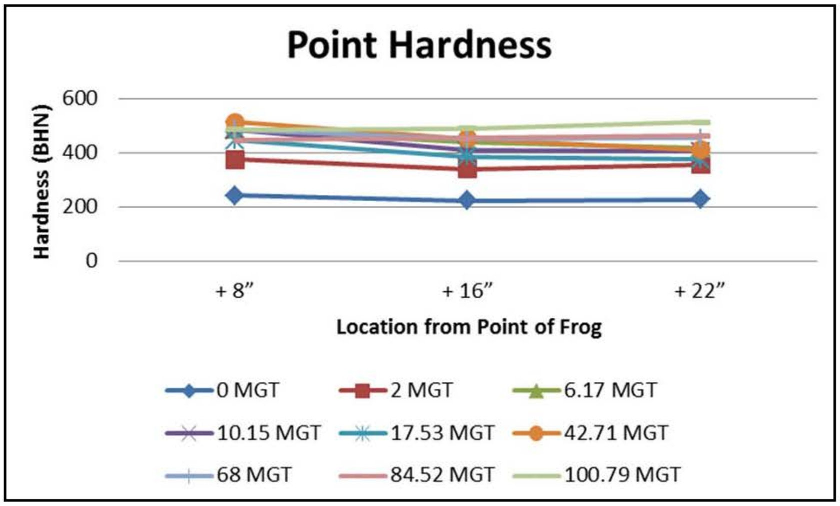

Figure 16. Frog point running surface hardness

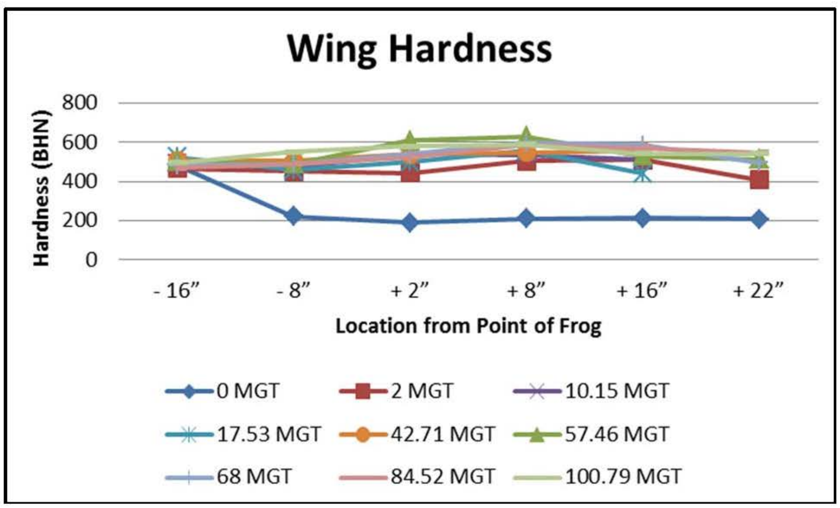

Figure 17. Wing rail running surface hardness

13

3.3 Track Geometry

The HTL, where the frog test was conducted, is maintained to FRA Class 4 track standards. There was no track geometry maintenance required during the period of performance.

3.4 Frog Components Maintenance

Table 4 lists the maintenance work performed on the test frog.

Table 4. Maintenance performed on Test Frog 2

Test Frog No. 2					
Item	**Date**	**Tonnage (MGT)**	**Description**	**Component**	**Measurements**
1	4/21/14	0	Weld Repair Flaw Inspection	Test Frog	Ultrasonic and Dye Penetrant
2	4/22/14	0	Installed in HTL Section 27	Test Frog	Profiles and Hardness
3	5/8/14	10.15	• Slight Vertical Dip (~0.027 inch) on the tread running surface • Ground Slight Bulge at Gage Face	Wing Rail	Profiles
4			Ground Metal Flow, Gage Corner, Entire Length of Frog Point	Frog Point	
5	5/15/14	17.53	Ground Metal Flow, Gage Corner, Entire Length of Frog Point and Wing Rail	Wing Rail	Profiles
6				Frog Point	

4.0 FINAL INSPECTION

Figures 18–20 show the condition of the running surface of the frog point, where spalling was developing at the two interface locations of the weld repair and the original casting material. There was minor pitting on the running surface of the wing rail at the wheel transfer location, Figure 21.

Figure 18. Final inspection: Running surface spalls developing on the frog point

Figure 19. Final inspection: Close-up of running surface spalls developing on the frog point

Figure 20. Final inspection: Close-up running surface spalls developing on the frog point

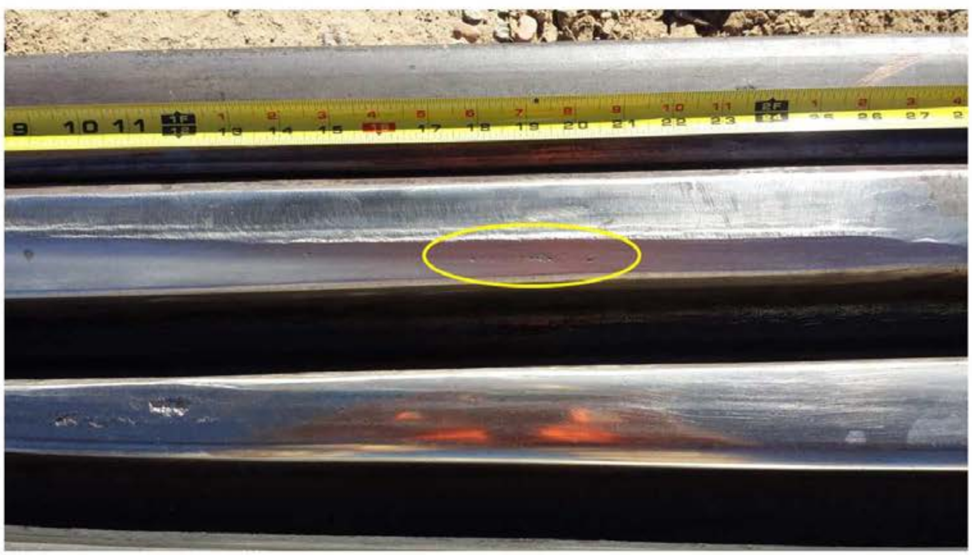

Figure 21. Final inspection: Minor running surface pitting on the wing rail

5.0 TEST TERMINATION

The test was terminated on November 4, 2014, when the frog was removed from the HTL in compliance with the contracted period of performance, which specified a minimum 100 MGT. The test frog was in service 118.16 MGT. Based on visual inspection at the time it was removed from track, the frog could have remained in service.

5.1 Disposition of Test Frogs

Frog 2 was cut to facilitate handling before it was returned to EWI (Figure 22). Frog 1 remains at TTCI.

Figure 22. Test Frog 2 cut and ready for return shipping to EWI

Attachment 1
Profiles

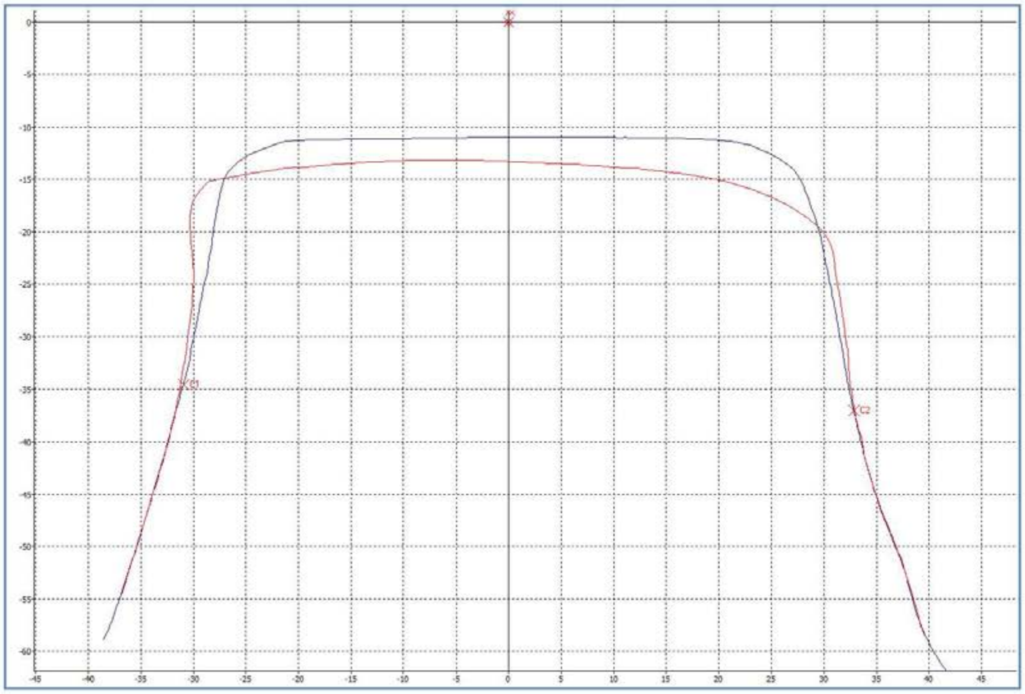

Overlay of two frog point profiles taken at 0 MGT (blue curve) and 100.79 MGT (red curve), 32 inches past the point of the frog (location 16).

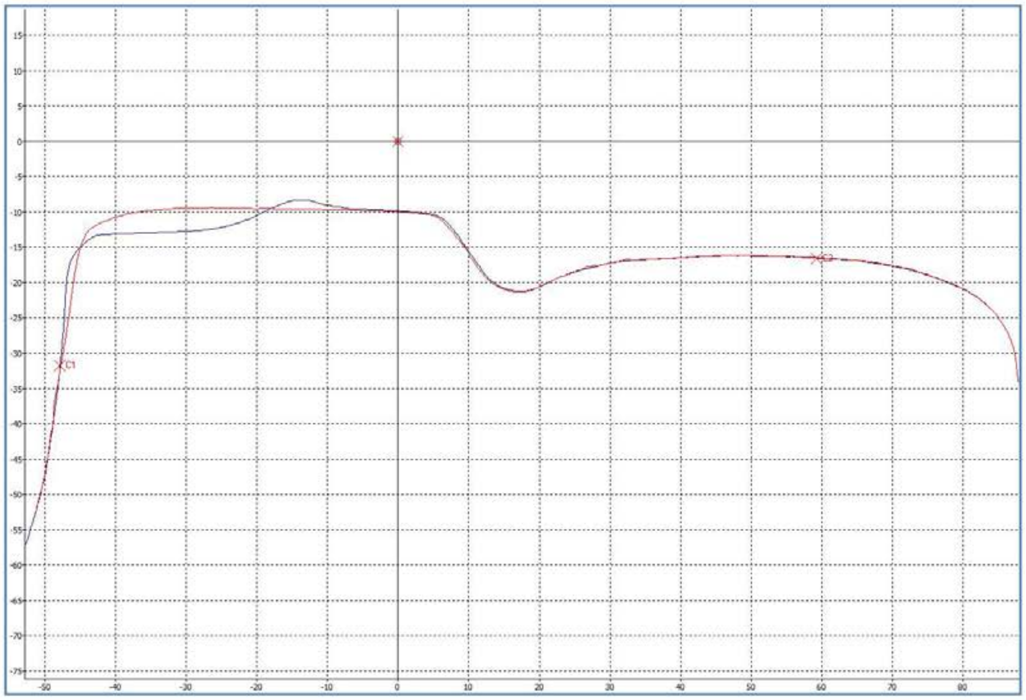

Overlay of two wing rail profiles taken at 0 MGT (blue curve) and 100.79 MGT (red curve), 8 inches ahead the point of the frog (location 25).

Sample A – Main (Gage) Wing

Location 19 (-16")

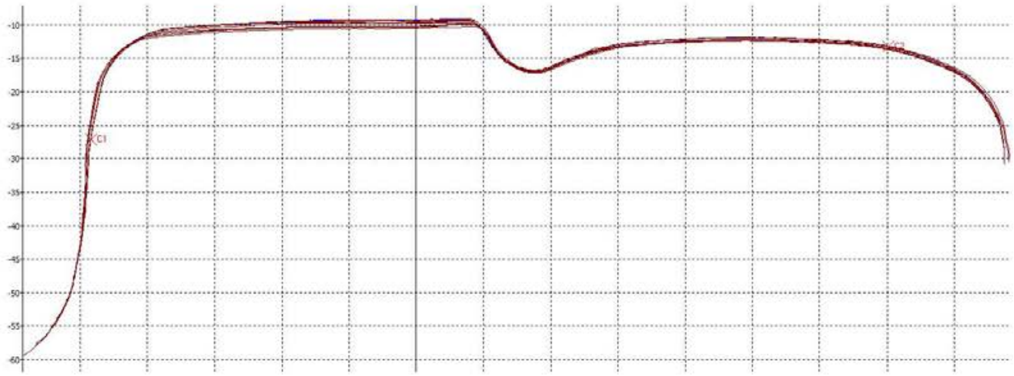

Location 20 (-8")

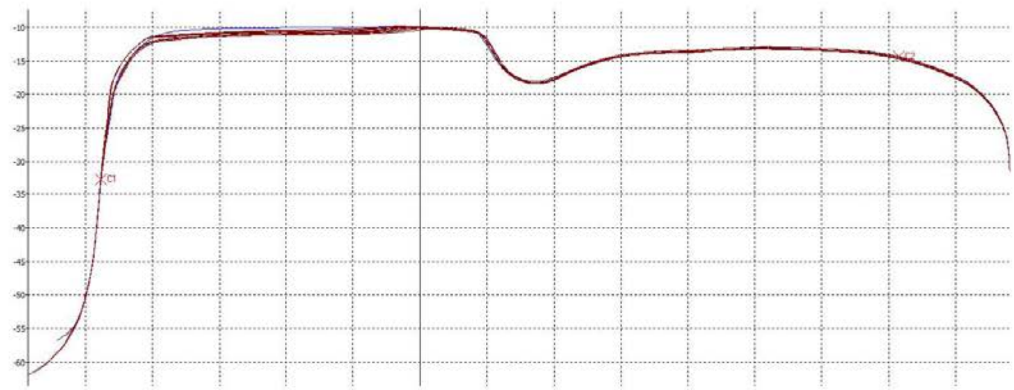

Location 21 (½" Point)

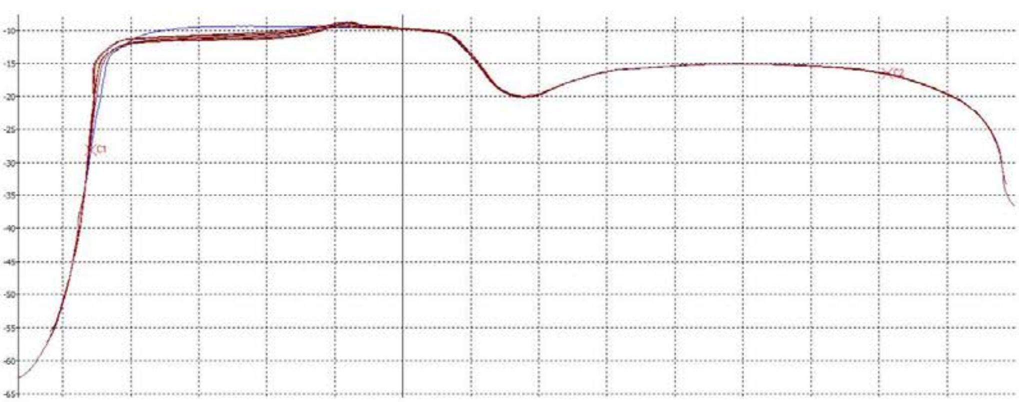

Location 22 (+2")

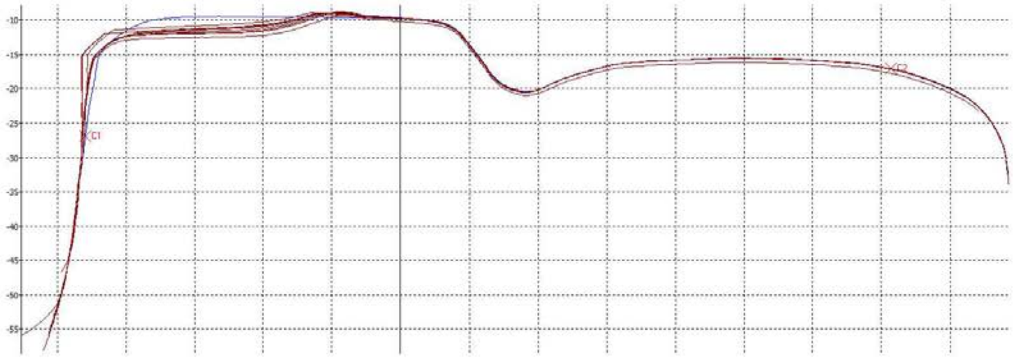

Location 23 (+4")

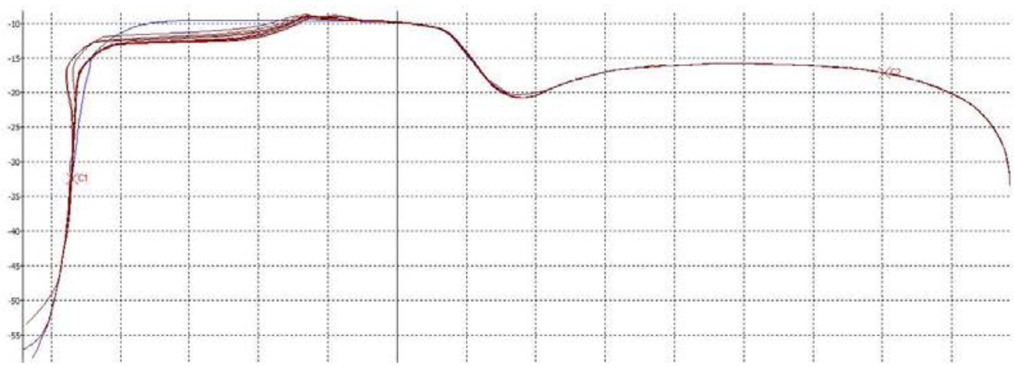

Location 24 (+6")

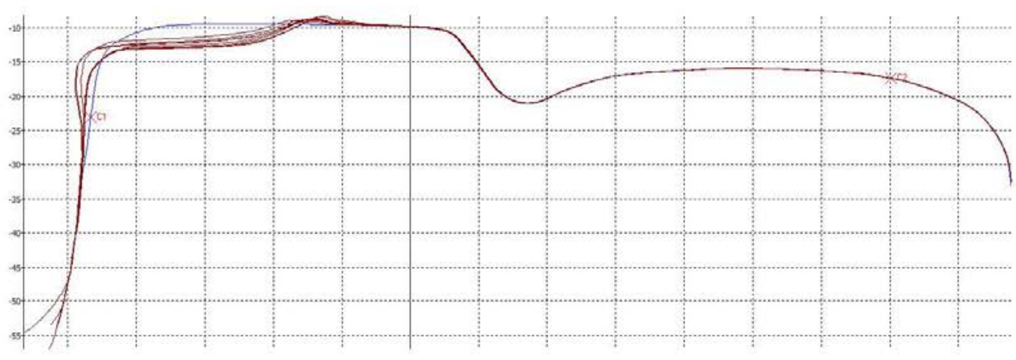

Location 25 (+8")

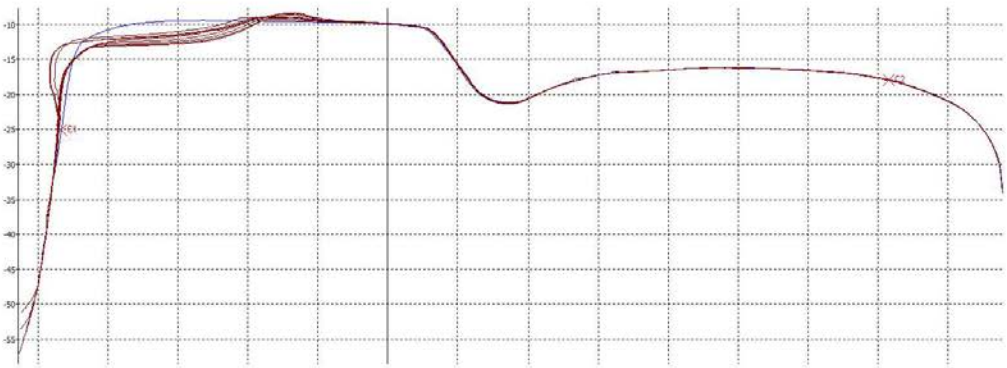

Location 26 (+10")

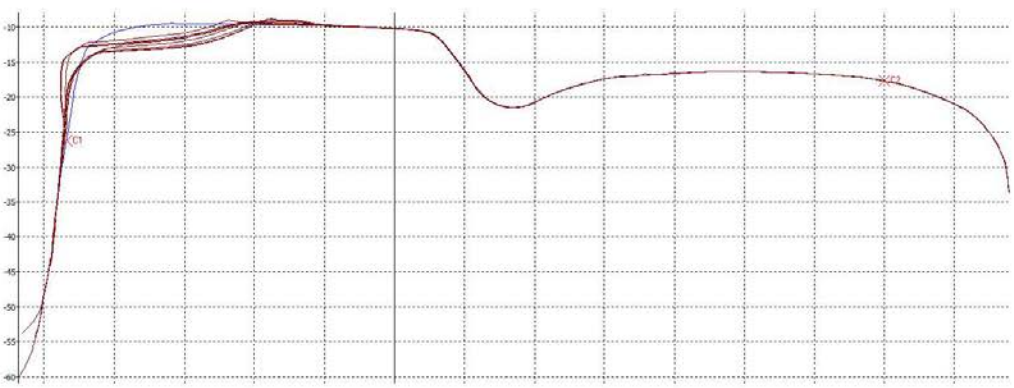

Location 27 (+12")

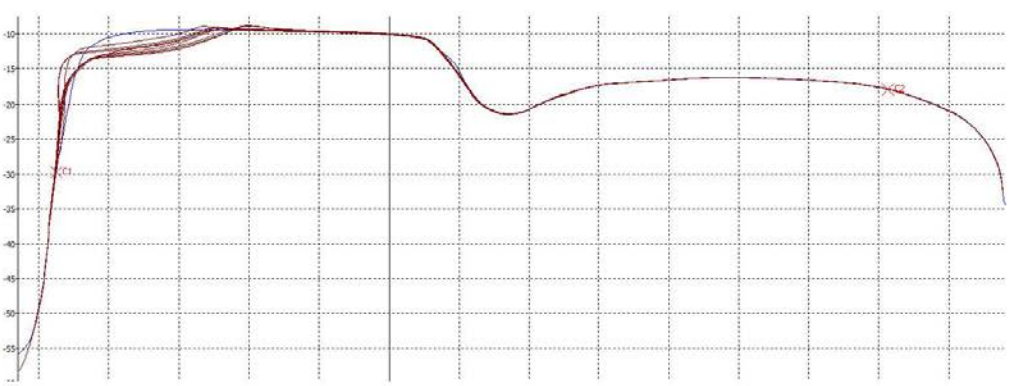

Location 28 (+14")

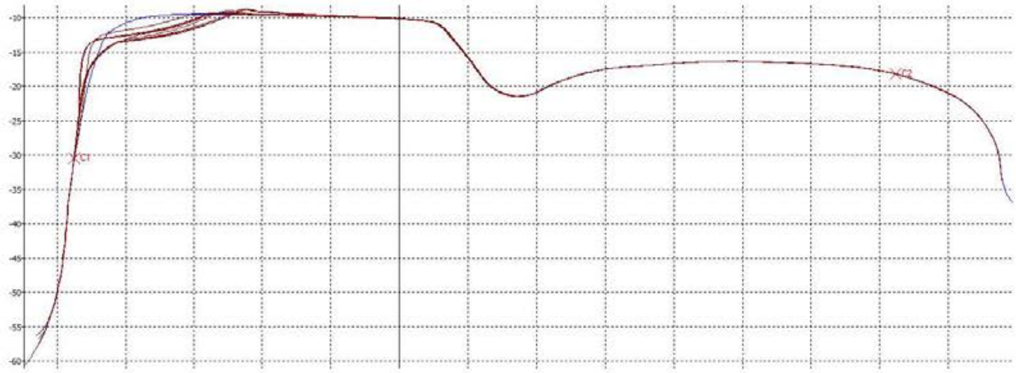

Location 29 (+16")

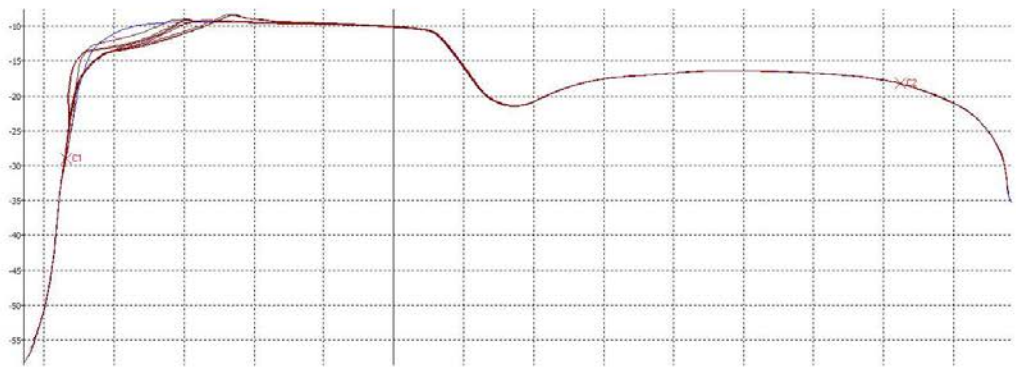

Location 30 (+18")

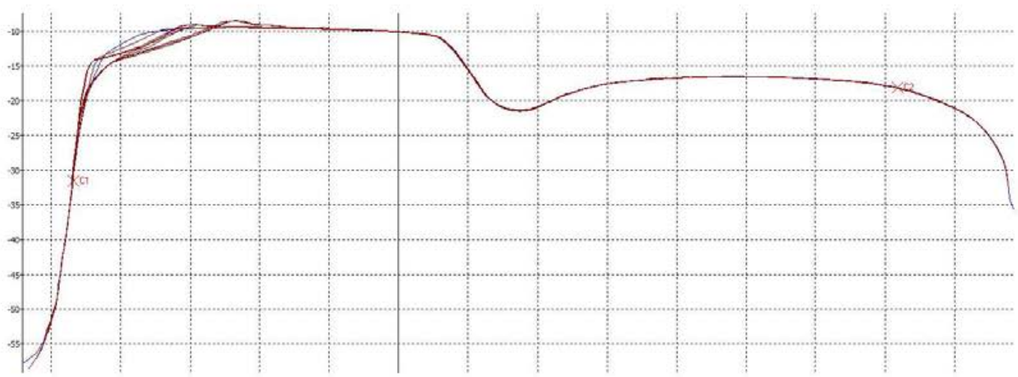

Location 31 (+20")

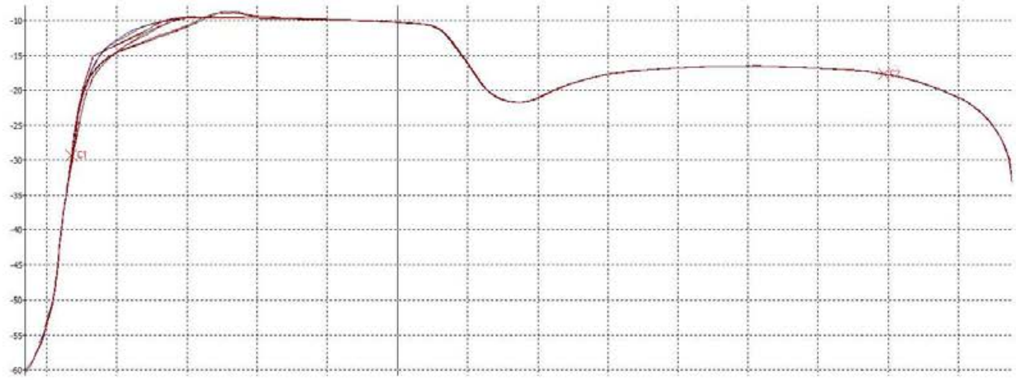

Location 32 (+22")

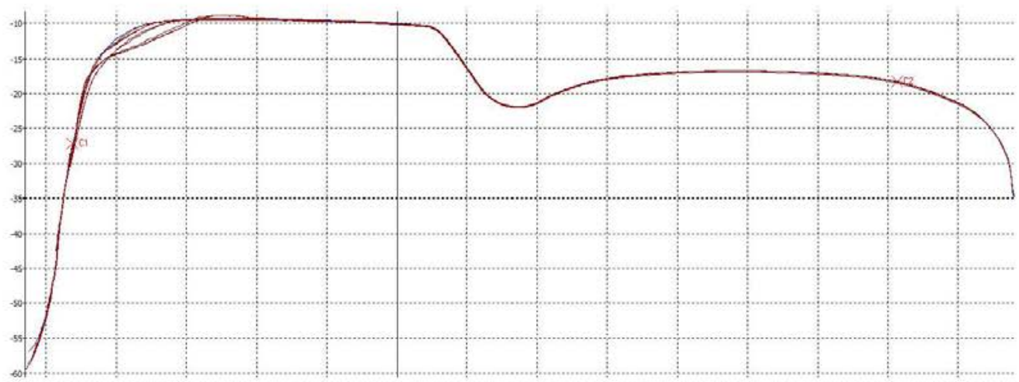

Location 33 (+24")

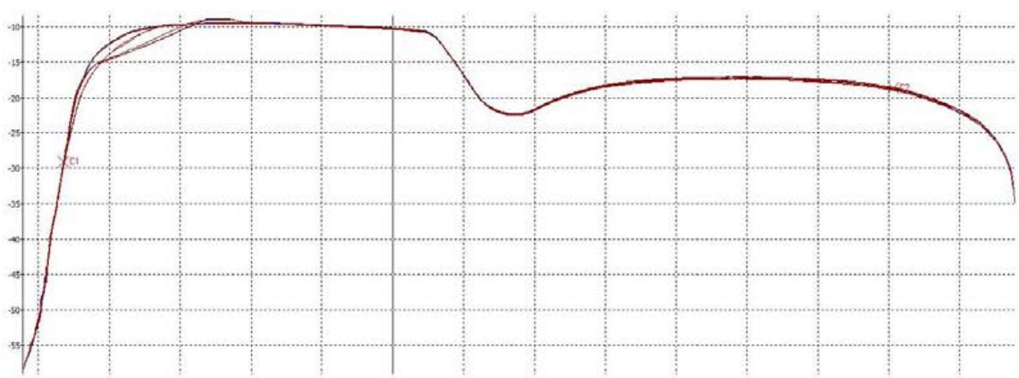

Location 34 (+26″)

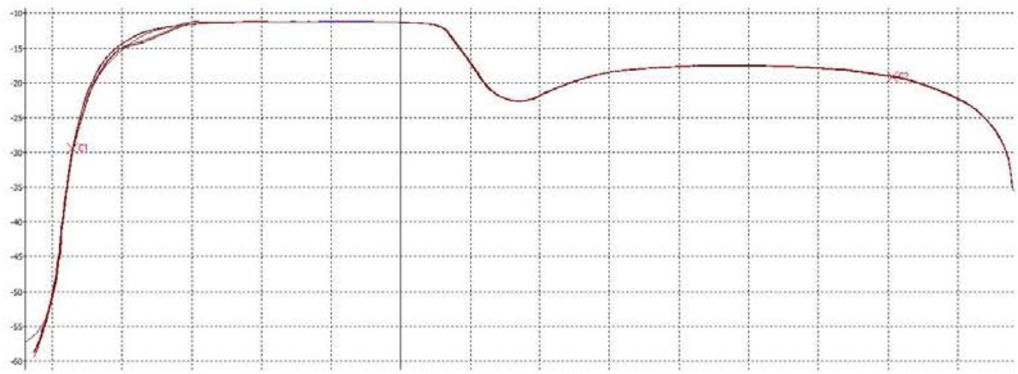

<u>Sample B – Point</u>

Location 1 (+2”)

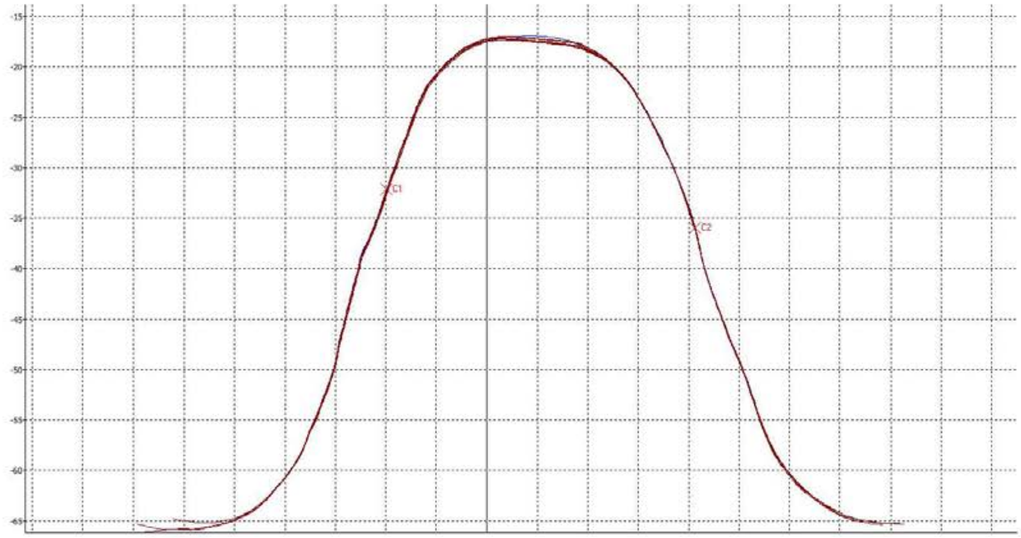

Location 2 (+4”)

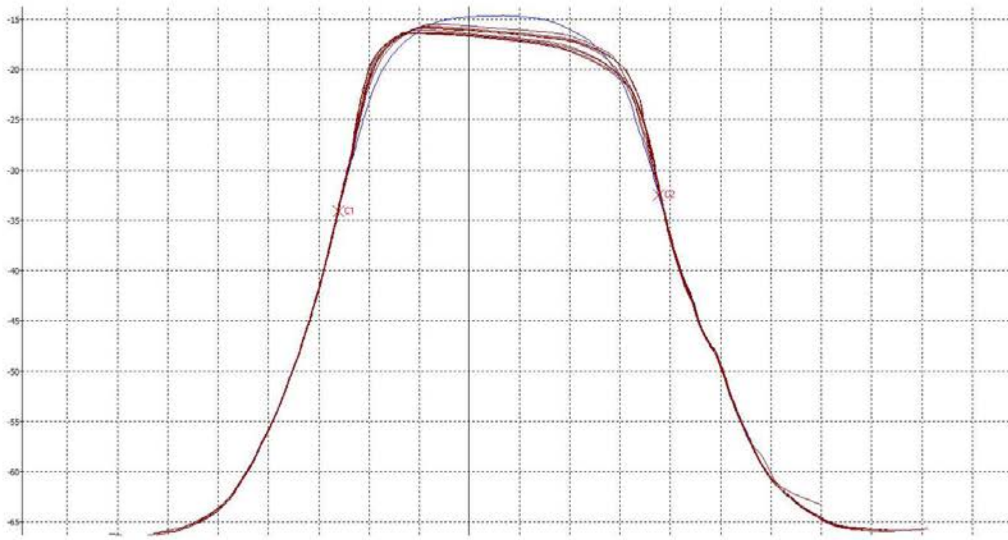

Location 3 (+6")

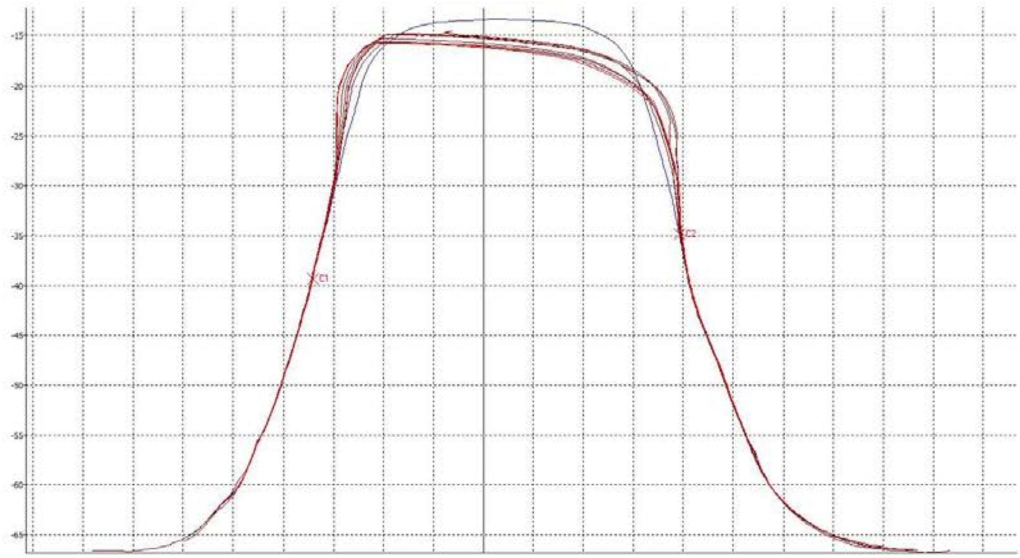

Location 4 (+8")

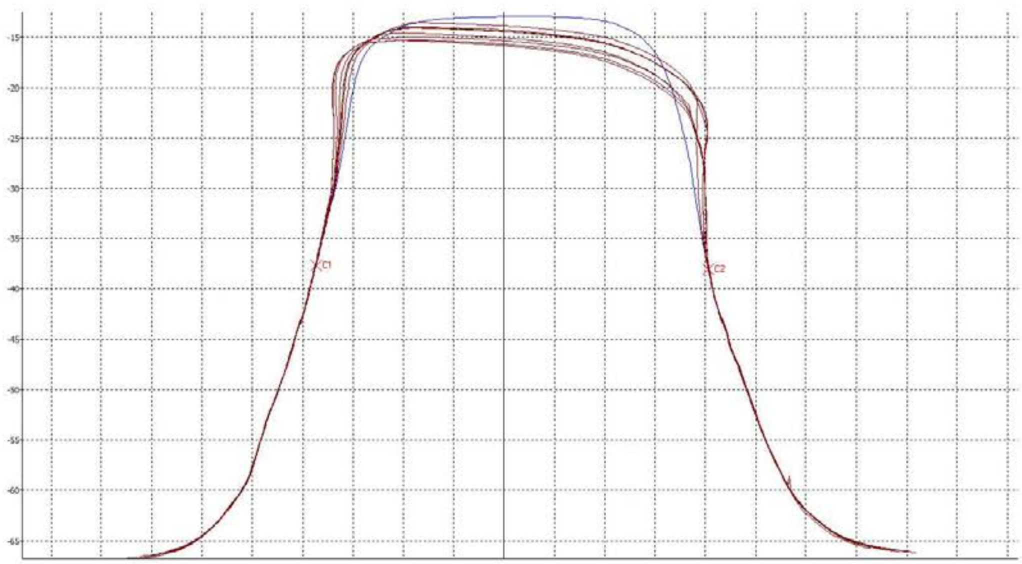

Location 5 (+10")

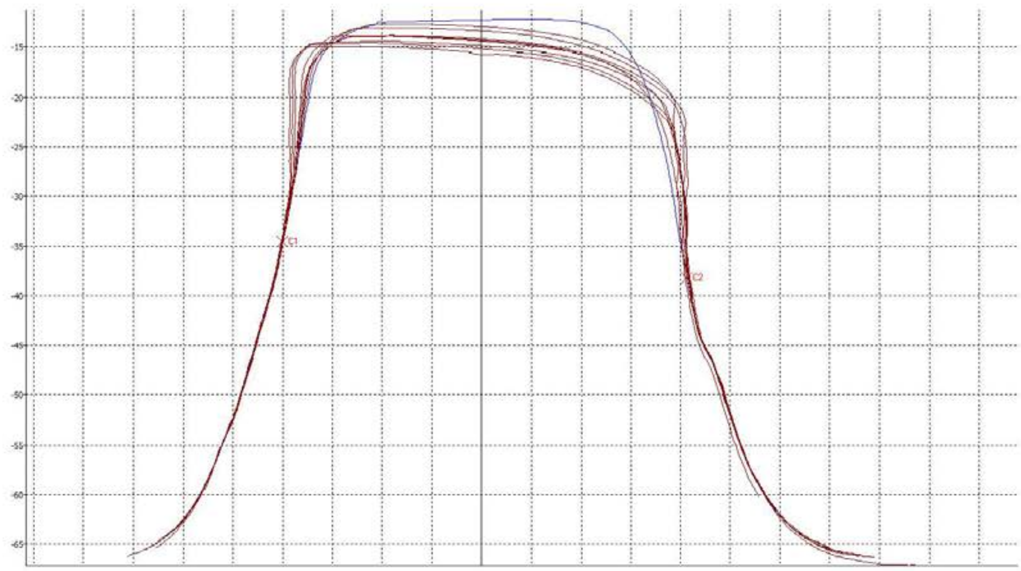

Location 6 (+12")

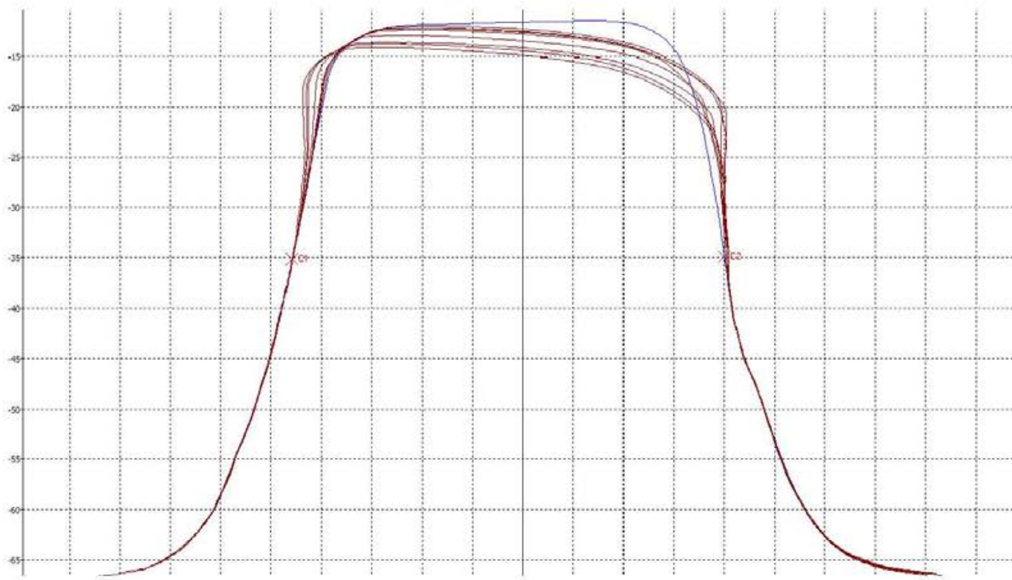

Location 7 (+14″)

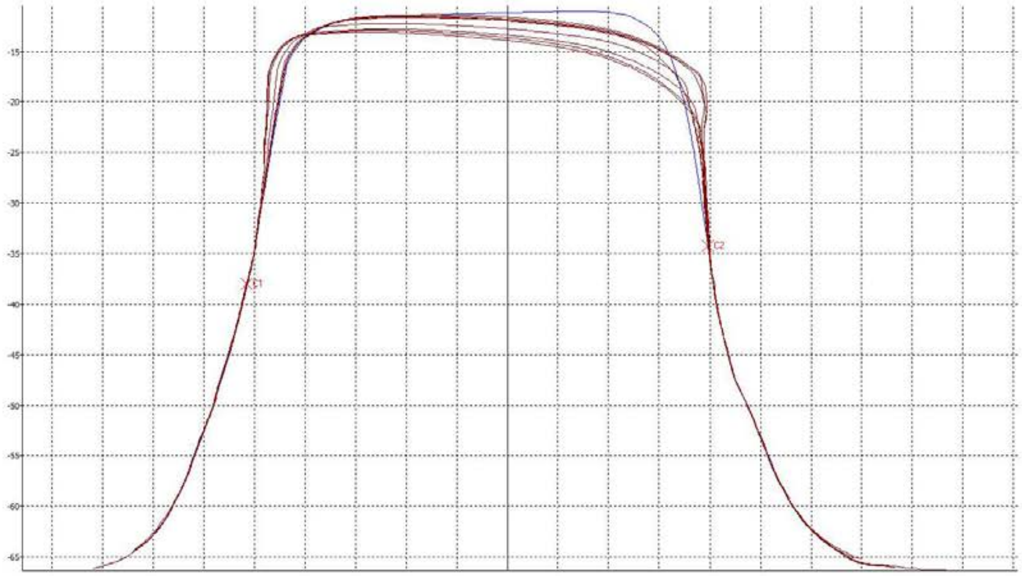

Location 8 (+16″)

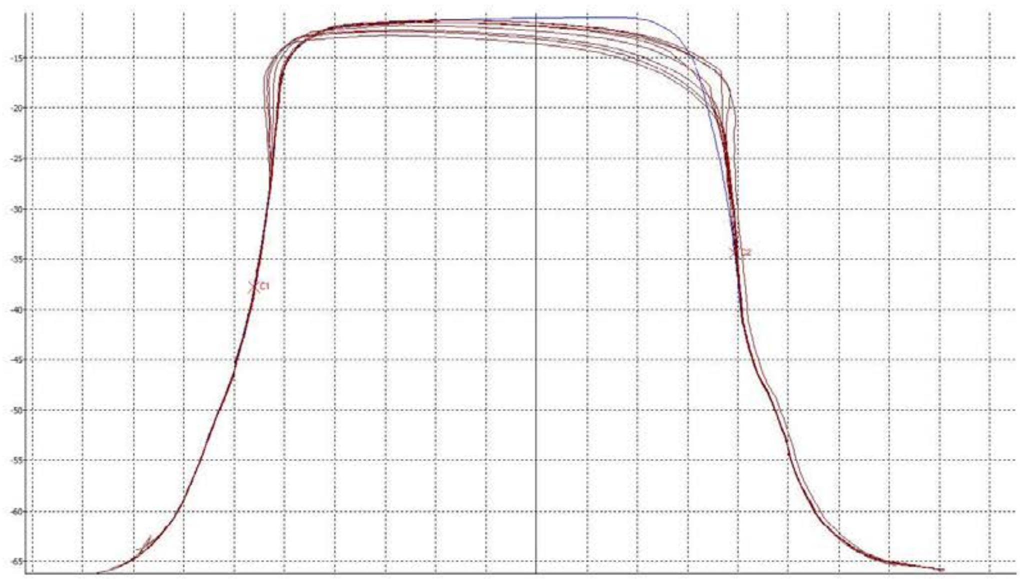

Location 9 (+18")

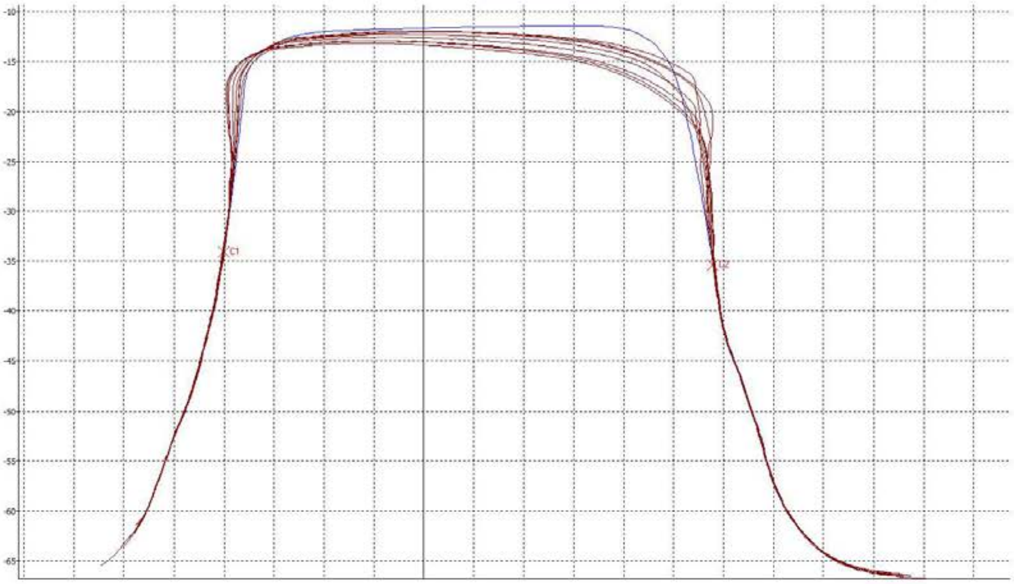

Location 10 (+20")

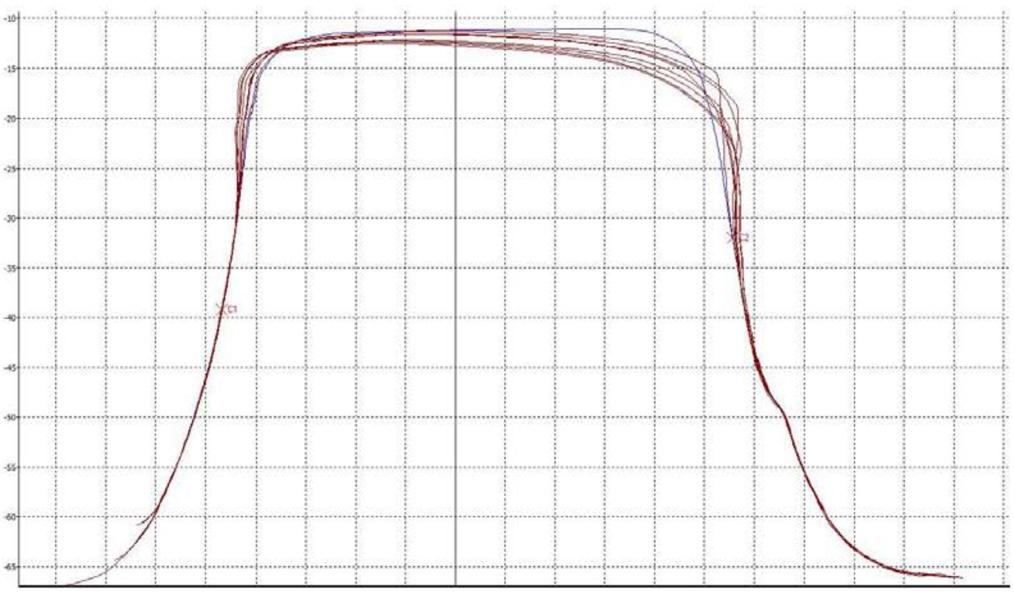

Location 11 (+22")

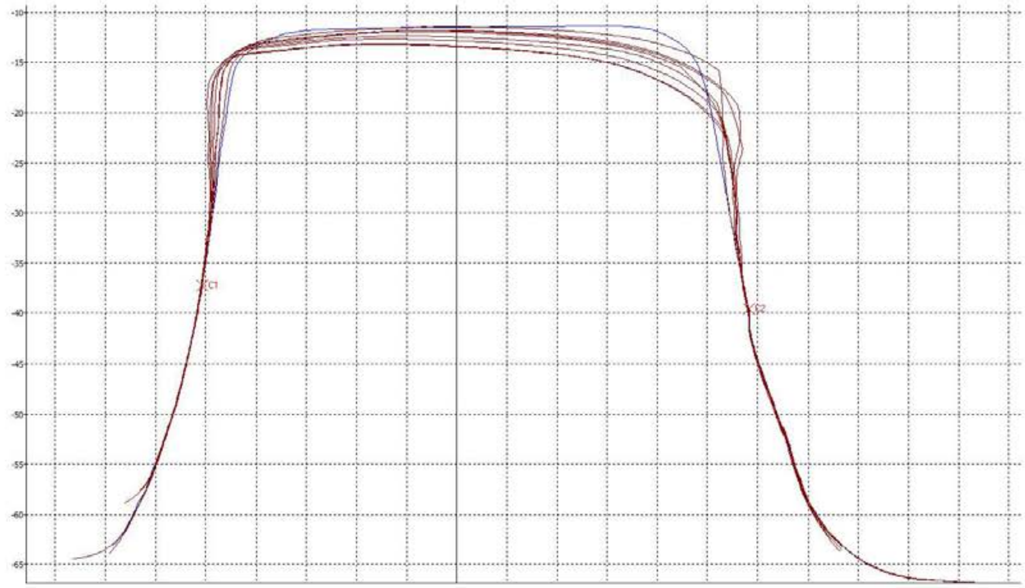

Location 12 (+24")

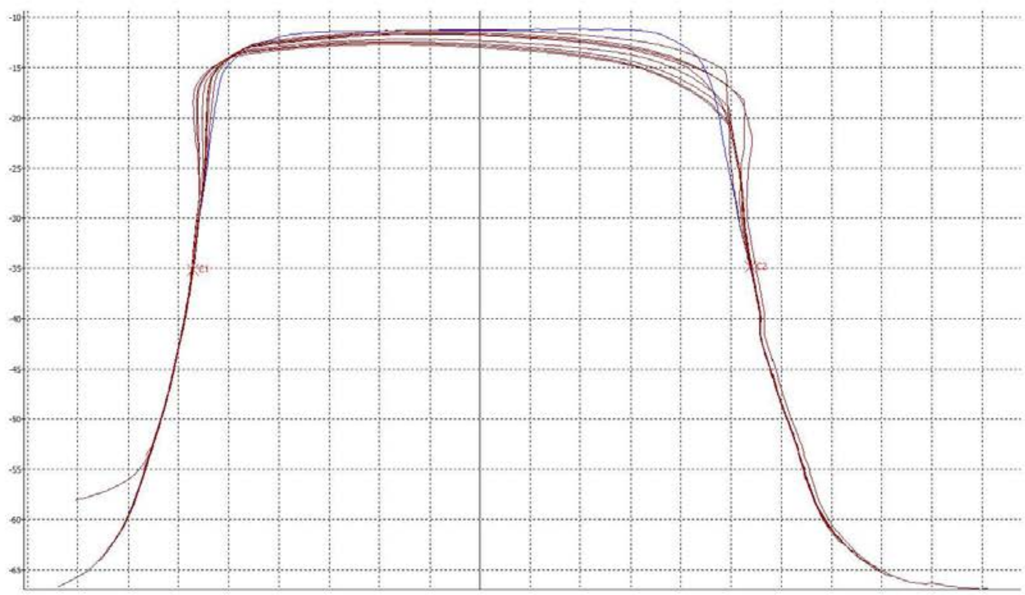

Location 13 (+26")

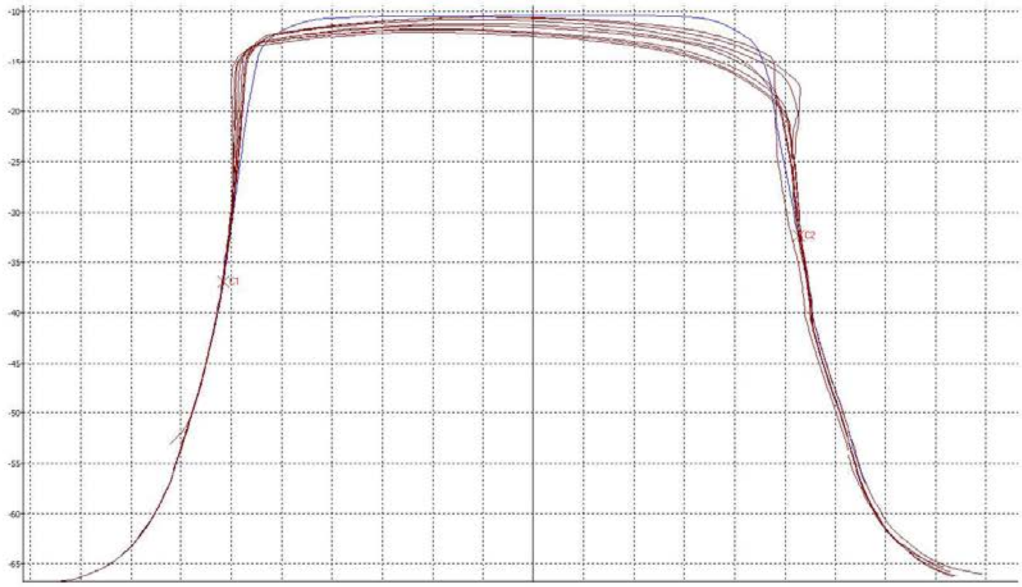

Location 14 (+28")

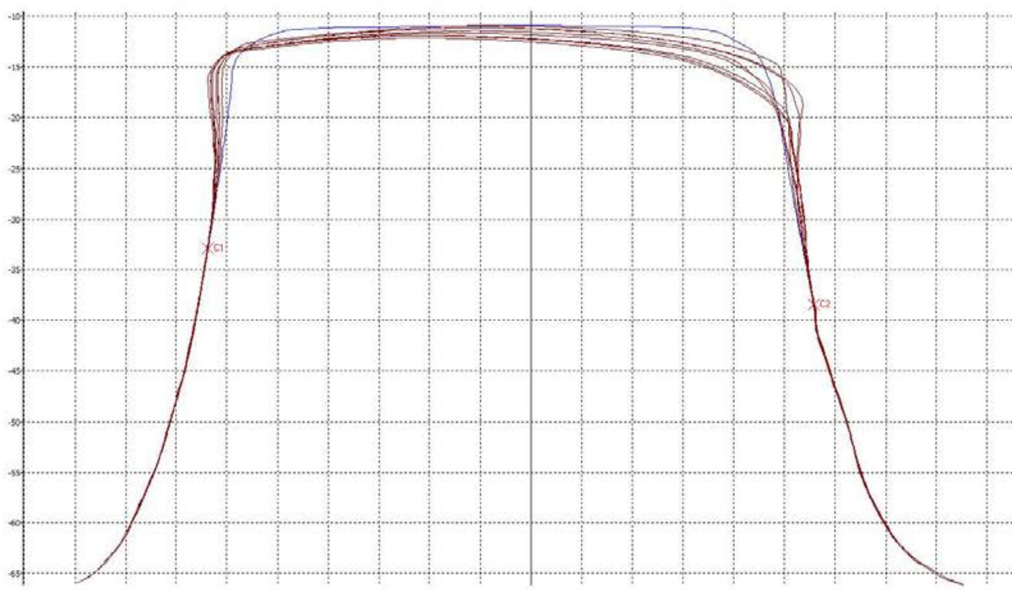

Location 15 (+30”)

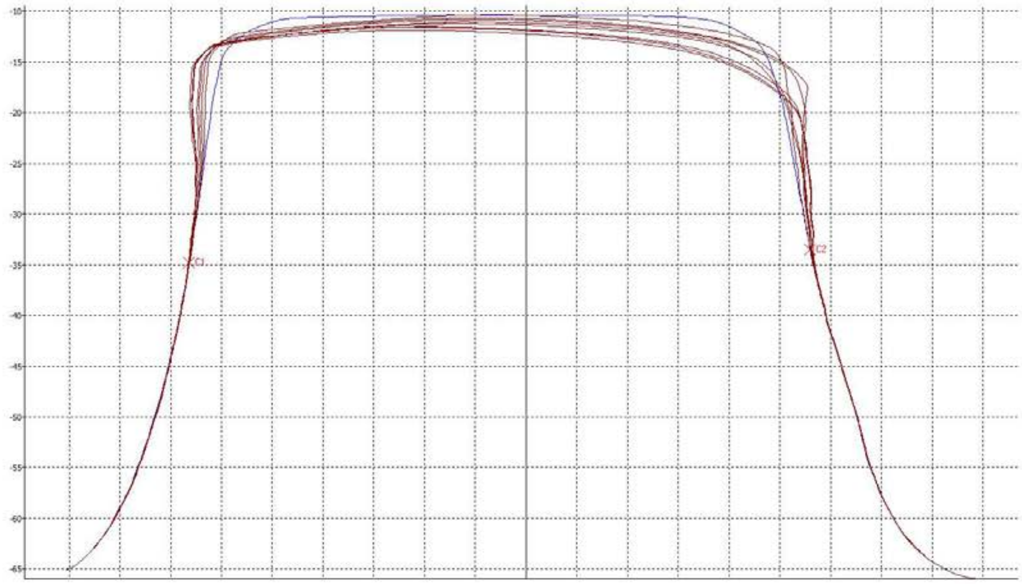

Location 16 (+32”)

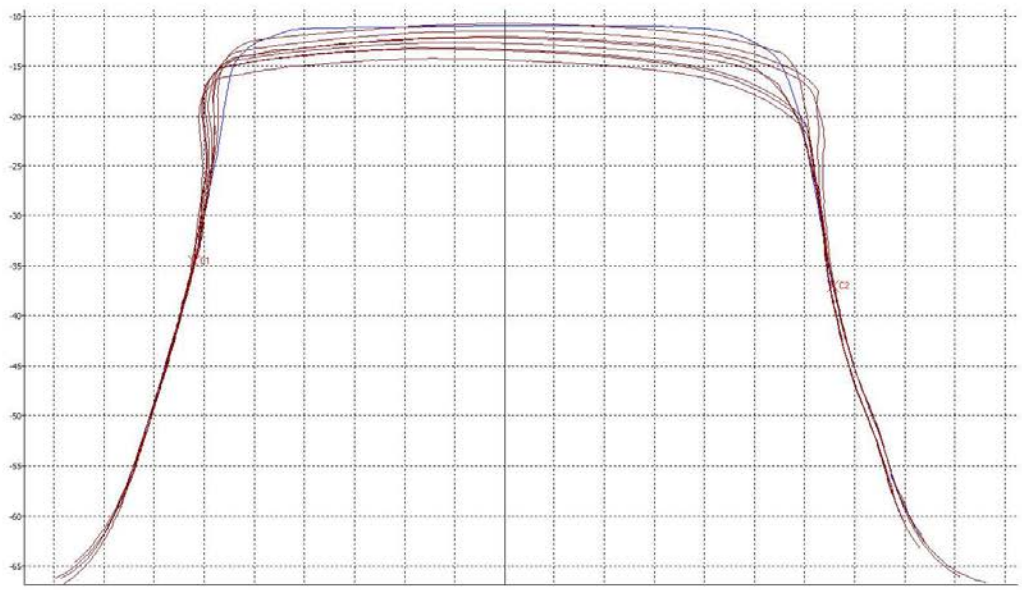

Location 17 (+34")

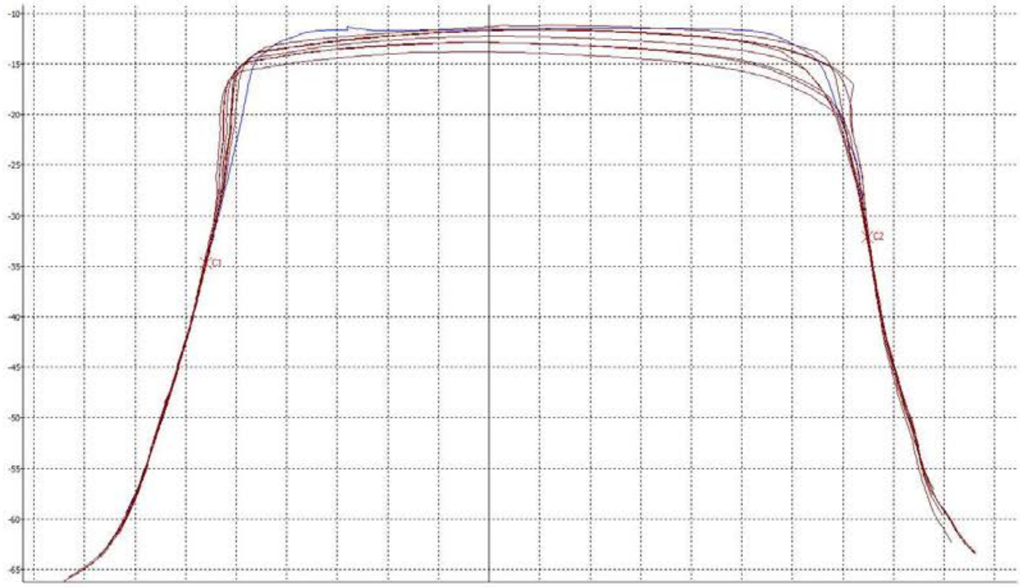

Location 18 (+36")

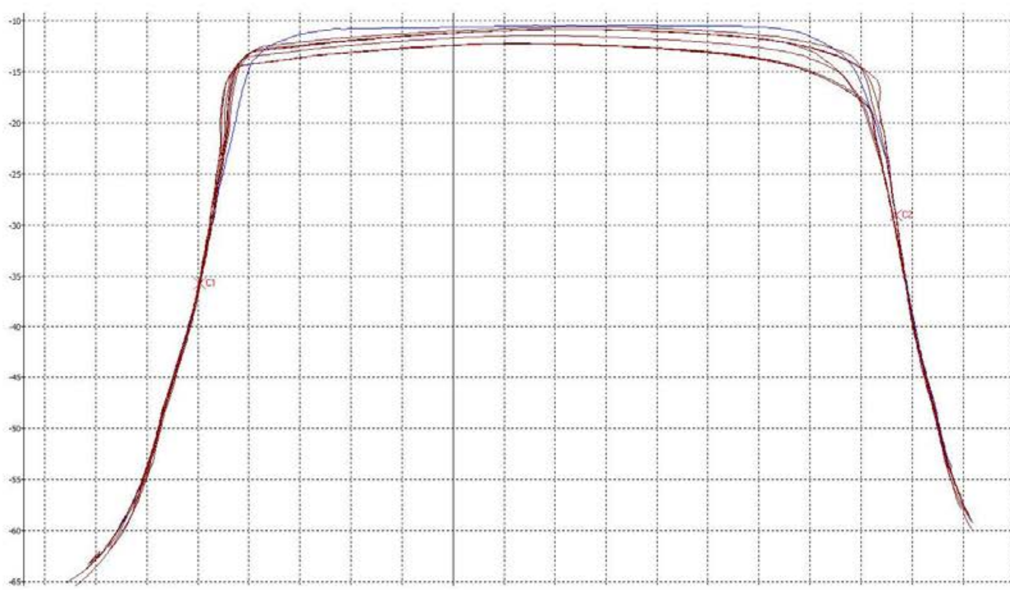

Attachment 2
Running Surface Wear Data Tables

Location 1 (+2")

MGT	Flow (mm^2)	Wear (mm^2)
0	0	0
2	1.878	1.081
6	2.034	1.484
10	1.393	1.458
18	0.682	2.332
60	1.659	4.757
68	0.196	5.189
85	0.195	5.394
101	0.091	6.885

Location 2 (+4")

MGT	Flow (mm^2)	Wear (mm^2)
0	0	0
2	12.746	14.337
6	18.268	19.443
10	19.579	21.799
18	12.780	22.950
60	16.849	30.32
68	18.264	33.307
85	18.476	36.012
101	20.208	37.973

Location 3 (+6")

MGT	Flow (mm^2)	Wear (mm^2)
0	0	0
2	26.051	38.830
6	35.225	42.028
10	33.115	42.81
18	23.139	40.447
60	30.410	56.598
68	32.212	61.896
85	32.102	65.842
101	32.670	68.821

Location 4 (+8")

MGT	Flow (mm^2)	Wear (mm^2)
0	0	0
2	24.524	24.785
6	35.296	37.000
10	35.519	39.195
18	35.340	40.028
60	31.198	59.860
68	35.192	67.177
85	37.529	78.521
101	37.314	83.460

Location 5 (+10")

MGT	Flow (mm^2)	Wear (mm^2)
0	0	0
2	22.914	23.550
6	34.459	36.251
10	38.265	57.866
18	11.411	63.411
60	28.456	63.078
68	36.350	78.158
85	37.086	88.768
101	39.350	101.38

Location 6 (+12")

MGT	Flow (mm^2)	Wear (mm^2)
0	0	0
2	22.605	27.805
6	28.720	34.338
10	27.957	35.770
18	13.462	41.613
60	20.653	61.700
68	29.737	87.611
85	29.823	99.484
101	33.049	113.646

Location 7 (+14")

MGT	Flow (mm^2)	Wear (mm^2)
0	0	0
2	20.686	20.505
6	22.676	24.917
10	20.692	28.157
18	9.668	32.678
60	15.909	56.027
68	24.143	81.939
85	24.563	93.038
101	25.695	101.455

Location 8 (+16")

MGT	Flow (mm^2)	Wear (mm^2)
0	0	0
2	17.861	18.505
6	20.991	19.905
10	26.622	26.477
18	11.716	31.731
60	17.304	45.733
68	22.658	69.532
85	23.701	79.668
101	26.160	97.075

Location 9 (+18")

MGT	Flow (mm^2)	Wear (mm^2)
0	0	0
2	17.869	30.793
6	25.949	31.550
10	24.003	33.676
18	15.715	48.411
60	22.235	62.425
68	26.945	84.133
85	26.796	89.711
101	28.124	100.590

Location 10 (+20")

MGT	Flow (mm^2)	Wear (mm^2)
0	0	0
2	13.681	15.250
6	31.120	26.451
10	32.099	37.714
18	20.271	40.741
60	26.129	66.366
68	35.426	75.113
85	35.349	85.966
101	37.859	93.161

Location 11 (+22")

MGT	Flow (mm^2)	Wear (mm^2)
0	0	0
2	16.592	15.130
6	35.481	36.486
10	35.413	40.014
18	22.198	47.758
60	27.160	65.851
68	30.427	86.195
85	32.992	113.331
101	32.845	116.077

Location 12 (+24")

MGT	Flow (mm^2)	Wear (mm^2)
0	0	0
2	16.106	15.301
6	30.494	31.145
10	38.296	37.548
18	18.752	44.358
60	26.396	66.550
68	31.805	84.280
85	31.400	94.753
101	32.722	102.094

Location 13 (+26")

MGT	Flow (mm^2)	Wear (mm^2)
0	0	0
2	11.837	28.331
6	32.526	33.411
10	28.845	48.292
18	20.095	69.568
60	23.003	78.708
68	29.573	102.349
85	30.077	110.928
101	33.004	122.193

Location 14 (+28")

MGT	Flow (mm^2)	Wear (mm^2)
0	0	0
2	19.214	20.374
6	32.756	35.434
10	30.027	36.519
18	17.349	56.286
60	21.594	64.549
68	29.271	84.611
85	28.245	89.714
101	30.773	101.882

Location 15 (+30")

MGT	Flow (mm^2)	Wear (mm^2)
0	0	0
2	18.796	21.150
6	35.513	38.705
10	37.150	46.491
18	25.528	62.990
60	33.048	68.314
68	41.588	92.288
85	40.648	98.415
101	42.650	112.604

Location 16 (+32")

MGT	Flow (mm^2)	Wear (mm^2)
0	0	0
2	21.262	11.078
6	31.571	48.094
10	31.645	80.631
18	13.629	94.105
60	18.609	117.974
68	24.021	154.346
85	25.464	163.244
101	27.069	213.000

Location 17 (+34")

MGT	Flow (mm^2)	Wear (mm^2)
0	0	0
2	19.768	11.042
6	26.010	30.291
10	23.741	30.225
18	14.288	44.289
60	17.362	75.884
68	21.550	111.124
85	21.785	114.744
101	24.088	167.901

Location 18 (+36")

MGT	Flow (mm^2)	Wear (mm^2)
0	0	0
2	12.537	24.706
6	18.616	40.900
10	18.117	42.375
18	12.038	55.111
60	13.546	90.294
68	16.529	138.535
85	16.022	140.314
101	16.334	141.598

Location 19 (-16")

MGT	Flow (mm^2)	Wear (mm^2)
0	0	0
2	0.101	2.105
6	0.064	6.442
10	0.082	12.06
18	0	21.341
60	6.564	38.201
68	8.466	42.315
85	8.284	44.607
101	11.63	56.368

Location 20 (-8")

MGT	Flow (mm^2)	Wear (mm^2)
0	0	0
2	8.886	13.585
6	9.204	17.945
10	9.305	23.441
18	0.549	35.296
60	0.984	36.083
68	1.241	35.830
85	1.150	43.155
101	1.505	45.719

Location 21 (1/2" point)

MGT	Flow (mm^2)	Wear (mm^2)
0	0	0
2	16.968	21.938
6	20.444	25.762
10	21.049	27.255
18	9.838	33.393
60	17.137	36.915
68	17.419	41.862
85	16.795	43.675
101	17.933	47.009

Location 22 (+2")

MGT	Flow (mm^2)	Wear (mm^2)
0	0	0
2	19.078	23.420
6	29.087	34.260
10	31.073	35.853
18	13.064	40.765
60	14.479	47.688
68	15.238	53.369
85	15.639	56.459
101	10.606	75.519

Location 23 (+4")

MGT	Flow (mm^2)	Wear (mm^2)
0	0	0
2	26.662	29.215
6	35.618	41.541
10	37.306	47.604
18	14.903	54.673
60	16.695	61.095
68	17.362	64.642
85	17.602	68.043
101	17.824	71.439

Location 24 (+6")

MGT	Flow (mm^2)	Wear (mm^2)
0	0	0
2	27.489	32.071
6	36.224	44.182
10	37.614	49.828
18	15.323	54.003
60	16.753	61.004
68	17.643	67.025
85	18.148	72.086
101	19.304	74.175

Location 25 (+8")

MGT	Flow (mm^2)	Wear (mm^2)
0	0	0
2	23.855	24.287
6	31.138	32.345
10	33.629	34.676
18	12.781	42.965
60	14.535	49.232
68	17.427	56.258
85	18.578	62.359
101	19.432	65.668

Location 26 (+10")

MGT	Flow (mm^2)	Wear (mm^2)
0	0	0
2	18.740	20.945
6	25.257	30.197
10	25.991	33.362
18	8.001	39.937
60	9.755	46.025
68	13.242	56.514
85	15.178	62.088
101	16.330	63.390

Location 27 (+12")

MGT	Flow (mm^2)	Wear (mm^2)
0	0	0
2	13.201	13.498
6	21.776	23.430
10	21.196	27.415
18	6.783	34.378
60	9.257	37.953
68	13.461	44.515
85	13.861	48.645
101	14.500	51.367

Location 28 (+14")

MGT	Flow (mm^2)	Wear (mm^2)
0	0	0
2	9.640	10.987
6	18.088	21.595
10	18.788	23.425
18	6.977	30.245
60	9.310	34.063
68	12.228	40.531
85	12.916	42.717
101	13.421	43.649

Location 29 (+16")

MGT	Flow (mm^2)	Wear (mm^2)
0	0	0
2	7.364	7.907
6	15.476	18.033
10	16.110	20.373
18	3.902	26.643
60	6.055	28.117
68	10.565	33.790
85	10.845	37.399
101	11.587	38.273

Location 30 (+18")

MGT	Flow (mm^2)	Wear (mm^2)
0	0	0
2	3.717	4.132
6	10.448	10.791
10	11.989	12.399
18	2.762	19.022
60	3.113	20.426
68	8.185	27.750
85	9.271	29.683
101	11.058	31.570

Location 31 (+20")

MGT	Flow (mm^2)	Wear (mm^2)
0	0	0
2	0.533	1.127
6	4.235	5.383
10	5.058	5.443
18	0.271	19.790
60	0.525	21.101
68	4.704	26.707
85	5.704	27.895
101	5.975	27.924

Location 32 (+22")

MGT	Flow (mm^2)	Wear (mm^2)
0	0	0
2	0.221	0.895
6	0.772	2.681
10	0.784	4.095
18	0.023	17.860
60	0.017	20.759
68	3.164	23.820
85	4.759	27.474
101	4.055	27.615

Location 33 (+24")

MGT	Flow (mm^2)	Wear (mm^2)
0	0	0
2	0.011	0.683
6	0	2.806
10	0	5.225
18	0.004	18.183
60	0.072	19.770
68	2.722	25.654
85	3.494	28.126
101	3.504	28.589

Location 34 (+26")

MGT	Flow (mm^2)	Wear (mm^2)
0	0	0
2	0.094	0.122
6	0.002	0.643
10	0.018	0.879
18	0	1.260
60	0	10.659
68	0.748	12.994
85	1.328	13.579
101	1.228	14.535

Attachment 3
Hardness Data Table

Hardness Data

	0 MGT		2 MGT		6.17 MGT		10.15 MGT		17.53 MGT		42.71 MGT		57.46 MGT	68 MGT		84.52 MGT		100.79 MGT	
Location Relative to POF	Main (wing)	Point	Main (wing)	Point	Main (wing)	Point	Main (wing)	Point	Main (wing)	Point	Main (wing)	Point	Main (wing) In Wearband	Main (wing)	Point	Main (wing)	Point	Main (wing)	Point
- 16"	486		466		494		494		527		508		501	482		471		496	
- 8"	222		454		501		471		460		506		491	492		491		552	
+ 2"	190		445		306		542		499		540		610	540		526		581	
+ 8"	210	243	505	377	314	487	538	484	557	447	548	513	632	599	487	587	448	589	486
+ 16"	215	223	510	341	238	438	510	410	441	387	558	453	531	587	452	571	456	544	491
+ 22"	207	228	408	358	220	418	250	405	223	377	267	411	513	497	455	550	464	542	513

Abbreviations and Acronyms

AMS	Austenitic Manganese Steel
AWS	American Welding Society
CSC	Controlled Short-Circuiting
CV	Constant Voltage
FCAW	Flux-Cored Arc Welding
FCAW-A	Flux-Cored Arc Welding Automated
GMAW	Gas Metal Arc Welding
HAL	Heavy Axle Load
HAZ	Heat-Affected Zone
HTL	High-Tonnage Loop
MGT	Million Gross Tons
RT	Radiographic Testing
RWF	Reciprocating Wire Feed
SA-FCAW	Semi-Automatic Flux-Cored Arc Welding
SMAW	Shielded Metal Arc Welding
TTCI	Transportation Technology Center, Inc.
UT	Ultrasonic Testing
UTS	Ultimate Tensile Strength
YS	Yield Strength